

CRISTIAN FELIPE ZULUAGA ARISTIZÁBAL

**SOLAR RADIATION IN BRAZIL: OBSERVATIONS, HISTORICAL
SIMULATIONS, PROJECTIONS AND APPLICATIONS**

Thesis submitted to the Applied Meteorology
Graduate Program of the Universidade Federal de
Viçosa in partial fulfillment of the requirements
for the degree of *Doctor Scientiae*.

Adviser: Flávio Barbosa Justino

**VIÇOSA - MINAS GERAIS
2021**

**Ficha catalográfica elaborada pela Biblioteca Central da Universidade
Federal de Viçosa - Campus Viçosa**

T

Z94s Zuluaga Aristizábal, Cristian Felipe, 1990-

2021 Solar radiation in Brazil : observations, historical
simulations, projections and applications / Cristian Felipe
Zuluaga Aristizábal. – Viçosa, MG, 2021.

98 f. : il. (algumas color.) ; 29 cm.

Inclui anexo.

Inclui apêndice.

Orientador: Flávio Barbosa Justino.

Tese (doutorado) - Universidade Federal de Viçosa.

Inclui bibliografia.

1. Radiação solar. 2. Climatologia - Modelos matemáticos.
3. Mudanças climáticas. 4. Sistemas de energia fotovoltaica.
I. Universidade Federal de Viçosa. Departamento de Engenharia
Agrícola. Programa de Pós-Graduação em Meteorologia
Agrícola. II. Título.

CDD 22. ed. 551.5271

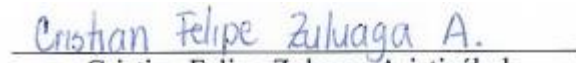
CRISTIAN FELIPE ZULUAGA ARISTIZÁBAL

**SOLAR RADIATION IN BRAZIL: OBSERVATIONS, HISTORICAL
SIMULATIONS, PROJECTIONS AND APPLICATIONS**

Thesis submitted to the Applied Meteorology
Graduate Program of the Universidade Federal de
Viçosa in partial fulfillment of the requirements
for the degree of *Doctor Scientiae*.

APPROVED: February 25, 2021.

Assent:


Cristian Felipe Zuluaga Aristizábal
Author


Flávio Barbosa Justino
Adviser

To my family.

ACKNOWLEDGEMENTS

To the Federal University of Viçosa, for the opportunity to complete the Applied Meteorology Graduate Program.

To the Coordenação de Aperfeiçoamento de Pessoal de Nível Superior (CAPES), to granting the scholarship.

This study was financed in part by the Coordenação de Aperfeiçoamento de Pessoal de Nível Superior – Brasil (CAPES) – Finance Code 001.

To my advisor Flávio Barbosa Justino for the great opportunity for learning and professional training he gave me, for teaching me quality science, for the support and for the trust in me.

Special thanks to my friend and colleague Álvaro Ávila for the coffees and scientific discussions shared during all these years.

To the colleagues who passed through the workroom during this time: Manuel, Vagna, Vanúcia, Gabriela, Alex, Guilherme, etc; as well as all the colleagues and professors of the Applied Meteorology Graduate Program.

To Graça, for her willingness, diligence and help (almost maternal). Here is my feeling of admiration.

To my family: Olga Lucía, Ximena and Vicente, for the support and unconditional love, even from a distance.

To all my soccer friends (peladas), especially Henry, Ángel, Nain, Marco, Renato, Kleiton, Daniel and Rodrigo. Thanks to each game, beer, barbecue and conversation with you, Viçosa became very special.

Finally, thanks to all who directly/indirectly contributed to finished this stage.

*“The world of things entered your infant mind
To populate that crystal cabinet.
Within its walls the strangest partners met,
And things turned thoughts did propagate their kind.
For, once within, corporeal fact could find
A spirit. Fact and you in mutual debt
Built there your little microcosm - which yet
Had hugest tasks to its small self assigned.*

*Dead men can live there, and converse with stars:
Equator speaks with pole, and night with day;
Spirit dissolves the world's material bars -
A million isolations burn away.
The Universe can live and work and plan,
At last made God within the mind of man.”*

Julian Huxley

ABSTRACT

ZULUAGA ARISTIZÁBAL, Cristian Felipe, D.Sc., Universidade Federal de Viçosa, February, 2021. **Solar Radiation in Brazil: Observations, Historical Simulations, Projections and Applications.** Adviser: Flávio Barbosa Justino.

Climate change is one of the greatest modern adaptation challenges facing humanity. Among the strategies to face this challenge is the use of renewable energies. The conversion of solar downward shortwave radiation (DSWR) to photovoltaic (PV) energy is considered a clean, sustainable and renewable energy technology that can help meet the energy demands of the growing world population, while reducing energy costs and the adverse human impacts of the use of fossil fuels. The main objective of this study is to evaluate the past and future changes in solar radiation in Brazil, and their consequences for the production of PV power potential (P_{PV}). Chapter 1 evaluates the spatiotemporal patterns of DSWR variability and trends in Brazil between 1980 and 2016, based on the most recent gridded datasets (observations, reanalysis and merging) and to explore the relationships between DSWR variability and decadal changes in cloud cover. The results showed that the ERA5 reanalysis delivered the DSWR values closest to the observations for all country regions. Also, DSWR shows a positive trend (“brightening”) for all of Brazil, particularly in the N, CW and SE regions. Strong correlations were found between cloud cover and observed DWSR, which indicated that the decadal changes in cloud cover are the main factor contributing to the “brightening” effect in Brazil. Chapter 2 evaluates how the CMIP6 models estimate the spatio-temporal variability of the DSWR and its causes in Brazil in the historical period 1981-2010. In addition, using an ensemble of the best models, it was estimated how the future changes (2021-2050 and 2071-2100) of DSWR, in two different scenarios of shared socioeconomic paths (SSP2-4.5 and SSP5-8.5), would affect the generation of photovoltaic systems in Brazilian territory. Future climate projections showed that P_{PV} will have slight increases only in the north of the N region, south of the NE region, and in the SE region, under all scenarios and periods, with maximum growth values of 2.5% under SSP5-8.5 for the immediate future (2021 - 2050). Despite the greater availability of solar radiation, the sensitivity of current P_{PV} systems’ technology to the increase in ambient temperature, would not allow increases in the yield of P_{PV} . On the contrary, as the temperature increases, the efficiency of the solar panels decreases, canceling the positive effect of the increase in DSWR.

Keywords: Solar radiation. CMIP6. Reanalyses. Climate changes. SSP

RESUMO

ZULUAGA ARISTIZÁBAL, Cristian Felipe, D.Sc., Universidade Federal de Viçosa, fevereiro de 2021. **Radiação Solar no Brasil: Observações, Simulações Históricas, Projeções e Aplicações.** Orientador: Flávio Barbosa Justino.

As mudanças climáticas são um dos maiores desafios modernos de adaptação que a humanidade está enfrentando. Entre as estratégias para afrontar este desafio está o uso de energias renováveis. A conversão da radiação solar (DSWR) por meio da energia fotovoltaica (PV) é considerado uma tecnologia de energia limpa, sustentável e renovável que pode ajudar a atender às demandas de energia da crescente população mundial, ao mesmo tempo que reduz os impactos adversos do uso de combustíveis fósseis. O objetivo principal deste estudo foi avaliar as mudanças atuais e futuras da radiação solar no Brasil, e suas consequências para a produção de energia PV (P_{PV}). Para isto, o capítulo 1 desta tese avaliou os padrões espaço-temporais de variabilidade e tendências de DSWR no Brasil entre 1980 e 2016, com base nos conjuntos de dados em grade mais recentes (observações, reanálise e merging) e explorar as relações entre a variabilidade de DSWR e mudanças na cobertura de nuvens. Os resultados mostraram que a reanálise ERA5 oferece os valores de DSWR mais próximos às observações para todo o país. Também, DSWR apresentou uma tendência positiva para todo Brasil, particularmente nas regiões N, CW e SE. Se encontraram fortes correlações entre a cobertura de nuvens e DSWR observada, que indicaram que as mudanças decadais na nebulosidade são o principal fator que contribui para o efeito de “brightening” no Brasil. O capítulo 2 avaliou como os recentes modelos do CMIP6 estimam a variabilidade espaço-temporal da DSWR e suas causas no Brasil, no período histórico 1981-2010. Além disso, foi estimado como as mudanças futuras (2021-2050 e 2071-2100) de DSWR, em dois cenários diferentes cenários econômicos e climáticos (SSP2-4.5 e SSP5-8.5), afetariam a geração dos sistemas fotovoltaicos no território brasileiro. As projeções climáticas futuras mostraram que P_{PV} terá aumentos leves apenas no norte da região N, sul da região NE, e na região SE, sob todos os cenários e períodos, com valores de crescimento máximos de 2.5 % sob SSP5-8.5 para o futuro imediato (2021 – 2050). Apesar da maior disponibilidade de radiação solar, a sensibilidade da tecnologia dos sistemas P_{PV} atuais ao aumento da temperatura, não permitiria incrementos no rendimento. Pelo contrário, na medida que a temperatura aumenta, a eficiência dos painéis solares diminui, cancelando o efeito positivo do incremento de DSWR.

Palavras-chave: Radiação solar. Brightening. CMIP6. Reanálises. Mudanças climáticas. SSP.

LIST OF FIGURES

CHAPTER 1

Figure 1. Identification of regions, States, altitude and localization of study area.	21
Figure 2. a) Spatial distribution of the mean annual DSWR climatology over Brazil from OBS_BR dataset and, annual bias between other datasets and OBS_BR, during 1980-2016, b) ERA5, c) MERRA2, d) JRA55, e) CFSR, f) GMFD and g) WFDEI. Significant differences at the 95% level of bias are dotted.....	27
Figure 3. a) Spatial distribution of the mean seasonal DSWR climatology over Brazil from OBS_BR dataset and, seasonal bias between other datasets and OBS_BR, during 1980-2016, b) ERA5, c) MERRA2, d) JRA55, e) CFSR, f) GMFD and g) WFDEI. The seasons are summer (DJF), autumn (MAM), winter (JJA) and spring (SON). Significant differences at the 95% level of bias are dotted.	29
Figure 4. Performance evaluation of datasets to estimate DSWR compared to that of the OBS_BR dataset, during 1980-2016. a) Bias, b) RMSE and c) KGE. Upper horizontal axis represents seasonal and annual time scales. The seasons are summer (DJF), autumn (MAM), winter (JJA) and spring (SON). Lower horizontal axis represents the North (N), Northeast (NE), Center-West (CW), Southeast (SE) and South (S) regions. Left vertical axis shows the reanalysis/merged products. Significant differences at the 95% level of bias have crosses.	31
Figure 5. DSWR annual anomaly trends (W/m^2 per decade) during the period 1980–2016 for all datasets, a) OBS_BR, b) ERA5, c) MERRA2, d) JRA55, e) CFSR, f) GMFD and g) WFDEI. Dots indicate where trends are significant at the 95% level. Colors signify dimming (blue) or brightening (red).	34
Figure 6. DSWR seasonal trends (W/m^2 per decade) during the period 1980–2016 for all datasets, a) OBS_BR, b) ERA5, c) MERRA2, d) JRA55, e) CFSR, f) GMFD and g) WFDEI. The seasons are summer (DJF), autumn (MAM), winter (JJA) and spring (SON). Dots indicate where trends are significant at the 95% level. Colors signify dimming (blue) or brightening (red).	36
Figure 7. Time series of the DSWR annual anomalies in the a) N, b) NE, c) CW, d) SE, and e) S regions from observations, reanalyses and merged datasets during the 1980-2016 period.	38
Figure 8. Time series of the DSWR seasonal anomalies in the a) N, b) NE, c) CW, d) SE, and e) S regions from observations, reanalyses and merged datasets, during the 1980-2016 period. The seasons are summer (DJF), autumn (MAM), winter (JJA) and spring (SON).	40
Figure 9. a) Annual mean CC climatology (fraction), b) annual CC trend (fraction per decade), c) seasonal mean CC climatology (fraction), and d) seasonal CC trend (fraction per decade) over Brazil during the 1980–2016 period. In maps (b-d), dots indicate statistical significance at the 95% level. Colors signify negative trends (blue) or positive trends (red). The seasons are summer (DJF), autumn (MAM), winter (JJA) and spring (SON). Dataset: ERA5.	42
Figure 10. Spatial distributions of the correlation coefficient (r) between DSWR and CC, at annual (ANN) and seasonal scales, during the 1980-2016 period. a) Correlation between DSWR from OBS_BR and CC from ERA5. b) Correlation between DSWR and CC, both from ERA5. Statistical significant correlations at the 95% level are dotted. The seasons are summer (DJF), autumn (MAM), winter (JJA) and spring (SON).	44
Figure A.1. KGE components values in the performance evaluation of datasets to estimate DSWR compared to that of the OBS_BR dataset, during 1980-2016. a) Correlation coefficient	

(r), b) bias ratio (β) and c) variability ratio (γ). Upper horizontal axis represents seasonal and annual time scales. The seasons are summer (DJF), autumn (MAM), winter (JJA) and spring (SON). Lower horizontal axis represents the North (N), Northeast (NE), Center-West (CW), Southeast (SE) and South (S) regions. Left vertical axis shows the reanalysis/merged products. Significant differences at the 95% level of r have crosses. 48

CHAPTER 2

Figure 1. Identification of study area. 60

Figure 2. a) Annual mean climatology and b) decadal trends of the RSDS, RSDSCS, CLT and TAS over Brazil during the historical period (1981 – 2010). In trend maps, dots indicate statistical significance at the 95% level. Reference dataset: ERA5. 63

Figure 3. Statistical performance for RSDS, RSDSCS, CLT and TAS for 47 ESMs from CMIP6 and a Multi-model-ensemble (M48), during the historical period (1981 – 2010) over Brazil. a) KGE, b) Correlation coefficient (r), c) Bias ratio (β) and d) Variability ratio (γ). Lower horizontal axis represents the North (1), Northeast (2), Center-West (3), Southeast (4) and South (5) regions. Left vertical axis shows the ESMs. Crosses indicate statistically significant correlations at the 95% level. 66

Figure 4. Comprehensive ranking based on KGE performance of ESMs calculating RSDS, RSDSCS, CLT and TAS. The y-axis represents the accumulation of ESMs ranking for the atmospheric variables. The first four ESMs are inside the red rectangle 68

Figure 5. Climatology of annual potential PV systems (a), and mean annual PV potential generation cycle by month for the b) N, c) NE, d) CW, e) SE and f) S regions, from ERA5 and OME over Brazil during the historical period (1981 – 2010). 70

Figure 6. Projected changes from OME in the annual mean of RSDS, CLT, TAS and RSDSCS for the near-term future (2021 – 2050) relative to the historical period (1981 – 2010), under a) SSP2-4.5 and b) SSP5-8.5 scenarios. Significant differences at the 95% level of changes are dotted. 71

Figure 7. Projected changes to the near-term future (2021-2050 versus 1981-2010) from OME in the annual cycle by month of a) RSDS, b) CLT, c) TAS and d) RSDSCS over five Brazilian regions under SSP2-4.5 (green) and SSP5-8.5 (orange) scenarios 73

Figure 8. Projected changes in annual potential PV systems (a), and in PV potential generation cycle by month for the b) N, c) NE, d) CW, e) SE and f) S regions, to the near-term future (2021-2050 versus 1981-2010) from OME under SSP2-4.5 (green) and SSP5-8.5 (orange) scenarios. In maps (a), significant differences at the 95% level of changes are dotted. 74

Figure 9. Projected changes in potential PV generation by a) isolated variation of RSDS ($P_{pv}(\Delta RSDS)$) and b) Isolated variation of TAS ($P_{pv}(\Delta TAS)$) for the near-term future (2021-2050 versus 1981-2010) from OME under SSP2-4.5 and SSP5-8.5 scenarios. Dots indicate significant differences at the 95% level. 75

Figure S1. Seasonal mean climatologies of the a) RSDS, b) RSDSCS, c) CLT and d) TAS over Brazil during the historical period (1981 – 2010). The seasons are summer (DJF), autumn (MAM), winter (JJA) and spring (SON). Dataset: ERA5. 82

Figure S2. Seasonal trends per decade of the a) RSDS, b) RSDSCS, c) CLT and d) TAS over Brazil during the historical period (1981 – 2010). The seasons are summer (DJF), autumn

(MAM), winter (JJA) and spring (SON). Dots indicate statistical significance at the 95% level Dataset: ERA5.	83
Figure S3. Seasonal KGE values for RSDS, RSDSCS, CLT and TAS for 47 ESMs from CMIP6 and a Multi-model-ensemble (M48), during the historical period (1981 – 2010) over Brazil. Lower horizontal axis represents the North (1), Northeast (2), Center-West (3), Southeast (4) and South (5) regions. Left vertical axis shows the ESMs.	84
Figure S4. Similar to Fig. S3, but for the correlation (r) values. Crosses indicate statistically significant correlations at the 95% level.	85
Figure S5. Similar to Fig. S3, but for the bias ratio (β) values.	86
Figure S6. Similar to Fig. S3, but for the variability ratio (γ) values.	87
Figure S7. Comprehensive ranking based on KGE performance of ESMs calculating RSDS, RSDSCS, CLT and TAS for the a) N, b) NE, c) CW, d) SE and e) S regions. The y-axis represents the accumulation of ESMs ranking for the atmospheric variables.	88
Figure S8. Projected changes from OME in the annual mean of RSDS, CLT, TAS and RSDSCS for the end-century future (2071 – 2100) relative to the historical period (1981 – 2010), under a) SSP2-4.5 and b) SSP5-8.5 scenarios. Significant differences at the 95% level of changes are dotted.	89
Figure S9. Projected changes to the end-century future (2071-2100 versus 1981-2010) from OME in the annual cycle by month of a) RSDS, b) CLT, c) TAS and d) RSDSCS over five Brazilian regions under SSP2-4.5 (green) and SSP5-8.5 (orange) scenarios.	90
Figure S10. Projected changes in annual potential PV generation (a), and in PV potential generation cycle by month for the b) N, c) NE, d) CW, e) SE and f) S regions, to the end-century future (2071-2100 versus 1981-2010) from OME under SSP2-4.5 (green) and SSP5-8.5 (orange) scenarios. In maps (a), significant differences at the 95% level of changes are dotted.	91
Figure S11. Projected changes in potential PV generation by a) isolated variation of RSDS (P_{pv} ($\Delta RSDS$)) and b) Isolated variation of TAS (P_{pv} (ΔTAS)) for the end-century future (2071-2100 versus 1981-2010) from OME under SSP2-4.5 and SSP5-8.5 scenarios. Dots indicate significant differences at the 95% level.	92

LIST OF TABLES

CHAPTER 1

Table 1. Characteristics of gridded datasets.	22
Table 2. Trends in DSWR (W/m^2 per decade) over the period 1980-2016, from various datasets/reanalyses. Values in bold indicate trends to be significant at 95% level. Signs signify dimming (-) or brightening (+).	37
Table 3. Trends in DSWR (W/m^2 per decade) and CC (fraction per decade) over the period 1980-2016, and correlation between DSWR trends and CC trends. Values in bold indicate the trends that significant at 95% level. Signs signify negative trends (-) or positive trends (+)...	45

CHAPTER 2

Table S1. ESMs from CMIP6 used in this study.	79
---	----

LIST OF ACRONYMS AND ABBREVIATIONS

CC	Cloud Cover Fraction
CFSR	Climate Forecast System Reanalysis
CLT	Cloud Cover Percentage
CMIP6	Couple Model Intercomparison Project Phase6
CW	Center-West
DSWR	Solar Downward Shortwave Radiation
ECMWF	European Centre for Medium-Range Weather Forecast
ERA5	Fifth Generation ECMWF atmospheric reanalysis
ESMs	Earth System Models
GMFD	Global Meteorological Forcing Dataset
JRA55	Japanese 55-year Reanalysis
KGE	Klinge-Gupta Efficiency metric
MERRA2	Modern-Era Retrospective Analysis for Research and Applications
N	North
NASA	National Aeronautics and Space Administration
NE	Northeast
OBS_BR	Observational Gridded Dataset for Brazil
OME	Optimal Model Ensemble
PPV	Photovoltaic Power Potential
RSDS	Solar Downward Shortwave Radiation.
RSDSCS	Solar Downward Shortwave Radiation for Clear Sky
S	South
SE	Southeast
SSP	Shared Socioeconomic Pathways
TAS	Air Temperature
WFDEI	WATCH Forcing Data Methodology Applied in ERA-Interim reanalysis

SUMMARY

GENERAL INTRODUCTION	15
CHAPTER 1. CLIMATOLOGY AND TRENDS OF DOWNWARD SHORTWAVE RADIATION OVER BRAZIL.....	17
1.1. Introduction	18
1.2. Materials and methods	21
1.2.1. Study Area.....	21
1.2.2. Datasets	22
1.2.3. Comparison and performance of datasets	25
1.2.4. Anomalies and Trends.....	26
1.3. Results	26
1.3.1. Performance of datasets	26
1.3.2. Temporal evolution of DSWR	33
1.3.3. Effects of cloud cover (CC) on DSWR variability.	41
1.4. Discussion and conclusions	45
1.5. Acknowledgments	47
1.6. Appendix	48
1.7. References	48
CHAPTER 2. THE CLIMATE CHANGE PERSPECTIVE OF ENERGY PHOTOVOLTAIC POTENTIAL IN BRAZIL	55
2.1. Introduction	56
2.2. Data and methodology	58
2.2.1. Reference dataset.....	58
2.2.2. ESMs from CMIP6	59
2.2.3. Ranking of the ESMs performance.	60
2.2.4. Projections of PV power potential	61
2.3. Results	62
2.3.1. Climatology and observed trends of atmospheric variables	62
2.3.2. Performance of CMIP6 models.....	65
2.3.3. Classification of EMSs.....	68
2.3.4. PV power potential (P_{PV}) during historical period.....	69
2.3.5. Projected changes and climate scenarios	71
2.3.5.1. Atmospheric variables	71
2.3.5.2. PV power potential	73
2.3.5.3. Contribution of RSDS and TAS to projected P_{PV} changes.....	74

2.4. Discussion and conclusions	76
2.5. Acknowledgments.....	78
2.6. Supplementary material	79
2.7. References	93
GENERAL CONCLUSIONS	97

GENERAL INTRODUCTION

Climate change - particularly global warming - is one of the greatest modern adaptation challenges facing humanity. Among the strategies to face this challenge, is the use of renewable energies (Kang et al., 2020). Easily available on the surface globally, solar energy is the most promising source of renewable energy. The use of solar downward shortwave radiation (DSWR) through photovoltaic (PV) energy is considered a clean, sustainable and renewable energy conversion technology that can help meet the energy demands of the growing world population while reduces the adverse human impacts of fossil fuel use (Jerez et al., 2015; Sawadogo et al., 2020).

The energy yields of PV systems initially depend on the amount of DSWR available. There is solid evidence that DSWR has undergone important variations in recent decades in various places in the world (Wild, 2016, 2012). However, these variations have not yet been extensively studied in Brazil. In addition to the previous one, there is also evidence that the increase in the ambient temperature - an aspect widely emphasized in climate change scenarios (Herring et al., 2020) - decreases the efficiency of PV systems (Crook et al., 2011; Jerez et al., 2015).

The scarcity of studies on DSWR in Brazil is due to the large amount of missing data and the lack of long-term data (stations in operation for more than 15 years), limiting the ability to clearly demonstrate the variability of the DSWR (Battisti et al., 2018). Among the options for overcoming these limitations are the recent gridded datasets (reanalyses) and the Earth System Models (ESMs), allowing the determination of the long-term variations of DSWR researching historical and future climate changes under different scenarios over the course of the year 21st century.

Objectives

The general objective is evaluate the current and future changes in solar radiation in Brazil, and their consequences for the production of photovoltaic power potential (P_{PV}).

However, this thesis consists of two chapters. Each chapter contains a separate article with its own introduction, objectives, literature review, methodology, results, conclusion and references.

- Chapter 1 aims to determine the spatiotemporal patterns of DSWR variability and trends over Brazil between 1980 and 2016, based on the most recent gridded datasets (observations, reanalysis and merged), and explore the relationships between DSWR variability and decadal changes in cloud cover.
- Chapter 2 aims to evaluate how the ESMs from CMIP6 estimate the DSWR spatiotemporal variability and its causes over Brazil, in the 1981-2010 historical period. Additionally, using the best models, the second objective is to estimate how the future changes (2015-2100) of DSWR, under two different Shared Socioeconomic Pathways (SSP) scenarios (SSP2-4.5 and SSP5-8.5), would affect the future electricity generation of PV systems in the Brazilian territory.

CHAPTER 1. CLIMATOLOGY AND TRENDS OF DOWNWARD SHORTWAVE RADIATION OVER BRAZIL

Published in Atmospheric Research 2021, v. 250; p. 105347, also available at:
[10.1016/j.atmosres.2020.105347](https://doi.org/10.1016/j.atmosres.2020.105347)

ABSTRACT

The solar downward shortwave radiation (DSWR) is the primary source of energy to Earth and a driving forcing for sensible/latent heat and water vapor fluxes over the terrestrial ecosystems and the atmosphere. Evaluation of the DSWR spatiotemporal patterns and trends is crucial to the understanding of weather and climate variability. In this study, DSWR is investigated over Brazil between 1980 and 2016 from contemporary state-of-the-art high-resolution gridded datasets (observations, reanalyses and merged products). The results show an increase in both annual and seasonal DSWR for all regions of Brazil, with large changes over the northern, west central, and southeastern parts of the country. The European Centre for Medium-Range Weather Forecast (ERA5) reanalysis proves to be an excellent option for investigating DSWR across Brazil, matching the observed climatology trends well. The best results are identified for the northeastern and southeastern regions during the months of March-April-May, and the poorest results for the center-west region during September-October-November. Changes in cloud cover (CC) are linked to changes in DSWR. Decadal fluctuations in CC are highly correlated with DSWR trends, with the strongest correlation ($r = -0.89$) in the southeast region, and weakest correlation ($r = -0.37$) in the north. We conclude that CC is a primary modulating factor of brightening across Brazil between 1980 and 2016. In a global context, our results agree with observations from other regions over the globe. Our results may indicate changes in the rainy seasons across Brazil, especially in the northeast. Future studies may use these results to further understand the impacts of brightening over Brazil on solar energy production and agriculture.

Keywords: Brightening; Cloud cover; Trends, Reanalysis; Gridded datasets; Solar radiation.

CLIMATOLOGY AND TRENDS OF DOWNWARD SHORTWAVE RADIATION OVER BRAZIL

Cristian Felipe Zuluaga ^a, Alvaro Avila-Diaz ^a, Flavio B. Justino ^a, Aaron B. Wilson ^{b,c}

^a Department of Agricultural Engineering, Universidade Federal de Viçosa, Viçosa 36570-900, MG, Brazil

^b Byrd Polar and Climate Research Center, The Ohio State University, Columbus 43210, OH, USA

^c OSU Extension – College of Food, Agricultural, and Environmental Sciences, The Ohio State University, Columbus 43210, OH, USA.

1.1.Introduction

The downward shortwave radiation (DSWR) is a main component of the surface radiation balance and a source of energy (or driving force) for the processes of heat (sensitive and latent) and gas (e.g., carbon dioxide, water vapor) exchanges between terrestrial/oceanic ecosystems and the atmosphere (Huang et al., 2019; Zhang et al., 2015). DSWR is not only of particular importance for modeling land surface processes and assessing the Earth's energy budget, but it is also needed for weather and climate predictions, and oceanic and atmospheric circulation studies (Zhang et al., 2016; 2017). In addition, it is also essential to have a complete understanding of the DSWR for use in renewable energy design and operation technologies in the energy sector (Babar et al., 2019; Molina et al., 2017). DSWR is also crucial for agriculture as evapotranspiration and irrigation require accurate estimates of the available surface energy (Stanhill and Cohen, 2001; Y. Yang et al., 2018).

The scientific community has devoted particular attention to DSWR and its global variability, principally since the 1990s (Perdigão et al., 2016; Wild, 2005). Experimental and modeling studies have shown that DSWR fluctuations in decadal time scales (i.e. global dimming and brightening) (Feng and Wang, 2019; Manara et al., 2018; Wild, 2016). Sanchez-Lorenzo et al. (2015) analyzed trends and decadal variations of DSWR over Europe from the Global Energy Balance Archive network for the period 1939–2012. They found that the annual average series showed a negative trend of -0.4 W/m^2 per decade, with a brightening period between 1940 and 1950, followed by solar dimming until the mid-1980s, and accompanied by

a brightening from the mid-1980s to 2012. Additionally, for the first time Sanchez-Lorenzo et al. (2017) calculated the DSWR trends from satellite-derived data in Europe (1983-2010). They showed a general increase across most of Europe of at least 2 W/m^2 per decade, which is in line with previous work. Jahani et al. (2018) investigated the spatiotemporal variations of DSWR between 1998 and 2015 over Iran and found a dimming that varied between 1.7 and 4.3% per decade, starting in the 2000s. In China, Wang et al. (2015), using observed, satellite and reanalysis data, determined that DSWR decreased (global dimming) at approximately 2.9 W/m^2 per decade, between 1961 and 1990, and remained stable thereafter. Soni et al. (2016) showed that DSWR across India declined between the 1970s and the late 1990s, at approximately 0.4 W/m^2 per year. Augustine and Dutton (2013) found a significant upward trend in DSWR (6.6 W/m^2 per decade) across the United States during the period 1996–2011. As mentioned by Wild (2008, 2009, 2016) DSWR at global level, showed a decrease of about $3\text{--}9 \text{ W/m}^2$ (global dimming) between the 1950s and 1980s and an increase of $1\text{--}4 \text{ W/m}^2$ since the 1980s (brightening period). According to some previously mentioned, decadal changes in DSWR are primarily attributed to changes in the transparency of the atmosphere due to variations in cloudiness and/or changes in anthropogenic emissions of aerosols.

Impacts of decadal DSWR changes have also been addressed by Wild et al. (2015), who investigated the influence of DSWR variations on photovoltaic energy in eight regions of the world. Based on climate change projections from 39 climate models from the 5th Intergovernmental Panel on Climate Change, they indicated statistically significant reductions (1% per year) in the production of photovoltaic energy in all regions, except in Germany and Spain, which project greater production due to the brightening caused by decreases in the cloud cover. On the other hand, Wang and Yang (2014) demonstrated that the trends of evaporation (from pan) and DSWR are in line during the same periods, suggesting possible implications of dimming/brightening on the hydrological cycle. These results are consistent with Wang et al. (2010) who demonstrated a high correlation between evapotranspiration and DSWR trends between 1982 and 2002, in particular over non-arid regions. Mercado et al. (2009) argued that changes in the DSWR diffuse fraction – largely associated with the period of dimming – increased the carbon sink by approximately 25% between 1960 and 1999.

Although several studies have examined DSWR trends in Europe, North America and Asia, trends over Brazil have not yet been studied extensively. Silva et al. (2010) determined the DSWR variability over northeastern Brazil from observations and reanalysis data

(NCEP/NCAR) for the 1948-2009 period. They found that DSWR decreased (dimming) by approximately 5.3 W/m^2 per decade. Raichijk (2012) analyzed the temporal series of monthly mean values of sunshine duration in five climatic regions of South America ($2^\circ\text{N} - 40^\circ\text{S}$; $77^\circ\text{W} - 36^\circ\text{W}$) between 1961 and 2004. They discussed a decreasing trend between 1961 and 1990 (average -0.35 hours/year) and an increasing trend from 1990 onwards (average of 0.4 hours/year). The sunshine duration may be associated with dimming/brightening since it varies inversely proportional to cloud cover and proportionally to solar radiation. According to Battisti et al. (2018), the main reasons for the lack of such studies in Brazil are fundamentally related to the low density of weather stations (especially in the center-west and northern regions). The large amount of missing data and lack of long-term data (stations in operation for more than 15 years) have averted the ability to clearly demonstrate the DSWR variability across Brazil. To overcome these problems, several recently composed datasets (global and regional), based on the combination of climate model simulations and interpolations of surface observations, have been generated (Gelaro et al., 2017; Hersbach et al., 2020; Sheffield et al., 2006; Xavier et al., 2016). According to Lilhare et al. (2019) these datasets tend to systematically agree with the temporal trends and spatial distribution of climate variables, but they often show notable differences at finer scales. Thus, inter-comparison and performance evaluation are essential prerequisites to guarantee their reliability, particularly for specific spatial and temporal domains (Troy and Wood, 2009).

Considering that a detailed study on the long-term variability of DSWR on regional and seasonal scales has not yet been carried out across Brazil, our research aims to partially alleviate this gap. The primary goals are to determine the spatiotemporal patterns of DSWR variability and trends over Brazil between 1980 and 2016, based on the most recent gridded datasets (observations, reanalysis and merged), and explore the relationships between DSWR variability and decadal changes in cloud cover. The paper is structured as follows. Section 2 introduces the study area, climate datasets and methods. Section 3 details the performance in estimating the variability and seasonal and annual trends of the DSWR based on different datasets for the northern, northeastern, midwestern, southeastern and southern regions of Brazil. The annual and seasonal cloud cover and their impacts on DSWR variability are also discussed. Finally, a general discussion and conclusions are presented in Section 4.

1.2. Materials and methods

1.2.1. Study Area

The study area extends over all of Brazil, which, due to its large territory (8.5 million km²) and influence of tropical and subtropical atmospheric circulation, has different climatic regimes. To meaningfully analyze the climatic latitudinal variability, the domain was segregated into five macroeconomic regions established by IBGE (Brazilian Institute of Geography and Statistics, 1969): north, northeast, center-west, southeast, and south, which constitute the 26 States and the Federal District (Figure 1).

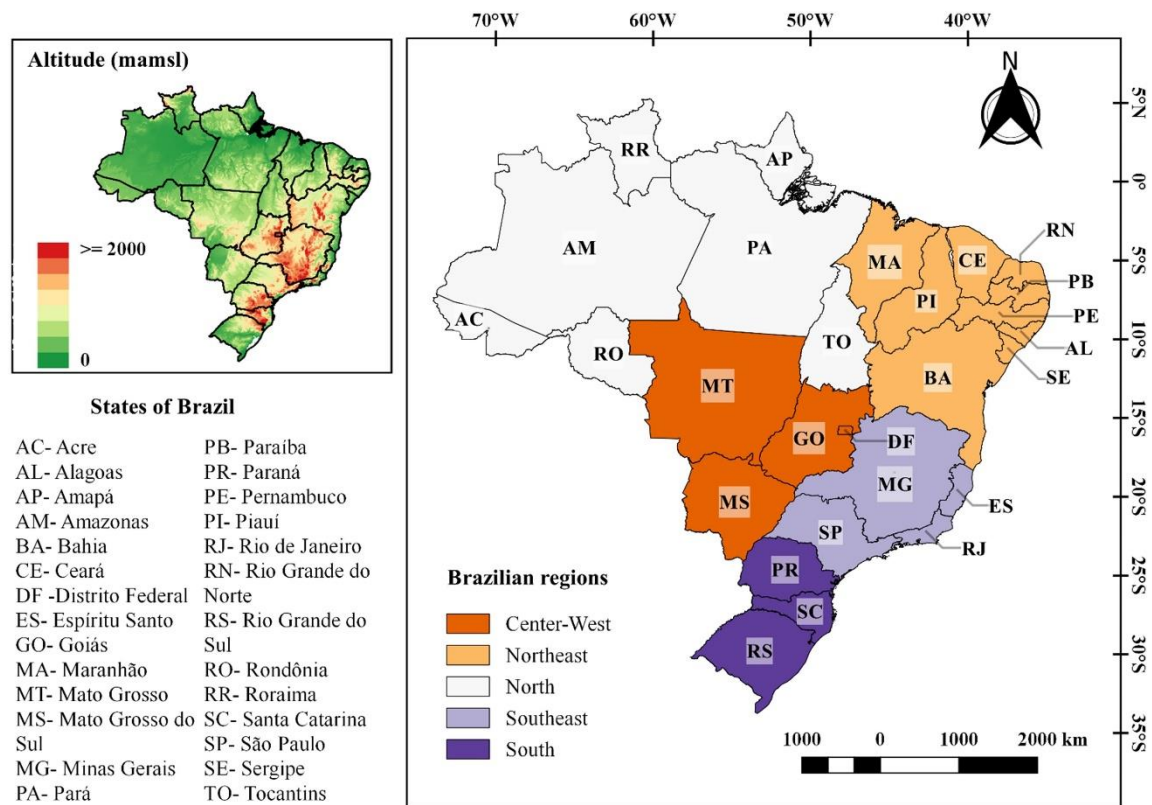


Figure 1. Identification of regions, States, altitude and localization of study area.

The north region (N) comprises seven States. This region has a rainy climate, with cloudiness associated with updrafts, disturbances in the Intertropical Convergence Zone (ITZC), and advection of maritime air from the Atlantic Ocean (Santos et al., 2015). The northeast region (NE) covers nine States, and despite its proximity to the Atlantic Ocean and trade winds blowing towards the continent, the formation of clouds and precipitation are scarce. NE is predominantly dominated by semi-arid climate, which is largely attributed to the

influence of the South Atlantic Tropical Anticyclone (Lima et al., 2016). The center-west (Federal District and three States; CW) and southeast (four States; SE) regions present a spring/summer rainy season dominated by the South Atlantic Convergence Zone (SACZ) and frontal systems and a dry winter season (Alvares et al., 2013; Zandonadi et al., 2015). The south region (S) comprises three States where precipitation and cloud cover are modulated by extratropical cyclones and associated cold fronts throughout the year (Pezzi et al., 2016).

1.2.2. Datasets

Seven different modern gridded datasets were used in this study to determine the spatiotemporal variability and trends of DSWR. Table 1 summarizes the characteristics of each dataset. All grid products provide DSWR in horizontal spatial resolutions ranging between 0.25° and 0.625°.

Table 1. Characteristics of gridded datasets.

Data name	Source	Resolution		Coverage	Period
		Spatial	Temporal		
Observation dataset					
OBS_BR	University of Texas/Universidade Federal de Espiritu Santo	0.25° x 0.25°	Daily	Brazil	1980 - 2016
Reanalysis dataset					
ERA5	ECMWF	0.25° x 0.25°	Hourly	Global	1979 - present
MERRA2	NASA-GMAO	0.5° x 0.625	Hourly		1980 - present
JRA55	JMA	0.5° x 0.5°	3 hourly		1958 - present
CFSR (v1)	NCEP - NOAA	0.312° x 0.312°	6 hourly		1979 - 2010
CFSR (v2)			Hourly		2011 - present
Merged dataset					
GMFD	Princeton University	0.25° x 0.25°	3 hourly	Global	1948 - 2016
WFDEI	WATCH	0.5° x 0.5°	3 hourly		1979 - 2016

The reference dataset (OBS_BR) was created from 735 weather stations (260 conventional and 475 automatic) over Brazil (see Figure 3 in Xavier et al., 2016). For conventional stations, the DSWR was estimated using the Ångström–Prescott equation (Eq. 1) (Paulescu et al., 2016),

$$DSWR = \left(a + b \frac{n}{N} \right) R_o \quad (1)$$

where n is the actual duration of sunshine (hour); N is the maximum possible duration of sunshine (hour); n/N expresses the sunshine percentage; R_o is the extraterrestrial radiation; a is a regression constant expressing the fraction of R_o on cloudy days ($n = 0$); and $a + b$ is the fraction of R_o on clear days ($n = N$) (Xia, et al., 2019). Xavier et al. (2016) assumed $a = 0.25$ and $b = 0.50$; extracted n from Campbell–Stokes heliograph measurements; and obtained N and R_o according to Allen et al. (1998).

In the automatic stations, the DSWR was directly measured using Eppley thermopile pyranometers, which generate a small voltage proportional to the temperature difference between two sensing areas. These instruments cover a spectral range of 300 to 2800 nm, and its measurement errors fluctuate around 5% with annual calibrations (Walter-Shea et al., 2019). DSWR values greater than R_o , or less than 30% of R_o , were excluded. Once DSWR was obtained for all stations, cross-validation was used to compare and validate different interpolation methods. Angular distance weighting (AWD) delivered the best DSWR interpolation at a horizontal resolution of 0.25° latitude/longitude and a daily frequency for the 1980-2016 period. In addition to the high spatial resolution, this dataset is based on data from ground stations located at different altitudes and land use. This allows a reasonable characterization of the effects of topography and land cover on surface climatic variables, difficult to be captured by satellite observations associated with cloud cover (Battisti et al., 2018; Bender and Sentelhas, 2018).

ERA5 is the fifth-generation reanalysis of the European Centre for Medium-Range Weather Forecast (ECMWF). It has a spatial resolution of $0.25^\circ \times 0.25^\circ$, with hourly temporal frequency from 1979 to present. Hersbach et al. (2020) describe two interesting points of the ERA5 radiation scheme. First, ERA5 assimilates several moisture-sensitive satellite channels using the all-sky approach, which provide new information in cloudy and precipitated areas. Second, uses the long-term forcing fields as available from the World Climate Research Programme (WCRP) initiative CMIP5, which include sea surface temperature, greenhouse gases, ozone and aerosols, such as stratospheric sulfates, fundamental to capture volcanic eruptions.

The second version of the Modern-Era Retrospective Analysis for Research and Applications (MERRA2) produced by NASA's GMAO (Global Modeling and Assimilation Office of the National Aeronautics and Space Administration) has a horizontal resolution of $0.5^\circ \times 0.625^\circ$ and hourly temporal resolution over the period 1980-present (Gelaro et al., 2017).

The DSWR parameterization of MERRA2 has a significant improvement over the first iteration of MERRA in the sense that it assimilates aerosol observations. This implies that the DSWR estimates have been improved with additional information such as aerosol optical depth (AOD) and volcanic aerosols data from platforms such as the Moderate Resolution Image Spectroradiometer (MODIS) and Advanced Very High Resolution Radiometer (AVHRR) (Feng and Wang, 2018; Gelaro et al., 2017).

The Japanese 55-year Reanalysis (JRA55) is the second Japanese global atmospheric reanalysis project, produced by the Japan Meteorological Agency (JMA). It is available from 1958 to present, with a spatial resolution of $0.5^\circ \times 0.5^\circ$, and 3-hour frequency (Kobayashi et al., 2015). This version includes a new radiation scheme, which calculates DSWR by a two-stream method with the delta-Eddington approximation and assumes a random cloud overlap within the cloudy fraction of a model grid (Zhang et al., 2016). Aerosol direct effects on DSWR are calculated using two atmospheric aerosol profiles from the World Meteorological Organization and AOD adjusted data from MODIS, not including volcanic aerosols (Kobayashi et al., 2015).

The Climate Forecast System Reanalysis (CFSR) is produced by the National Centers for Environmental Prediction (NCEP). Version 1 (Saha et al., 2010) provides information between 1979 and 2010, and version 2 (Saha et al., 2014) between 2011 to the present. Both versions are available in a horizontal spatial resolution of $0.312^\circ \times 0.312^\circ$. Differences between versions include an increase in temporal resolution (from 6 hours in version 1 to 1 hour in version 2), as well as an improvement in the cloud-radiation interaction scheme. DSWR parameterizations use random cloud overlap for cloudy sky radiative transfer, and a climatological aerosol scheme provides a global distribution of AOD and stratospheric volcanic aerosols (Saha et al., 2010, 2014; Zhang et al., 2016). We used both versions to span the period of our work (1980-2016).

The Global Meteorological Forcing Dataset (GMFD) of the Princeton University is a merging of the NCEP reanalysis and satellite observational datasets, available in spatial resolution of $0.25^\circ \times 0.25^\circ$, and frequency of 3 hours, for the 1948-2016 period (Sheffield et al., 2006). The WATCH Forcing Data Methodology Applied to ERA-Interim Reanalysis (WFDEI) is a dataset that incorporates in-situ observations in the ERA-Interim reanalysis, enhanced by an elevation correction for numerous variables. It is available from 1979 to 2016, with a spatial resolution of ~ 56 km ($0.5^\circ \times 0.5^\circ$) and 3-hour frequency (Weedon et al., 2014).

In both datasets, the monthly bias correction to DSWR is made using the Climatic Research Unit (CRU) average cloud cover and the effects of interannual changes in atmospheric aerosol loading (Schmied et al., 2016; Weedon et al., 2014).

This large variation in the temporal ranges and horizontal spatial resolutions among the datasets necessitated a regridding procedure. All datasets were horizontally regridded using bilinear interpolation to a $0.25^\circ \times 0.25^\circ$ (latitude x longitude) grid on a monthly timescale. It should be noted that we selected the 1980-2016 period (37 years) due to the availability of observations in the reference dataset (OBS_BR).

1.2.3. Comparison and performance of datasets

Reanalyses and merged products were compared to OBS_BR at annual (ANN) and seasonal scales over the five regions of Brazil (Figure 1). Metrics used include the bias, the root-mean-square error (RMSE), and the Kling-Gupta Efficiency (KGE). For seasonal analysis, seasons were delineated as summer (December, January and February - DJF), autumn (March, April and May - MAM), winter (June, July and August - JJA) and spring (September, October and November - SON).

The bias (Eq. 2) indicates the tendency of error. The RMSE (Eq. 3) provides information about the overall forecast errors in relation to the actual measured values. Biases and RMSEs closer to zero indicate better performance of the model. Many published studies on the inter-comparison of datasets use bias and RMSE (Babar et al., 2019; Porfirio et al., 2020; Salazar et al., 2020; Zhang et al., 2016). The KGE metric (Eq. 4), that was proposed by Gupta et al. (2009) and modified by Kling et al. (2012), provides interesting diagnostic information about the performance of the models due to the combination of three components: the correlation coefficient (r ; Eq. 5), the bias ratio (β ; Eq. 6) and the variability ratio (γ ; Eq. 7).

$$\text{Bias} = \bar{P} - \bar{O} \quad (2)$$

$$\text{RMSE} = \sqrt{\frac{1}{N} \sum_{i=1}^N (P_i - O_i)^2} \quad (3)$$

$$\text{KGE} = 1 - \sqrt{(r - 1)^2 + (\beta - 1)^2 + (\gamma - 1)^2} \quad (4)$$

$$r = \frac{\sum_{i=1}^N (O_i - \bar{O})(P_i - \bar{P})}{\sqrt{\sum_{i=1}^N (O_i - \bar{O})^2} \sqrt{\sum_{i=1}^N (P_i - \bar{P})^2}} \quad (5)$$

$$\beta = \frac{\mu_P}{\mu_O} \quad (6)$$

$$\gamma = \frac{CV_P}{CV_O} \quad (7)$$

where N is the number of observations, μ is the mean value, CV is the coefficient of variation, P is the predicted value and O is the observed reference value. The optimal value of KGE and its components is one (+1.0) (Kling et al., 2012; Schmied et al., 2016).

1.2.4. Anomalies and Trends

In order to remove the seasonal cycle, annual and seasonal anomalies were calculated as the difference between the corresponding actual annual (or seasonal) value and the climatic average annual (or seasonal) value (Mateos et al., 2014). Trend magnitude was calculated by applying the Sen's slope method (Sen, 1968) and its statistical significance estimated by the Mann-Kendall (MK) non-parametric test at the 95% significance level ($p\text{-value} \leq 0.05$) (Kendall, 1975; Mann 1945). According to Jahani et al. (2018), the MK does not require data to be normally distributed, has low sensitivity to sudden interruptions caused by the lack of data in the series, and is not sensitive to outliers. The MK is a method widely used to identify trends in climate variables such as DSWR (Jahani et al., 2018; Long et al., 2009; Manara et al., 2017; Sanchez-Lorenzo et al., 2015). For each region of Brazil, zones of brightening or dimming during the period from 1980 to 2016 were identified.

1.3. Results

1.3.1. Performance of datasets

Figure 2a shows the annual mean values of DSWR delivered by OBS_BR during the 1980-2016 period. Of great global importance due to the Amazon rainforest, the N region

experiences a heterogeneous distribution of DSWR, with minimum values ($<180 \text{ W/m}^2$) west of the Amazon basin (States of AC and AM), and maximum values ($>220 \text{ W/m}^2$) over the southeastern corner of the State of TO. The NE region presents the highest annual DSWR value (243 W/m^2). The CW region has the second highest annual value of DSWR, with an average annual value of 206 W/m^2 . In the SE region, the distribution of DSWR fits the altitude (topography) profile as illustrated by Figure 1. The lowest values ($<180 \text{ W/m}^2$) are found on the east (windward) side of the mountainous region (RJ, ES and east of MG and SP) and the highest values ($>230 \text{ W/m}^2$) are observed on the leeward (northern extent of MG). As expected, the southernmost part of Brazil, the S region exhibits the lowest DSWR values ($<170 \text{ W/m}^2$ over the State of SC and east of PR).

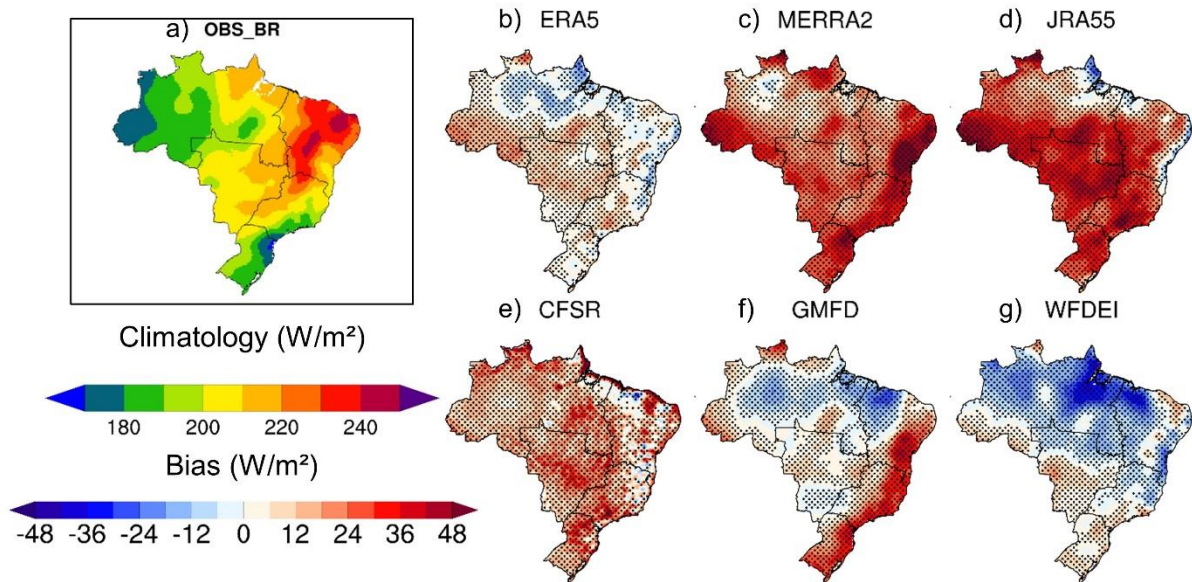


Figure 2. a) Spatial distribution of the mean annual DSWR climatology over Brazil from OBS_BR dataset and, annual bias between other datasets and OBS_BR, during 1980-2016, b) ERA5, c) MERRA2, d) JRA55, e) CFSR, f) GMFD and g) WFDEI. Significant differences at the 95% level of bias are dotted.

Figure 2b-g shows the differences (bias) between the mean DSWR values from other datasets (reanalyses and merged) and OBS_BR during the 1980-2016 period. The dots show the locations where, using the t-test, the differences between the dataset's means are significantly different from zero at the 95% confidence level. ERA5 (Figure 2b) presents DSWR closest to OBS_BR (bias close to zero and without statistical significance). Biases range between $\pm 20 \text{ W/m}^2$ with lower values over the NE region and higher values for the CW region. MERRA2 (Figure 2c), JRA55 (Figure 2d) and CFSR (Figure 2e) overestimate DSWR (bias $>$

15 W/m² and statistical significance) over most of the country. However, they differ regionally; for instance, MERRA2 shows larger values along the NE coast, whereas JRA55 exceeds observations in the CW, SE, and S regions. Differences between OBS_BR and CFSR are very small indicating a good performance by the reanalysis. GMFD (Figure 2f) displays differences in line with the pattern shown by the MERRA2 and JRA55 along the Brazilian coast. However, differences between the GMFD and OBS_BR are much smaller elsewhere (without statistical significance). The WFDEI (Figure 2g) slightly underestimates DSWR over the northern part of the Brazilian Amazon but shows very good correspondence with observations in general.

Figure 3a shows seasonal mean values of the OBS_BR dataset and Figure 3b-g shows the differences between this dataset and the reanalyses/merged data. The dots show where the seasonal means are significantly different among the products. According to Da Rocha et al. (2004), the N region has two well-defined seasons, wet (January-June) and dry (July-December) due to the dominance of the annual cycle of ITCZ and SACZ (Santos et al., 2017). This affects the DSWR seasonality as well, which presents values greater than 205 W/m² for JJA and SON and less than 182 W/m² for DJF and MAM (Figure 3a). The NE region presents the maximum value (275 W/m²) during spring, in the States of CE and RN (Figure 3a). The minimum value of this region is in southern BA during JJA (160 W/m²). In the CW region, the greatest DSWR values occur during SON and DJF (≈ 295 W/m²) and the weakest during MAM and JJA (≈ 195 W/m²). The SE region displays a seasonality of DSWR values, where the strongest value (230.41 W/m²) occurs during DJF and the weakest (174.83 W/m²) during JJA. The S region shows values greater than those in the SE (242.73 W/m²) during the summer and the lowest value (128.38 W/m²) in the winter (Figure 3a). The S region experiences the largest amplitude of the seasonal cycle.

It must be mentioned that MERRA2 (Figure 3c), JRA55 (Figure 3d) and CFSR (Figure 3e) overestimate DSWR in all seasons, with bias values between 6 and 44 W/m². ERA5 exhibits very small differences (in most cases differences without statistical significance) with values of about ± 20 W/m² in all seasons, except during SON, where it delivers an overestimation in N and CW (Figure 3b). Biases between merged datasets and OBS_BR show disagreement between these products as well. The WFDEI opposes the main pattern of reanalyses, i.e. underestimates DSWR for all seasons except SON over the CW, SE, and S regions (Figure 3g).

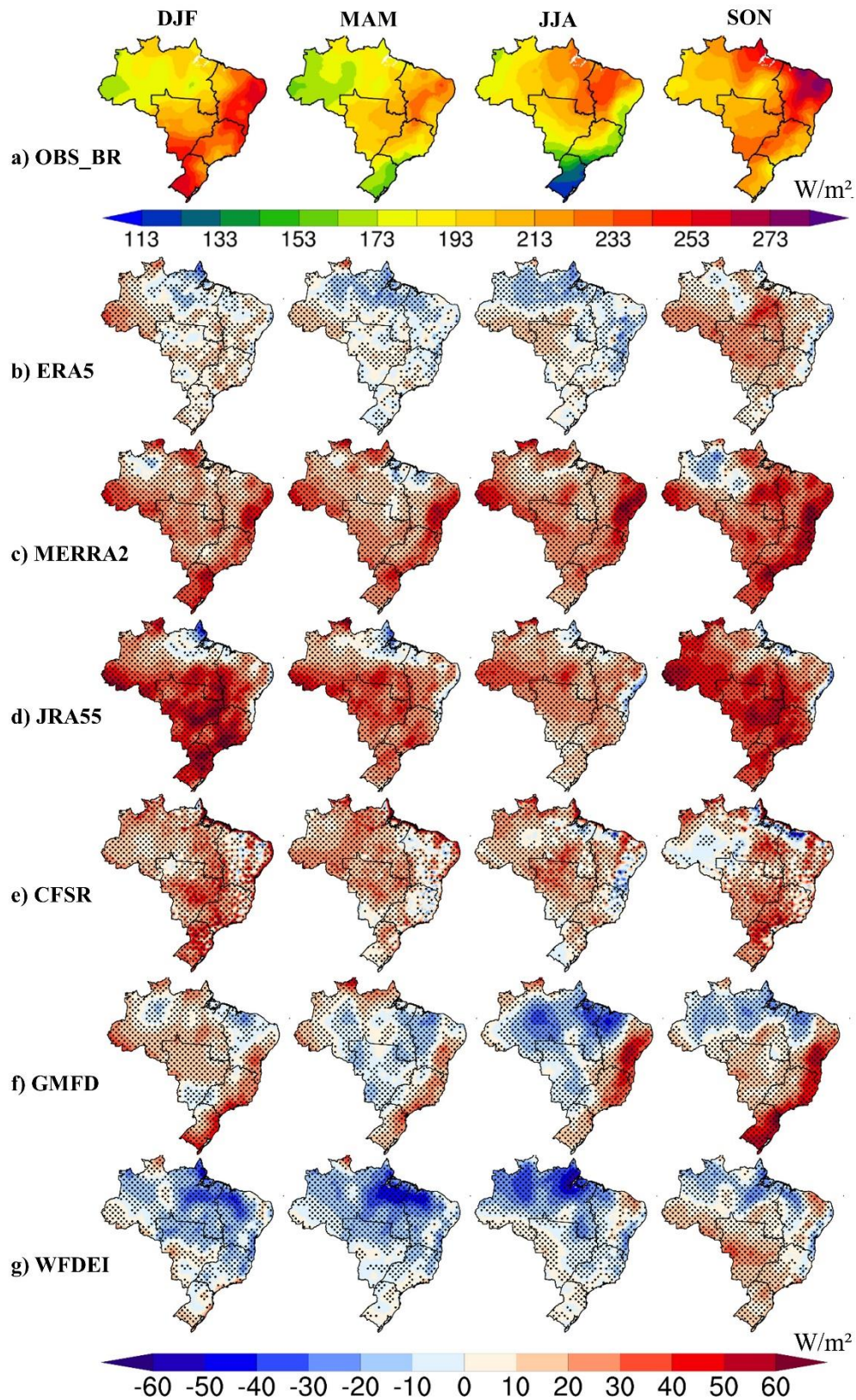


Figure 3. a) Spatial distribution of the mean seasonal DSWR climatology over Brazil from OBS_BR dataset and, seasonal bias between other datasets and OBS_BR, during 1980-2016, b) ERA5, c) MERRA2, d) JRA55, e) CFSR, f) GMFD and g) WFDEI. The seasons are summer (DJF), autumn (MAM), winter (JJA) and spring (SON). Significant differences at the 95% level of bias are dotted.

Larger differences of DSWR from GMFD are found in JJA and SON seasons (Figure 3f). One highlighted feature that emerges by comparing the OBS_BR to the other datasets are differences over the Brazilian coastline. This region experiences greater variability throughout the year related to the advection of maritime warm and humid air, which can induce different cloud types. Moreover, it has steep orographic terrain that rises from sea level to 2000 m at 300 km of the coast (Figure 1). These factors affect the accuracy of datasets interpolations (Borges et al., 2016). However, the high density of stations over this part of Brazil, used in OBS_BR, allowed reducing errors and finding the best interpolation performances (Xavier et al., 2016). On the other hand, the coarse horizontal resolutions from the reanalyses and merged products constrain their abilities to adequately represent land characteristics and meso-scale processes over this complex topography, showing the need to incorporate more observations to overcome these limitations.

Figure 4 shows the performance in statistical metrics for all datasets over each region. The crosses in Figure 4a show where biases between the datasets means are significant. In the N, the best annual values of RMSE and KGE are presented by ERA5 (6.4 W/m² and 0.36) and GMFD (5.4 W/m² and 0.19), respectively (Figures 4b-c). Seasonally, ERA5 and GMFD exhibit similar values, except in the SON, where the error of ERA5 is twice that of GMFD. The largest disagreements are noted in MERRA2, JRA55, and CFSR. WFDEI shows lower RMSE and KGE (Figure 4b-c), but still far from ERA5 and GMFD.

The best performing dataset for the NE region is ERA5, with annual values of bias = 0.6 W/m², RMSE = 3.2 W/m² and KGE = 0.83 (Figure 4a-c). Best results are shown during MAM (bias = 4 W/m², RMSE = 6 W/m² and KGE = 0.85), but larger differences occur during SON (bias = 8 W/m², RMSE = 9 W/m² and KGE = 0.81). Except for WFDEI (bias = -9 W/m²), all datasets overestimate DSWR values, with biases ranging between 6.4 and 30 W/m² (Figure 4a). CFSR and WFDEI also perform well in this region, with values of RMSE < 20 W/m² and KGE > 0.4 (Figure 4b-c). The worst performing datasets (annual and seasonal) are MERRA2 and JRA55.

Over CW, all datasets overestimate DSWR, except WFDEI and GMFD during MAM and JJA (Figure 4a). As shown for the N region, SON is the season with the worst performance of all reanalyses/merged data, with biases between 12 and 44 W/m² (statistically significant), RMSEs between 17 and 46 W/m², and maximum KGE of 0.4 (Figure 4a-c). The best

performances are delivered by ERA5, GMFD and WFDEI, and weaker ones are noted for JRA55, MERRA2 and CFSR.

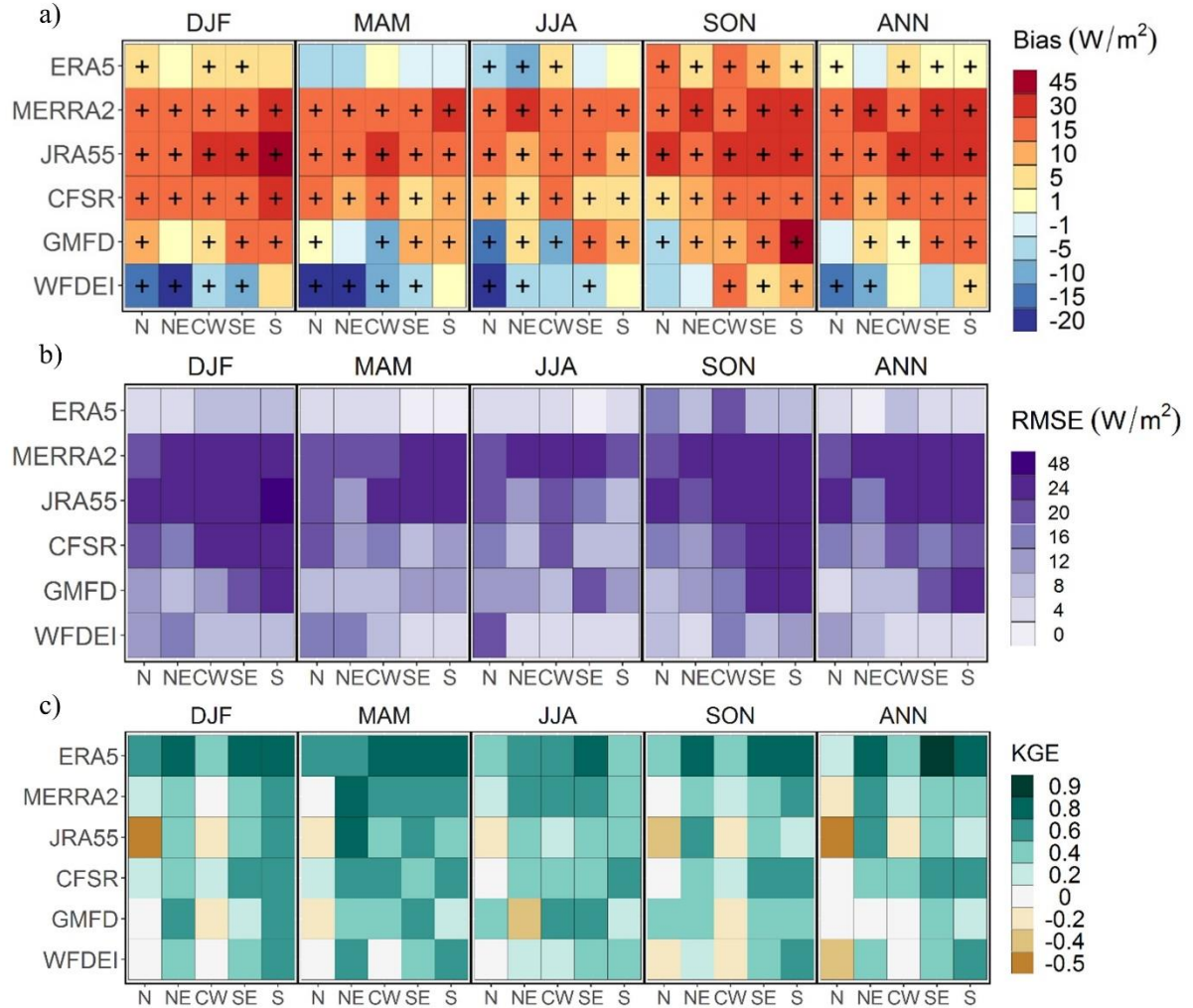


Figure 4. Performance evaluation of datasets to estimate DSWR compared to that of the OBS_BR dataset, during 1980-2016. a) Bias, b) RMSE and c) KGE. Upper horizontal axis represents seasonal and annual time scales. The seasons are summer (DJF), autumn (MAM), winter (JJA) and spring (SON). Lower horizontal axis represents the North (N), Northeast (NE), Center-West (CW), Southeast (SE) and South (S) regions. Left vertical axis shows the reanalysis/merged products. Significant differences at the 95% level of bias have crosses.

In SE, apart from WFDEI, all datasets overestimate the DSWR values (Figure 4a). WFDEI, along with ERA5, has similar performance insofar with respect to the RMSEs and biases (absolute value). However, the KGE value of ERA5 is twice larger than that of WFDEI, turning the ERA5 most suitable dataset for this region (Figure 4a-c). Like CW, the worst

performances of the datasets are during SON, followed by DJF. The other four datasets (MERRA2, JRA55, CFSR, and GMFD) performed well below the best values.

For the S, although all datasets overestimate the DSWR values (Figure 4a), ERA5 and WFDEI have very low annual and seasonal biases (and without statistical significance during DJF, MAM and JJA). For other metrics, ERA5 and WFDEI show good performance, with values of $RMSE < 15 \text{ W/m}^2$ and $KGE > 0.4$ (Figure 4b-c). MERRA2 and JRA55 should be used with care due to large values of RMSE and low KGE (Figure 4b-c).

In general, all datasets show a large limitation during SON but the best performance in MAM. These results are likely related to changes in cloudiness and atmospheric transmissivity due to seasonal variability of precipitation, driven by the South American Monsoon (SAMS). According to Garcia and Kayano (2015), the wet stage of this atmospheric system initiates in the equatorial Amazon during austral spring (SON) and propagates rapidly eastward and southeastward, reaching central Brazil during DJF, when it becomes fully developed, with the main convective activity associated with the SACZ. Precipitation is very regular during spring and so too are the cloud conditions associated with large systems. During MAM, however, intense rainfall reduces over the Amazon and gradually migrates northwestward, marking the SAMS demise. Precipitation in MAM is more related to the thunderstorms and mesoscale system with erratic distribution of clouds across Brazil. The coarse resolution of reanalyses limits their ability to reproduce these atmospheric features. In Figure A.1c, $\gamma \neq 1$ reveals differences between the variability of OBS_BR and the reanalyses/merged datasets. During SON, except for ERA5 and CFSR, all datasets present $\gamma < 0.8$, showing the inability to capture the DSWR variability in relation to observations. On the other hand, in MAM, γ varies between 0.8 and 1.2 in all datasets (except WFDEI), probably due to decreased variability in CC and lower DSWR magnitudes.

Strictly speaking, ERA5 delivers the best performance for all regions. It has shown the highest accuracy (RMSE, bias and KGE) in estimating the spatial values of DSWR with respect to OBS_BR. As a recently released dataset, ERA5 has not been evaluated in detail at a regional basis. Urraca et al. (2018) evaluated DSWR estimates of ERA5 using some surface stations across the world. They pointed out that the most relevant improvement in the ERA5 is the reduction in the positive bias compared to that for ERA-Interim (EI). This improvement is directly related to a better estimate of the mean sea level pressure (MSLP) and the surface

pressure (SP) by ERA5, with respect to EI and other reanalyses (Dullaart et al., 2020; Malakar et al., 2020). Thus, proper MSLP and SP estimates lead to an adequate identification of low (high) pressure systems associated with clouds and precipitation (clear skies) areas.

Similar to previous studies that evaluated the performance for MERRA2 and JRA55 attributed the overestimation of DSWR to an underestimation of CC. This has been a common feature in both reanalyses (Feng and Wang, 2018; Zhang et al., 2016) and is primarily linked to higher values of MSLP and SP. This induces an increase in anticyclonic circulation that produces a negative bias of CC over South America (Gelaro et al., 2017; Kobayashi et al., 2015; Malakar et al., 2020). CFSR shows limitations in reproducing DSWR in the N and CW (Saha et al., 2010). All reanalyses use surface observations in their assimilation schemes (for instance, temperature, MSLP and SP), and regions with sparse coverage of data may experience more significant biases in simulating derived variables like DSWR.

Merged products show an underestimation of DSWR, except for mountainous areas in GMFD, but prove to be an adequate representation over N, NW, and CW. The WFDEI dataset is also suitable for all regions, except for N. It must be considered that this dataset is forced by EI, and ECMWF is updating it with ERA5 data to launch a new version (WFDE5, see: <https://cds.climate.copernicus.eu/cdsapp#!/dataset/derived-near-surface-meteorological-variables?tab=overview>). Improving the representation of CC and MSLP should produce a more accurate radiation balance.

1.3.2. Temporal evolution of DSWR

The last three decades have been punctuated by increases in global temperatures and higher frequency of climate/weather extremes worldwide (Herring et al., 2020) and in Brazil (Avila-Diaz et al., 2020a). Since DSWR is the main source of energy to the climate system, it is important to evaluate any changes that may contribute to a better understanding of climate change and its extremes. Based on our investigation, the OBS_BR DSWR trend is characterized by a generalized increase (brightening) throughout the period across most of Brazil. However, other datasets present distinct regional patterns (Figure 5).

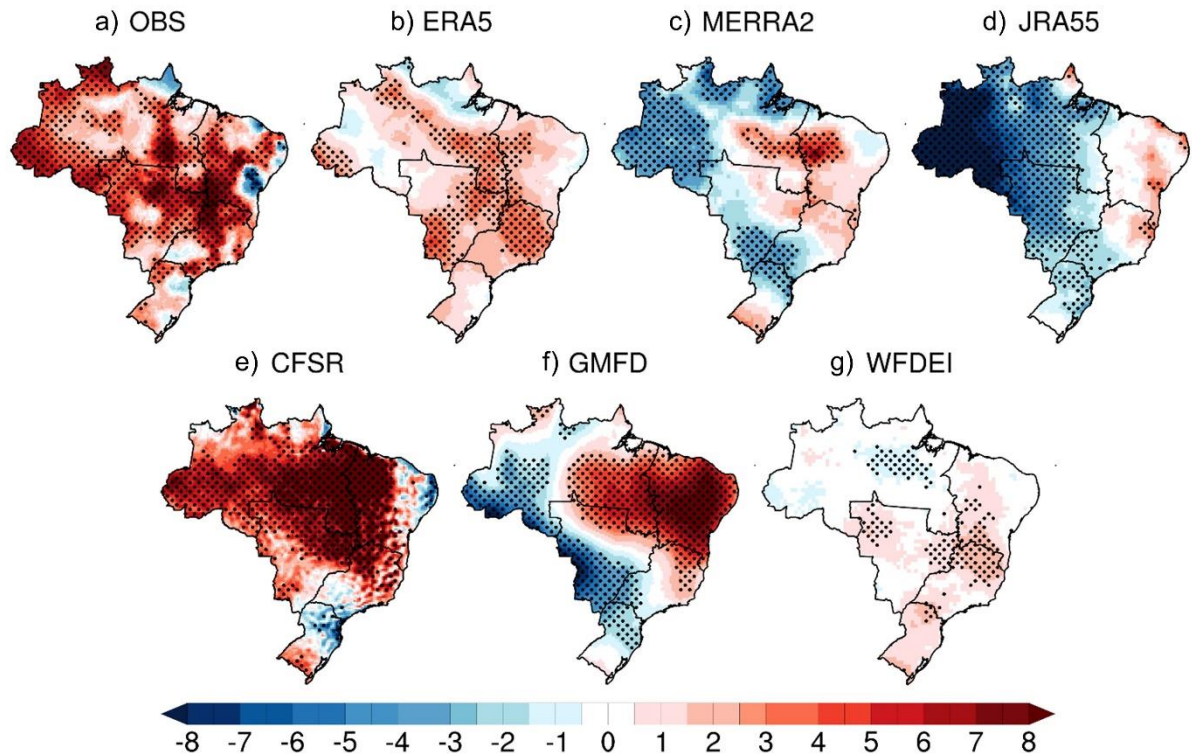


Figure 5. DSWR annual anomaly trends (W/m^2 per decade) during the period 1980–2016 for all datasets, a) OBS_BR, b) ERA5, c) MERRA2, d) JRA55, e) CFSR, f) GMFD and g) WFDEI. Dots indicate where trends are significant at the 95% level. Colors signify dimming (blue) or brightening (red).

In the N, which includes the Amazon basin, areas with large increases include parts of the PA State, west of AM, and the States of RO, AC and the RR (i.e. the Brazilian frontier limits). Central Amazon and the western part of PA show small trends, while AP depicts negative trends (Figure 5a). ERA5 (Figure 5b) and CFSR (Figure 5e) show similarities with OBS_BR in the trend values, but CFSR represents higher values across the central portions of AM and PA. The NE region shows that positive trends are concentrated in the countryside, whereas in most cases along the coast, negative trends are dominant. The CW region in OBS_BR, ERA5, and CFSR is characterized by atmospheric brightening. This feature is completely different in JRA55 (Figure 5d), MERRA2 (Figure 5c), and GMFD (Figure 5f) where negative trends are dominant. It should be stressed that these three datasets show very similar spatial distributions insofar as trends are concerned. For WFDEI, trends are much weaker, and most part of Brazil does not show statistically significant values (Figure 5g).

In the SE region, the greatest brightening values are in the north of the MG State and the coastal extent SP, regions with distinctly different climates. This usefully serves to highlight

the complexity of analyzing DSWR (Figure 5a). The former area is characterized as semi-arid, whereas the latter has a subtropical climate with a well-defined rainy season. ERA5 (Figure 5b), CFSR (Figure 5e), and WFDEI (Figure 5g) trends are similar. MERRA2, GMFD, and JRA55 differ greatly from OBS_BR, especially over the western part of the country (Figure 5c, d, f). The S region exhibits the weakest brightening and fewest statistically significant values of the DSWR trends for OBS_BR (Figure 5a). The highest values are located across the western part of RS and northern sections of PR. WFDEI and ERA5 deliver similar patterns of trends to those depicted by OBS_BR.

Figure 6 shows that seasonal trends in OBS_BR are mostly positive (brightening) for all seasons and regions, in agreement with Figure 5a. CFSR (Figure 6e) and ERA5 (Figure 6b) have similar patterns to OBS_BR (Figure 6a) in the N region, with the exception of MAM where ERA5 delivers a negative trend throughout the region. The other datasets do not show a regionally-dominant pattern. In DJF, merged data/reanalyses show similar negative trends over most of western Brazil, but this is not reproduced by OBS_BR.

Based on two surface stations and NCEP/NCAR reanalysis, Silva et al. (2010) found a negative trend (dimming) in the NE region between 1948 and 2009. OBS_BR shows a small area of negative trend values in all seasons, located across northern BA and western PE (Figure 6a). Nevertheless, Silva et al. (2010) only used two stations. Therefore, it is doubtful this dataset can reproduce the overall characteristics in the NE State as depicted in our study. This reinforces the need for utilizing robust grid data (spatially distributed) that can adequately represent the spatial variability of DSWR. Except for ERA5 (Figure 6b) in JJA, and JRA55 (Figure 6d) and WFDEI (Figure 6g) in DJF, all datasets reproduce the same brightening trends across the NE region.

In CW, MERRA2, JRA55, and GMFD exhibit opposite trends to that of OBS_BR (Figure 6a, c, d and f), except for JJA. ERA5 (Figure 6b) and GMFD (Figure 6f) present trends very close to that of OBS_BR, but statistical significance only covers small areas. In the SE region, ERA5 and WFDEI (Figure 6g) show trends like those of OBS_BR for all seasons. It is worth noting that all datasets reproduce the negative trend over the southern portion of the SE region during DJF season. In the S region, except for ERA5 and WFDEI, all datasets show opposite patterns of trends in relation to OBS_BR.

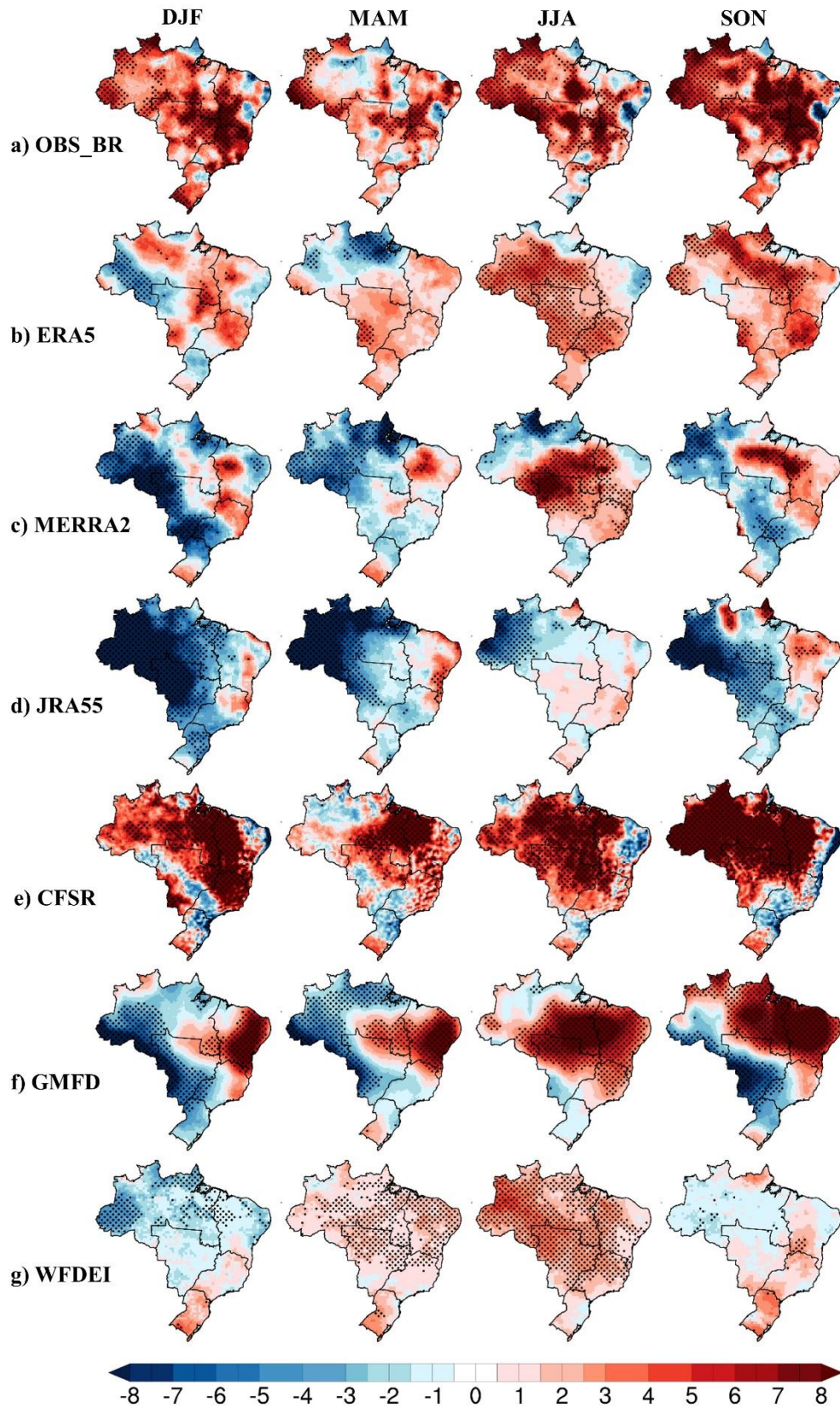


Figure 6. DSWR seasonal trends (W/m² per decade) during the period 1980–2016 for all datasets, a) OBS_BR, b) ERA5, c) MERRA2, d) JRA55, e) CFSR, f) GMFD and g) WFDEI. The seasons are summer (DJF), autumn (MAM), winter (JJA) and spring (SON). Dots indicate where trends are significant at the 95% level. Colors signify dimming (blue) or brightening (red).

Table 2. Trends in DSWR (W/m^2 per decade) over the period 1980-2016, from various datasets/reanalyses. Values in bold indicate trends to be significant at 95% level. Signs signify dimming (-) or brightening (+).

Region	Season	OBS_BR	ERA5	MERRA2	JRA55	CFSR	GMFD	WFDEI
N	DJF	+3.2	+0.2	-3.6	-10.3	+4.9	-2.5	-2.0
	MAM	+1.8	-1.2	-4.3	-8.0	+2.5	-2.0	+0.6
	JJA	+3.7	+2.3	+0.7	-2.3	+5.4	+2.7	+2.4
	SON	+5.1	+2.7	-1.1	-3.4	+8.7	+3.6	-0.2
	ANN	+3.2	+1.1	-2.1	-5.6	+4.3	+0.4	-0.2
NE	DJF	+2.6	+0.4	+0.1	-0.7	+6.7	+5.2	-1.3
	MAM	+2.8	+1.7	+1.6	+1.8	+5.3	+6.0	+1.8
	JJA	+1.0	-0.2	+1.5	+0.1	+2.2	+6.1	+1.5
	SON	+3.8	+2.3	+2.3	+1.7	+6.0	+8.9	+0.7
	ANN	+2.5	+1.3	+1.4	+0.9	+5.2	+6.4	+0.5
CW	DJF	+4.5	+1.5	-4.7	-8.4	+3.9	-3.7	-1.1
	MAM	+2.5	+2.0	-1.6	-2.2	+1.8	-1.4	+0.8
	JJA	+4.8	+2.7	+3.8	+0.4	+5.5	+3.9	+2.7
	SON	+3.9	+1.6	-2.1	-3.9	+5.5	-3.6	0.0
	ANN	+3.9	+2.0	-1.0	-3.3	+4.3	-1.3	+0.5
SE	DJF	+5.3	+2.4	-1.3	-0.9	+6.4	0.0	+0.6
	MAM	+1.8	+1.4	-1.0	-1.0	+1.2	+0.1	+0.7
	JJA	+3.3	+3.2	+1.6	+0.9	+3.2	+2.1	+1.6
	SON	+3.7	+3.4	-0.5	-1.3	-0.2	-1.0	+1.1
	ANN	+3.6	+2.5	-0.5	-0.6	+2.8	+0.8	+0.9
S	DJF	+2.7	-1.1	-1.5	-2.8	-0.4	-2.1	+2.1
	MAM	+0.8	+1.2	+0.1	-0.8	-0.9	+0.1	+1.6
	JJA	+0.3	+1.6	-0.9	+0.2	0.0	-0.4	+0.5
	SON	+3.5	+2.0	-0.7	-0.8	+0.5	-1.7	+2.3
	ANN	+1.7	+0.9	-0.5	-1.4	-0.5	-1.3	+1.3

Table 2 summarizes the average values of annual and seasonal trends from all datasets in each region of Brazil. OBS_BR shows positive trends (brightening) across the N region, varying between 1.8 and 3.7 W/m^2 per decade in all seasons. CFSR follows the same positive trends (and statistical significance) as OBS_BR but with a slight overestimation. ERA5 shows the same pattern as OBS_BR (with slight underestimations), except in MAM (-1.2 W/m^2 per decade). MERRA2, WFDEI, and GMFD reflect the same direction of the OBS_BR trends in some regions but with larger differences. Over the NE region, OBS_BR has a positive annual trend (statistically significant brightening) of 2.5 W/m^2 per decade, varying between 3.8 W/m^2 per decade (SON) and 1 W/m^2 per decade (JJA). Except for ERA5 in JJA (-0.2 W/m^2 per decade), JRA55 DJF (-0.7 W/m^2 per decade), and WFDEI DJF (-1.3 W/m^2 per decade), all other products have the same trends (brightening) as OBS_BR. Although CFSR and GMFD

show statistical significance in all their trends, they overestimate all values. In this sense, ERA5 and MERRA2 show values closest to observations.

The CW region presents the strongest annual brightening value (3.9 W/m^2 per decade) across the country. The seasonal trends show statistical significance, with the lowest values in MAM (2.5 W/m^2 per decade) and the greatest during JJA (4.8 W/m^2 per decade). In JJA, all datasets present the same trend with statistical significance (except JRA55). ERA5 and CFSR show trends closest to those observed (Table 2). The SE region has the second strongest annual DSWR trend from OBS_BR (3.6 W/m^2 per decade). In this region, the greatest brightening value in the whole country (5.3 W/m^2 per decade) is found during DJF. ERA5 trends in JJA, SON, and ANN are almost equal to those observed. The trends in the S region vary between 2.7 W/m^2 per decade in DJF and 0.3 W/m^2 per decade in JJA. WFDEI shows the best performance, followed by ERA5 that only showed an opposite trend in DJF (-1.1 W/m^2 per decade).

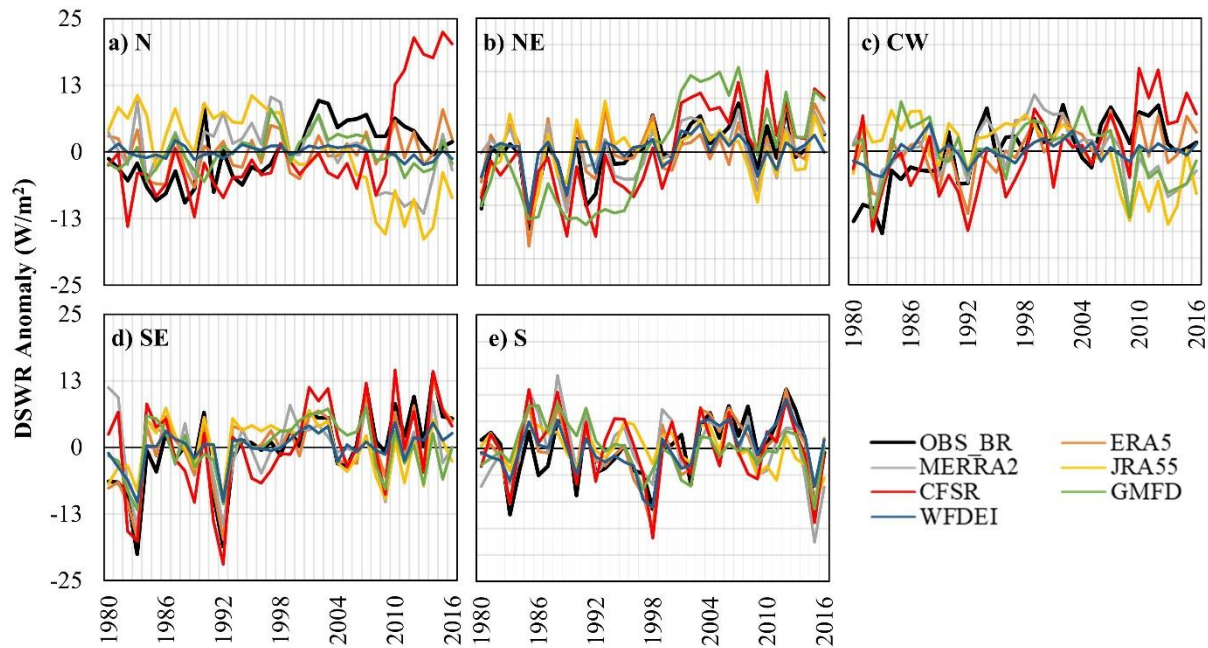


Figure 7. Time series of the DSWR annual anomalies in the a) N, b) NE, c) CW, d) SE, and e) S regions from observations, reanalyses and merged datasets during the 1980-2016 period.

Figure 7 shows the temporal evolution of the annual DSWR anomalies from all datasets and within each region during the period 1980-2016. In the N region, JRA55 and MERRA2 show

a downward trend, opposite to that of OBS_BR, ERA5, and GMFD (Figure 7a). DSWR reanalysis trends are related to the quantity and quality of the observations assimilated in the model, mainly that of CC, SP, and MSLP (Gelaro et al., 2017; Kobayashi et al., 2015). Regional averages across the NE (Figure 7b), CW (Figure 7c), and SE (Figure 7d) regions show strong negative anomalies in 1992. Swingedouw et al. (2017) attribute the worldwide changes in the DSWR in that year to the Mount Pinatubo eruption in June 1991. They argued that the release of gases (e.g., sulfur dioxide) by volcanic eruptions modified the DSWR dispersion, leading to a change in the opacity of the atmosphere and cooling of the surface that reached up to ~ -0.5 K nearly 18 months after the eruption (Soden et al., 2002). It is noteworthy that all datasets captured this negative trend. However, only datasets with a specific parameterization for volcanic aerosols (ERA5, MERRA2, and CFSR) were close to the OBS_BR values. The reason for capturing the anomaly (with underestimation) of datasets JRA55, GMFD, and WFDEI - without parameterization for volcanic aerosols - is probably related to the effect of aerosols on the properties of clouds. According to Matsui et al. (2004), high aerosol concentrations can increase cloud albedo up to 30%.

Interestingly, CFSR shows diverging behavior after 2011 (when version 2 began). The new parameterization leads to an amplification of positive anomalies of DSWR, which were negative until 2011. This is likely due to an increase in the DSWR values in 2011-2016 that modifies the mean value particularly in the N region (Figure 7a). The CW region shows similarities in the behavior of the CFSR (Figure 7c). GMFD, JRA55, and MERRA2 display negative trends in contrast to OBS_BR, ERA5, and CFSR. WFDEI does not show any marked anomalies. In the S region, negative anomalies are observed in 1998 based on all dataset calculations (Figure 7e), probably related to a high density of surface observations (Melo et al., 2015). WFDEI does not exhibit a clear pattern of increasing/decreasing trends of DSWR.

Figure 8 shows the temporal evolution of the seasonal DSWR anomalies for each region during the period 1980-2016. In the N region (Figure 8a), JRA55 and MERRA2 reflect negative anomalies after 2008, mainly during DJF and MAM. The extreme anomalies of the CFSR persist throughout all seasons; however, this is only prevalent across the N region and to a lesser extent in the CW region in DJF and SON (Figure 8c). In the NE region (Figure 8b), an increase in positive anomalies for all seasons is demonstrated. Anomalies in 1992 are present in all seasons for the SE region, and in SON and DJF for the CW and NE regions (Figure 8d). The large anomaly of the S region (1998) is depicted in all seasons, but weaker in JJA (Figure

8e). In this region, except for OBS_BR, ERA5 and WFDEI, the datasets show downward trends.

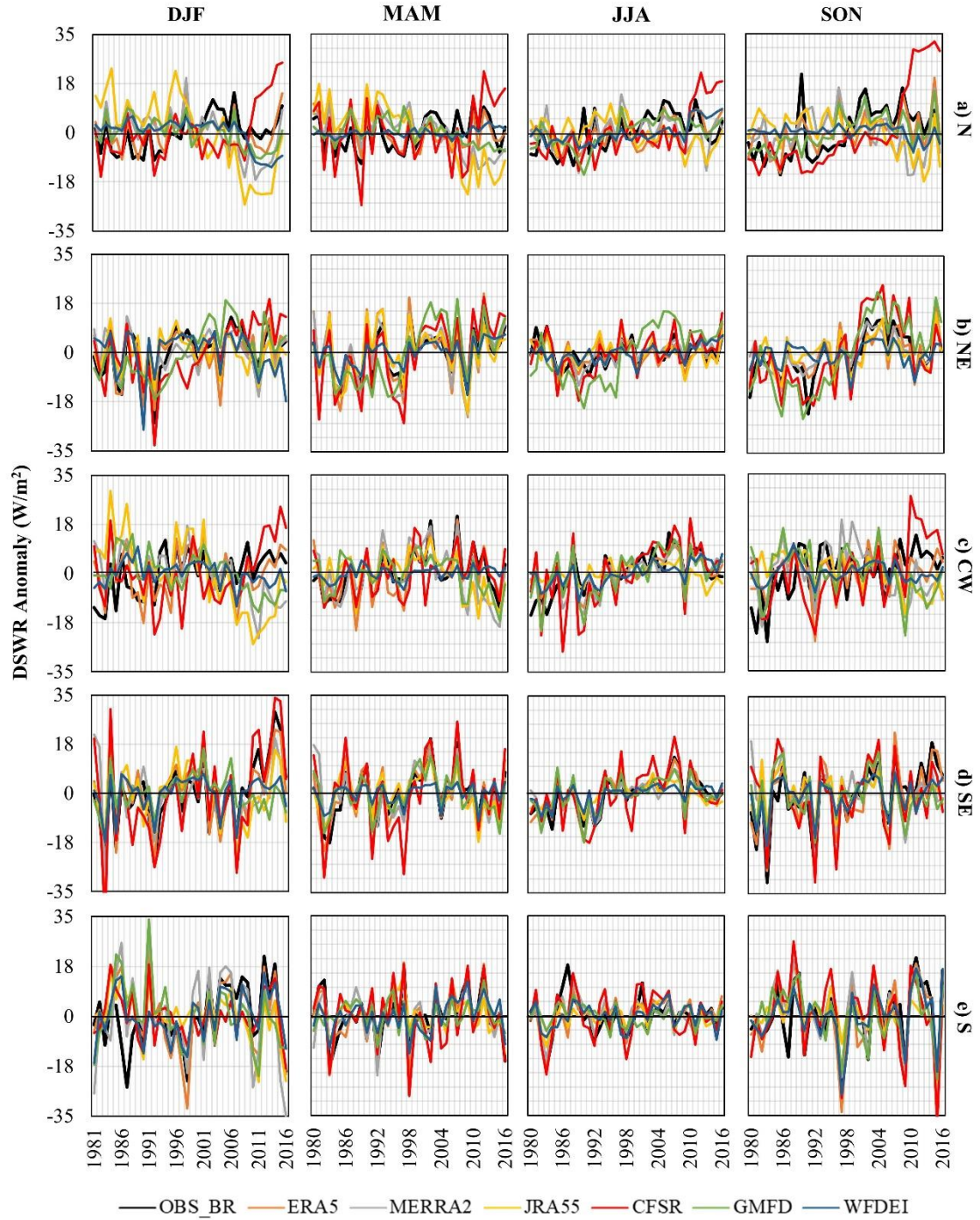


Figure 8. Time series of the DSWR seasonal anomalies in the a) N, b) NE, c) CW, d) SE, and e) S regions from observations, reanalyses and merged datasets, during the 1980-2016 period. The seasons are summer (DJF), autumn (MAM), winter (JJA) and spring (SON).

All results suggest that ERA5 can be used to study the long-term aspects and temporal evolution of DSWR for Brazil. However, its relationship with CC, considering that in Brazil there are no databases of this variable, should be further evaluated (Perdigão et al., 2016; Sanchez-Lorenzo et al., 2017; Zhang et al., 2016).

1.3.3. Effects of cloud cover (CC) on DSWR variability.

It has long been argued that the local distribution of clouds modifies the amount of solar radiation reaching the surface. To assess the influence of CC on the spatiotemporal variability of DSWR, CC climatology and trends from ERA5 at annual and seasonal scales are analyzed (Figure 9). According to Danso et al. (2019), ERA5 provides diagnostic CC fractions on 2D single atmospheric layers (namely low-level, mid-level, high-level and total atmospheric column). We used the total atmospheric column, which integrates all clouds from the surface level to the top of the atmosphere.

Figure 9a shows that northern Brazil (N region) delivers the greatest CC, ranging from 0.82 in northwest AM to 0.57 in southeast TO. The highest CC values (> 0.80) occur from DJF to MAM, which correspond to the wet season (Figure 9c). The region with the lowest CC is NE, with minimum values lower than 0.46 extending across the States of CE, RN, PI, and BA (Figure 9a). These values are particularly low during JJA (< 0.40) over MA and PI, and a large part of BA (Figure 9c). In the SE region, in line with DSWR, CC is highly correlated with altitude, showing the smallest annual values (≈ 0.56) on the leeward side of the mountains (northwest of SP and MG). Whereas the greatest values (≈ 0.68 , Figure 9a) are located on the windward side (RJ, ES, and eastern MG and SP). The CC seasonal variation in this region shows its maxima during the rainy season (DJF) and the smallest CC during the dry season (JJA). The CW region exhibits the largest annual CC values in northern MT (bordering the Amazon region) and the lowest in southern MS. Turning to the S region, a high degree of CC is found in eastern PR and SC. Seasonally the CW and S regions show maximum CC values in DJF and minima in JJA (Figure 9c), in line with summer and winter seasons.

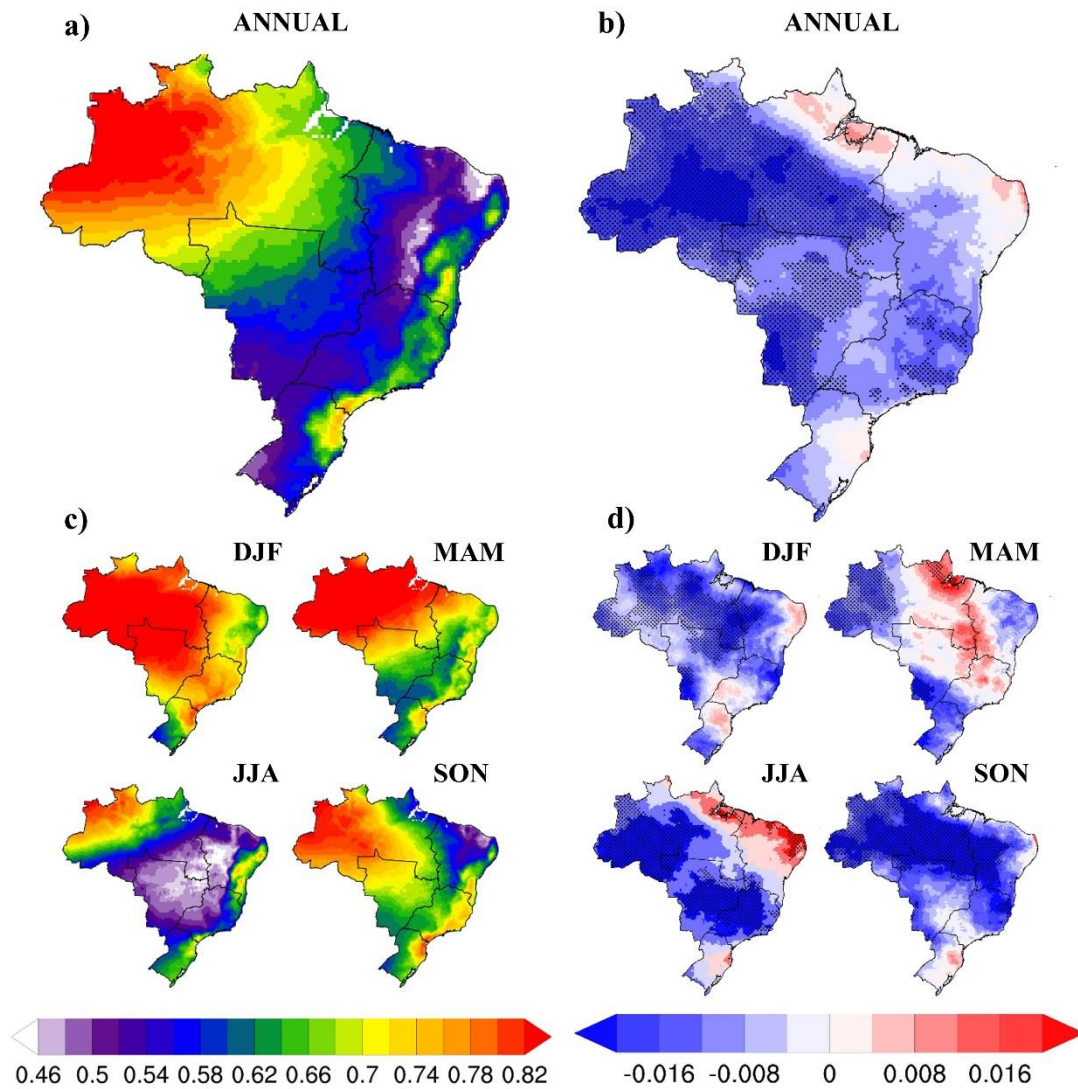


Figure 9. a) Annual mean CC climatology (fraction), b) annual CC trend (fraction per decade), c) seasonal mean CC climatology (fraction), and d) seasonal CC trend (fraction per decade) over Brazil during the 1980–2016 period. In maps (b-d), dots indicate statistical significance at the 95% level. Colors signify negative trends (blue) or positive trends (red). The seasons are summer (DJF), autumn (MAM), winter (JJA) and spring (SON). Dataset: ERA5.

In general, CC across the country is decreasing with large negative trends in the center and western portions of the N and CW regions, as well as in the SE region (Figure 9b). It should be stressed that the trends exhibit large spatial variability among seasons, though the S region does not show large trend. Figure 9d shows that the N and CW regions experience the largest reduction in CC during DJF, JJA, and SON (≈ -0.02 per decade). On the other hand, there exists a slight increase in the MAM season in most of Brazil, specifically over MA, TO, PI, BA, GO, and north of MG and the DF. The largest CC increases in JJA in the northern part of the NE

region are connected to wetter conditions, including events of more intense precipitation, and a possible shift of the rainy season from MAM to JJA (Hänsel et al., 2016).

Figure 10 illustrates the correlation (r) between DSWR and CC (from OBS_BR and ERA5) at annual and seasonal scales. Figure 10b shows that only the west side of AM during DJF and MAM does not show statistically significant correlation, likely depicting modeling issues with the rainy season (ERA5) or related to the lower surface station density. As expected, OBS_BR DSWR (Figure 10a) has a lower correlation with CC compared to that of ERA5. However, their correlations are highly negative ($r < -0.55$ with statistical significance) in the NE, SE, and S regions during all seasons (except JJA for the NE region). Weak correlations (without statistical significance) are observed during JJA and SON in the PA in the N region and MT in CW (Figure 10a). In these localities, which correspond to the west side of the border between Cerrado (Savannas) and Amazon Forest biomes, both measured DSWR and ERA5 CC's show negative trends (Figures 6a and 9d, respectively). This shows quantitatively that, during JJA and SON (dry season), CC does not play a relevant role in explaining the DSWR variations. On the other hand, during these seasons, frequent burning of native vegetation occurs as a traditional agricultural practice, injecting large amounts of aerosols into the atmosphere (Pivello, 2011; Reis et al., 2018). Therefore, it is reasonable to suppose that variations in the aerosol-cloud interaction are probably the main factor influencing the negative DSWR decadal variability in these regions.

In Table 3, the DSWR trends from OBS_BR and ERA5 are presented again, but the ERA5 CC trends are added, as well as the correlation between CC and DSWR. Except for JJA in the NE region, MAM in the SE region, and JJA and SON in the S region, CC shows negative trends ranging from -0.022 per decade to -0.003 per decade. The results of the correlations between DSWR and CC for both datasets are similar, which show that the decision to use the CC time series from ERA5 is robust. All correlations are statistically significant ($p < 0.05$). The correlations vary between -0.37 and -0.89 for OBS_BR, and between -0.75 and -0.96 for ERA5, as anticipated. The N region shows the weakest correlation between CC and DSWR for OBS_BR, mainly during the dry season (JJA and MAM), while the strongest is during JJA for the SE region. The strong negative pattern correlation between CC and DSWR suggests that variations in CC can substantially influence the inter-annual and inter-seasonal variability of DSWR as changes in the cloudiness directly impacts the incident solar radiation at the surface. In other words, reduction in the amount of CC can, to a certain extent, be considered as one of

the possible factors to increase the amount of DSWR received (brightening) in almost all of Brazil between 1980 and 2016.

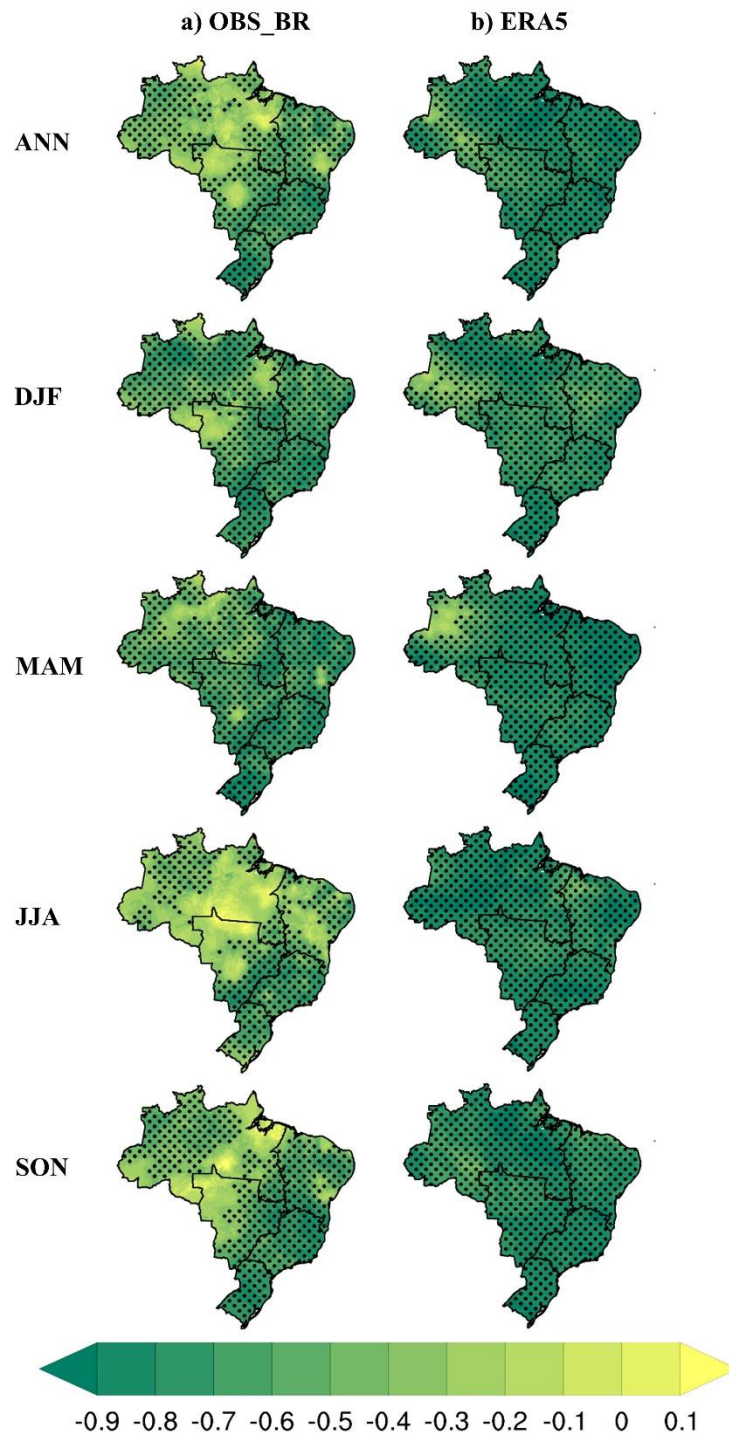


Figure 10. Spatial distributions of the correlation coefficient (r) between DSWR and CC, at annual (ANN) and seasonal scales, during the 1980-2016 period. a) Correlation between DSWR from OBS_BR and CC from ERA5. b) Correlation between DSWR and CC, both from ERA5. Statistical significant correlations at the 95% level are dotted. The seasons are summer (DJF), autumn (MAM), winter (JJA) and spring (SON).

Table 3. Trends in DSWR (W/m^2 per decade) and CC (fraction per decade) over the period 1980-2016, and correlation between DSWR trends and CC trends. Values in bold indicate the trends that significant at 95% level. Signs signify negative trends (-) or positive trends (+).

Region	Season	Decadal Trends			Correlation	
		DSWR OBS_BR	DSWR ERA5	CC ERA5	OBS_BR	ERA5
N	DJF	+3.2	+0.2	-0.011	-0.78	-0.84
	MAM	+1.8	-1.2	-0.003	-0.74	-0.87
	JJA	+3.7	+2.3	-0.016	-0.37	-0.92
	SON	+5.1	+2.7	-0.021	-0.57	-0.93
	ANN	+3.2	+1.1	-0.014	-0.53	-0.90
NE	DJF	+2.6	+0.4	-0.009	-0.78	-0.75
	MAM	+2.8	+1.7	-0.007	-0.88	-0.96
	JJA	+1.0	-0.2	+0.006	-0.56	-0.86
	SON	+3.8	+2.3	-0.014	-0.80	-0.85
	ANN	+2.5	+1.3	-0.005	-0.71	-0.90
CW	DJF	+4.5	+1.5	-0.010	-0.69	-0.76
	MAM	+2.5	+2.0	-0.003	-0.82	-0.87
	JJA	+4.8	+2.7	-0.022	-0.62	-0.85
	SON	+3.9	+1.6	-0.011	-0.48	-0.87
	ANN	+3.9	+2.0	-0.011	-0.60	-0.79
SE	DJF	+5.3	+2.4	-0.008	-0.83	-0.84
	MAM	+1.8	+1.4	0.000	-0.88	-0.84
	JJA	+3.3	+3.2	-0.020	-0.89	-0.91
	SON	+3.7	+3.4	-0.012	-0.81	-0.88
	ANN	+3.6	+2.5	-0.011	-0.83	-0.89
S	DJF	+2.7	-1.1	-0.004	-0.82	-0.91
	MAM	+0.8	+1.2	-0.013	-0.88	-0.92
	JJA	+0.3	+1.6	0.000	-0.58	-0.87
	SON	+3.5	+2.0	0.000	-0.83	-0.89
	ANN	+1.7	+0.9	-0.003	-0.86	-0.85

1.4. Discussion and conclusions

This study has evaluated the downward shortwave radiation (DSWR) based on the most recent gridded products over Brazil during the 1980-2016 period. Four reanalyses (ERA5, MERRA2, JRA55, and CFSR) and two merged products (GMFD and WFDEI) were compared to gridded observations. Indicators that estimate the accuracy (RMSE, bias and KGE) of the datasets were analyzed at annual and seasonal scales for five regions of Brazil.

Overall, results showed that ERA5 delivers the best performance for all regions of the country. The worst performances (overestimation) were noted in MERRA2 and JRA55, while CFSR demonstrated an intermediate performance. Malakar et al. (2020) found the same performance for these reanalyses when evaluating the mean sea-level pressure (MSLP) and

surface pressure (SP) products. These variables are fundamental in determining cloud cover (CC), since accurate estimates of MSLP and SP allow an adequate identification of low (high) pressure systems associated with clouds and precipitation (clear skies). CC and aerosols are the most important factors determining the DSWR variations. The limitations to the calculation of MSLP, SP, DSWR, and CC may be linked to poor data availability and quality across South America (Gelaro et al., 2017; Hersbach et al., 2018; Kobayashi et al., 2015; Saha et al., 2010). Merged products underestimated DSWR in the N, NE, and CW regions. In the SE and S regions, they showed opposite results. For instance, the GMFD overestimated DSWR whereas WFDEI underestimated in the N and CW regions. However, both merged products had better agreement with observations than CFSR, MERRA2 and JRA55.

The observations demonstrated a positive trend (brightening) in DSWR for the whole country in 1980-2016, particularly in the N, CW, and SE regions. Our results are in line with Raichijk (2012). For the NE region, Silva et al. (2010) found dimming; however, their study was only based on two stations. Thus, it should be emphasized that the use of gridded data provides a spatially-broader view of trends and variability. In a global context, our results agree with observations in other regions, such as the United States and Europe (Wild, 2012, 2009). Annual and seasonal ERA5 trends in all regions of Brazil are highly consistent with observations. Strong correlations between CC and observed DWSR showed that decadal changes in CC are the main contributing factor to the brightening effect in Brazil. However, during JJA and SON in the N and CW regions, the correlations were very weak, suggesting that a different factor influences the DSWR variability during these seasons. In fact, these are fire seasons when biomass burning is frequent along the border between Cerrado and the Amazon forest (Silva et al., 2020).

It is reasonable to argue that aerosols (from biomass burning) should be considered as the main influencing factor for DSWR decadal variability during this period. Wild (2012) pointed out that the aerosol-cloud interactions can increase the DSWR variation in unexplored regions; on the other hand, it can suppress variations in polluted regions. In addition, it is important to study the contribution of each type of cloud (high, mid and low) to the DSWR variability, as suggested by Kambezidis et al. (2016). Analyses presented here deliver the first assessment of the spatiotemporal patterns of variability and trends of DSWR and their relationship with CC at annual and seasonal scales. Although this work revealed strong evidence of brightening in

Brazil, more evidence should be sought from additional information on more widely meteorological variables (e.g., sunshine duration, diurnal temperature range or evaporation).

Future investigation should seek to demonstrate how aerosols and clouds (main modulators of atmospheric transparency) interact and contribute to changes in DSWR. The aerosol-radiation interactions occurs in two ways, direct and indirect (Padma Kumari and Goswami, 2010). The direct interactions consists of scattering, reflecting and absorption the incident radiation at the top of the atmosphere (Wang et al., 2020). Scattering and reflection are mainly produced by aerosol sulfate particles (from volcanoes or anthropic activities), while absorption is generated by black carbon (from fuel combustion and burning biomass) (Kuniyal and Guleria, 2019; Norris and Wild, 2009). At the same time, indirect interactions consists of modification of the optical properties of clouds due to the aerosols loading, resulting in an increasing in their albedo, and consequently in a higher reflection of DSWR at the surface of the Earth (Schwartz et al., 2002; Serrano et al., 2015). However, the multiple ways through which aerosol-radiation and aerosol-cloud interactions take place are major sources of uncertainties in climate modeling and prediction (Kuniyal and Guleria, 2019). Therefore a better understanding of the causes and magnitudes of DSWR changes may be used to improve climate models and reduce uncertainties in future climate projections (Wild, 2009). Additionally, exploration of the variability in all radiation fluxes (both from the surface and the top of the atmosphere) is needed to gain a better understanding of the anthropogenic and natural disturbances in the radiation balance that underlies global climate change (Wild et al., 2018). A positive trend in DSWR over Brazil has far-reaching implications and should also be evaluated through other perspectives, such as outcomes on the solar energy sector and/or agriculture.

1.5. Acknowledgments

We acknowledge the Coordination for the Improvement of Higher Education Personnel (CAPES) for supporting this research. We acknowledge all the Institutions that make their datasets available. The authors acknowledge Alexandre Xavier, Carey King, and Bridget Scanlon that provided daily climate data for Brazil. The author thanks the graduate program in Applied Meteorology at the Universidade Federal de Viçosa.

1.6. Appendix

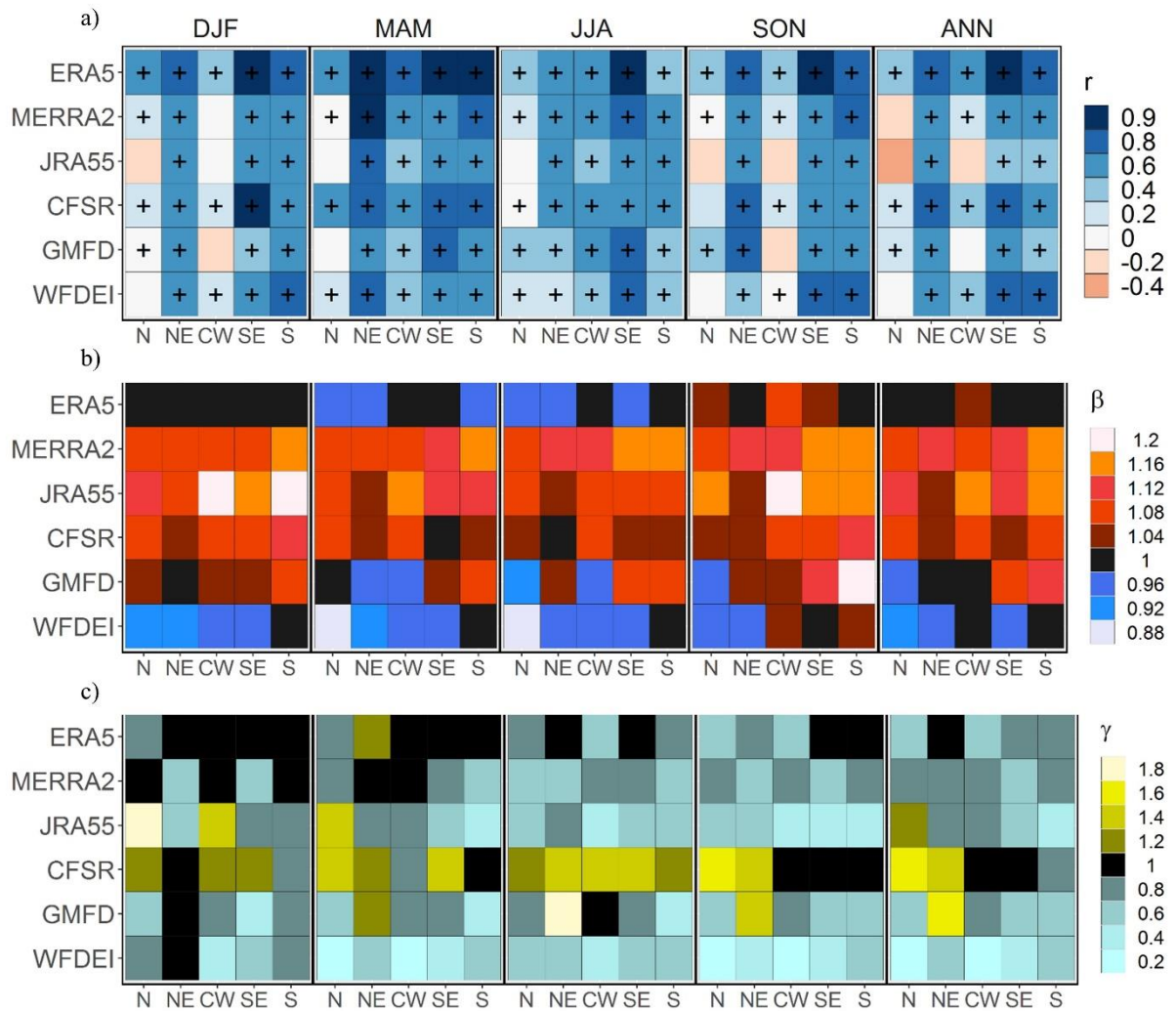


Figure A.1. KGE components values in the performance evaluation of datasets to estimate DSWR compared to that of the OBS_BR dataset, during 1980-2016. a) Correlation coefficient (r), b) bias ratio (β) and c) variability ratio (γ). Upper horizontal axis represents seasonal and annual time scales. The seasons are summer (DJF), autumn (MAM), winter (JJA) and spring (SON). Lower horizontal axis represents the North (N), Northeast (NE), Center-West (CW), Southeast (SE) and South (S) regions. Left vertical axis shows the reanalysis/merged products. Significant differences at the 95% level of r have crosses.

1.7. References

- Allen, G.R., Pereira, S.L., Raes, D., Smith, M., 1998. Crop Evapotranspiration - Guidelines for computing crop water requirements. FAO Irrigation and drainage paper 56, 1-15. Available online: https://appgeodb.nancy.inra.fr/biljou/pdf/Allen_FAO1998.pdf (Accessed on 4 May 2020)

- Alvares, C.A., Stape, J.L., Sentelhas, P.C., De Moraes Gonçalves, J.L., Sparovek, G., 2013. Köppen's climate classification map for Brazil. *Meteorol. Zeitschrift* 22, 711–728. <https://doi.org/10.1127/0941-2948/2013/0507>
- Augustine, J.A., Dutton, E.G., 2013. Variability of the surface radiation budget over the United States from 1996 through 2011 from high-quality measurements. *J. Geophys. Res. Atmos.* 118, 43–53. <https://doi.org/10.1029/2012JD018551>
- Avila-Diaz, A., Abrahão, G., Justino, F., Torres, R., Wilson, A., 2020. Extreme climate indices in Brazil: evaluation of downscaled earth system models at high horizontal resolution. *Clim. Dyn.* 54, 5065–5088. <https://doi.org/10.1007/s00382-020-05272-9>
- Babar, B., Graversen, R., Boström, T., 2019. Solar radiation estimation at high latitudes: Assessment of the CMSAF databases, ASR and ERA5. *Sol. Energy* 182, 397–411. <https://doi.org/10.1016/j.solener.2019.02.058>
- Battisti, R., Bender, F.D., Sentelhas, P.C., 2018. Assessment of different gridded weather data for soybean yield simulations in Brazil. *Theor. Appl. Climatol.* 1–11. <https://doi.org/10.1007/s00704-018-2383-y>
- Bender, F.D., Sentelhas, P.C., 2018. Solar Radiation Models and Gridded Databases to Fill Gaps in Weather Series and to Project Climate Change in Brazil. *Adv. Meteorol.* 2018, 1–15. <https://doi.org/10.1155/2018/6204382>
- Borges, P. de A., Franke, J., da Anunciação, Y.M.T., Weiss, H., Bernhofer, C., 2016. Comparison of spatial interpolation methods for the estimation of precipitation distribution in Distrito Federal, Brazil. *Theor. Appl. Climatol.* 123, 335–348. <https://doi.org/10.1007/s00704-014-1359-9>
- Da Rocha, H.R., Goulden, M.L., Miller, S.D., Menton, M.C., Pinto, L.D.V.O., De Freitas, H.C., E Silva Figueira, A.M., 2004. Seasonality of water and heat fluxes over a tropical forest in eastern Amazonia. *Ecol. Appl.* 14, 22–32. <https://doi.org/10.1890/02-6001>
- Danso, D.K., Anquetin, S., Diedhiou, A., Lavaysse, C., Koba, A., Touré, N.E., 2019. Spatio-temporal variability of cloud cover types in West Africa with satellite-based and reanalysis data. *Q. J. R. Meteorol. Soc.* 145, 3715–3731. <https://doi.org/10.1002/qj.3651>
- Dullaart, J.C.M., Muis, S., Bloemendaal, N., Aerts, J.C.J.H., 2020. Advancing global storm surge modelling using the new ERA5 climate reanalysis. *Clim. Dyn.* 54, 1007–1021. <https://doi.org/10.1007/s00382-019-05044-0>
- Feng, F., Wang, K., 2018. Does the modern-era retrospective analysis for research and applications-2 aerosol reanalysis introduce an improvement in the simulation of surface solar radiation over China? *Int. J. Climatol.* <https://doi.org/10.1002/joc.5881>
- Feng, F., Wang, K., 2019. Determining Factors of Monthly to Decadal Variability in Surface Solar Radiation in China: Evidences From Current Reanalyses. *J. Geophys. Res. Atmos.* 124, 9161–9182. <https://doi.org/10.1029/2018jd030214>
- Garcia, S.R., Kayano, M.T., 2015. Multidecadal variability of moisture and heat budgets of the South American monsoon system. *Theor. Appl. Climatol.* 121, 557–570. <https://doi.org/10.1007/s00704-014-1265-1>
- Gelaro, R., McCarty, W., Suárez, M.J., Todling, R., Molod, A., Takacs, L., Randles, C.A., Darmenov, A., Bosilovich, M.G., Reichle, R., Wargan, K., Coy, L., Cullather, R., Draper, C., Akella, S., Buchard, V., Conaty, A., da Silva, A.M., Gu, W., Kim, G.K., Koster, R., Lucchesi, R., Merkova, D., Nielsen, J.E., Partyka, G., Pawson, S., Putman, W., Rienecker, M., Schubert, S.D., Sienkiewicz, M., Zhao, B., 2017. The modern-era retrospective analysis for research and applications, version 2 (MERRA-2). *J. Clim.* 30, 5419–5454. <https://doi.org/10.1175/JCLI-D-16-0758.1>
- Gupta, H. V., Kling, H., Yilmaz, K.K., Martinez, G.F., 2009. Decomposition of the mean squared error and NSE performance criteria: Implications for improving hydrological modelling. *J. Hydrol.* 377, 80–91. <https://doi.org/10.1016/j.jhydrol.2009.08.003>

- Hänsel, S., Medeiros, D.M., Matschullat, J., Petta, R.A., de Mendonça Silva, I., 2016. Assessing homogeneity and climate variability of temperature and precipitation series in the capitals of North-Eastern Brazil. *Front. Earth Sci.* 4, 1–21. <https://doi.org/10.3389/feart.2016.00029>
- Herring, S.C., Christidis, N., Hoell, A., Hoerling, M.P., Stott, P.A., 2020. Explaining Extreme Events of 2018 from a Climate Perspective. *Bull. Am. Meteorol. Soc.* 101, S1–S134. <https://doi.org/10.1175/BAMS-ExplainingExtremeEvents2018.1>
- Hersbach, H., Bell, B., Berrisford, P., Hirahara, S., Horányi, A., Muñoz-Sabater, J., Nicolas, J., Peubey, C., Radu, R., Schepers, D., Simmons, A., Soci, C., Abdalla, S., Abellan, X., Balsamo, G., Bechtold, P., Biavati, G., Bidlot, J., Bonavita, M., Chiara, G., Dahlgren, P., Dee, D., Diamantakis, M., Dragani, R., Flemming, J., Forbes, R., Fuentes, M., Geer, A., Haimberger, L., Healy, S., Hogan, R.J., Hólm, E., Janisková, M., Keeley, S., Laloyaux, P., Lopez, P., Lupu, C., Radnoti, G., Rosnay, P., Rozum, I., Vamborg, F., Villaume, S., Thépaut, J., 2020. The ERA5 global reanalysis. *Q. J. R. Meteorol. Soc.* qj.3803. <https://doi.org/10.1002/qj.3803>
- Huang, G., Li, Z., Li, X., Liang, S., Yang, K., Wang, D., Zhang, Y., 2019. Estimating surface solar irradiance from satellites: Past, present, and future perspectives. *Remote Sens. Environ.* 233, 111371. <https://doi.org/10.1016/j.rse.2019.111371>
- Jahani, B., Dinpashoh, Y., Wild, M., 2018. Dimming in Iran since the 2000s and the potential underlying causes. *Int. J. Climatol.* 38, 1543–1559. <https://doi.org/10.1002/joc.5265>
- Kambeizidis, H.D., Kaskaoutis, D.G., Kalliampakos, G.K., Rashki, A., Wild, M., 2016. The solar dimming/brightening effect over the Mediterranean Basin in the period 1979–2012. *J. Atmos. Solar-Terrestrial Phys.* 150–151, 31–46. <https://doi.org/10.1016/j.jastp.2016.10.006>
- Kendall, M., 1975. Rank correlation methods, 4th ed. London.
- Kling, H., Fuchs, M., Paulin, M., 2012. Runoff conditions in the upper Danube basin under an ensemble of climate change scenarios. *J. Hydrol.* 424–425, 264–277. <https://doi.org/10.1016/j.jhydrol.2012.01.011>
- Kobayashi, S., Ota, Y., Harada, Y., Ebata, A., Moriya, M., Onoda, H., Onogi, K., Kamahori, H., Kobayashi, C., Endo, H., Miyaoka, K., Kiyotoshi, T., 2015. The JRA-55 reanalysis: General specifications and basic characteristics. *J. Meteorol. Soc. Japan* 93, 5–48. <https://doi.org/10.2151/jmsj.2015-001>
- Kuniyal, J.C., Guleria, R.P., 2019. The current state of aerosol-radiation interactions: A mini review. *J. Aerosol Sci.* 130, 45–54. <https://doi.org/10.1016/j.jaerosci.2018.12.010>
- Lilhare, R., Déry, S.J., Pokorný, S., Stadnyk, T.A., Koenig, K.A., 2019. Intercomparison of Multiple Hydroclimatic Datasets across the Lower Nelson River Basin, Manitoba, Canada. *Atmosphere-Ocean* 0, 1–17. <https://doi.org/10.1080/07055900.2019.1638226>
- Lima, F., Martins, F.R., Pereira, E.B., Lorenz, E., Heinemann, D., 2016. Forecast for surface solar irradiance at the Brazilian Northeastern region using NWP model and artificial neural networks. *Renew. Energy* 87, 807–818. <https://doi.org/10.1016/j.renene.2015.11.005>
- Long, C.N., Dutton, E.G., Augustine, J.A., Wiscombe, W., Wild, M., McFarlane, S.A., Flynn, C.J., 2009. Significant decadal brightening of downwelling shortwave in the continental United States. *J. Geophys. Res.* 114, D00D06. <https://doi.org/10.1029/2008JD011263>
- Malakar, P., Kesarkar, A.P., Bhate, J.N., Singh, V., Deshamukhya, A., 2020. Comparison of Reanalysis Data Sets to Comprehend the Evolution of Tropical Cyclones Over North Indian Ocean. *Earth Sp. Sci.* 7, 1–15. <https://doi.org/10.1029/2019EA000978>
- Manara, V., Brunetti, M., Maugeri, M., Sanchez-Lorenzo, A., Wild, M., 2017. Sunshine duration and global radiation trends in Italy (1959–2013): To what extent do they agree? *J. Geophys. Res. Atmos.* 122, 4312–4331. <https://doi.org/10.1002/2016JD026374>
- Manara, V., Bassi, M., Brunetti, M., Cagnazzi, B., Maugeri, M., 2018. 1990 – 2016 surface

- solar radiation variability and trend over the Piedmont region (northwest Italy). *Theor. Appl. Climatol.* <https://doi.org/https://doi.org/10.1007/s00704-018-2521-6>
- Mann, H.B. 1945. Non-parametric tests against trend. *Econometrica*. 13, 245–259.
- Mateos, D., Sanchez-Lorenzo, A., Antón, M., Cachorro, V.E., Calbó, J., Costa, M.J., Torres, B., Wild, M., 2014. Quantifying the respective roles of aerosols and clouds in the strong brightening since the early 2000s over the Iberian Peninsula. *J. Geophys. Res. Atmos.* 119, 10,382–10,393. <https://doi.org/10.1002/2014JD022076>
- Matsui, T., Masunaga, H., Pielke, R.A., Tao, W.K., 2004. Impact of aerosols and atmospheric thermodynamics on cloud properties within the climate system. *Geophys. Res. Lett.* 31, 2–5. <https://doi.org/10.1029/2003gl019287>
- Melo, D. de C.D., Xavier, A.C., Bianchi, T., Oliveira, P.T.S., Scanlon, B.R., Lucas, M.C., Wendland, E., 2015. Performance evaluation of rainfall estimates by TRMM Multi-satellite Precipitation Analysis 3B42V6 and V7 over Brazil. *J. Geophys. Res. Atmos.* 120, 9426–9436. <https://doi.org/10.1002/2015JD023797>
- Mercado, L.M., Bellouin, N., Sitch, S., Boucher, O., Huntingford, C., Wild, M., Cox, P.M., 2009. Impact of changes in diffuse radiation on the global land carbon sink. *Nature* 458, 1014–1017. <https://doi.org/10.1038/nature07949>
- Molina, A., Falvey, M., Rondanelli, R., 2017. A solar radiation database for Chile. *Sci. Rep.* 7, 1–11. <https://doi.org/10.1038/s41598-017-13761-x>
- Norris, J.R., Wild, M., 2009. Trends in aerosol radiative effects over China and Japan inferred from observed cloud cover, solar “dimming,” and solar “brightening.” *J. Geophys. Res. Atmos.* 114. <https://doi.org/10.1029/2008JD011378>
- Padma Kumari, B., Goswami, B.N., 2010. Seminal role of clouds on solar dimming over the Indian monsoon region. *Geophys. Res. Lett.* 37, 1–5. <https://doi.org/10.1029/2009GL042133>
- Paulescu, M., Stefu, N., Calinoiu, D., Paulescu, E., Pop, N., Boata, R., Mares, O., 2016. Ångström–Prescott equation: Physical basis, empirical models and sensitivity analysis. *Renew. Sustain. Energy Rev.* 62, 495–506. <https://doi.org/10.1016/j.rser.2016.04.012>
- Perdigão, J.C., Salgado, R., Costa, M.J., Dasari, H.P., Sanchez-Lorenzo, A., 2016. Variability and trends of downward surface global solar radiation over the Iberian Peninsula based on ERA-40 reanalysis. *Int. J. Climatol.* 36, 3917–3933. <https://doi.org/10.1002/joc.4603>
- Pezzi, L.P., Souza, R.B., Farias, P.C., Acevedo, O., Miller, A.J., 2016. Air-sea interaction at the Southern Brazilian Continental Shelf: In situ observations. *J. Geophys. Res. Ocean.* 121, 6671–6695. <https://doi.org/10.1002/2016JC011774>
- Pivello, V.R., 2011. The use of fire in the cerrado and Amazonian rainforests of Brazil: Past and present. *Fire Ecol.* 7, 24–39. <https://doi.org/10.4996/fireecology.0701024>
- Porfirio, A.C.S., Ceballos, J.C., Britto, J.M.S., Costa, S.M.S., 2020. Evaluation of Global Solar Irradiance Estimates from GL1.2 Satellite-Based Model over Brazil Using an Extended Radiometric Network. *Remote Sens.* 12, 1331. <https://doi.org/10.3390/rs12081331>
- Raichijk, C., 2012. Observed trends in sunshine duration over South America. *Int. J. Climatol.* 32, 669–680. <https://doi.org/10.1002/joc.2296>
- Reis, S.M., Marimon, B.S., Marimon Junior, B.H., Morandi, P.S., de Oliveira, E.A., Elias, F., Das Neves, E.C., de Oliveira, B., Nogueira, D. da S., Umetsu, R.K., Feldpausch, T.R., Phillips, O.L., 2018. Climate and fragmentation affect forest structure at the southern border of amazonia. *Plant Ecol. Divers.* 11, 13–25. <https://doi.org/10.1080/17550874.2018.1455230>
- Saha, S., Moorthi, S., Pan, H.L., Wu, X., Wang, Jiande, Nadiga, S., Tripp, P., Kistler, R., Woollen, J., Behringer, D., Liu, H., Stokes, D., Grumbine, R., Gayno, G., Wang, Jun, Hou, Y.T., Chuang, H.Y., Juang, H.M.H., Sela, J., Iredell, M., Treadon, R., Kleist, D., Van Delst, P., Keyser, D., Derber, J., Ek, M., Meng, J., Wei, H., Yang, R., Lord, S., Van Den

- Dool, H., Kumar, A., Wang, W., Long, C., Chelliah, M., Xue, Y., Huang, B., Schemm, J.K., Ebisuzaki, W., Lin, R., Xie, P., Chen, M., Zhou, S., Higgins, W., Zou, C.Z., Liu, Q., Chen, Y., Han, Y., Cucurull, L., Reynolds, R.W., Rutledge, G., Goldberg, M., 2010. The NCEP climate forecast system reanalysis. *Bull. Am. Meteorol. Soc.* 91, 1015–1057. <https://doi.org/10.1175/2010BAMS3001.1>
- Saha, S., Moorthi, S., Wu, X., Wang, J., Nadiga, S., Tripp, P., Behringer, D., Hou, Y.T., Chuang, H.Y., Iredell, M., Ek, M., Meng, J., Yang, R., Mendez, M.P., Van Den Dool, H., Zhang, Q., Wang, W., Chen, M., Becker, E., 2014. The NCEP climate forecast system version 2. *J. Clim.* 27, 2185–2208. <https://doi.org/10.1175/JCLI-D-12-00823.1>
- Salazar, G., Gueymard, C., Galdino, J.B., de Castro Vilela, O., Fraidenraich, N., 2020. Solar irradiance time series derived from high-quality measurements, satellite-based models, and reanalyses at a near-equatorial site in Brazil. *Renew. Sustain. Energy Rev.* 117, 109478. <https://doi.org/10.1016/j.rser.2019.109478>
- Sanchez-Lorenzo, A., Enriquez-Alonso, A., Wild, M., Trentmann, J., Vicente-Serrano, S.M., Sanchez-Romero, A., Posselt, R., Hakuba, M.Z., 2017. Trends in downward surface solar radiation from satellites and ground observations over Europe during 1983–2010. *Remote Sens. Environ.* 189, 108–117. <https://doi.org/10.1016/j.rse.2016.11.018>
- Sanchez-Lorenzo, A., Wild, M., Brunetti, M., Guijarro, J.A., Hakuba, M.Z., Calbó, J., Mystakidis, S., Bartok, B., 2015. Reassessment and update of long-term trends in downward surface shortwave radiation over Europe (1939–2012). *J. Geophys. Res. Atmos.* 120, 9555–9569. <https://doi.org/10.1002/2015JD023321>
- Santos, E.B., Lucio, P.S., Santos e Silva, C.M., 2017. Synoptic patterns of atmospheric circulation associated with intense precipitation events over the Brazilian Amazon. *Theor. Appl. Climatol.* 128, 343–358. <https://doi.org/10.1007/s00704-015-1712-7>
- Santos, E.B., Lucio, P.S., Santos e Silva, C.M., 2015. Precipitation regionalization of the Brazilian Amazon. *Atmos. Sci. Lett.* 16, 185–192. <https://doi.org/10.1002/asl2.535>
- Schmied, H.M., Müller, R., Sanchez-Lorenzo, A., Ahrens, B., Wild, M., 2016. Evaluation of radiation components in a global freshwater model with station-based observations. *Water (Switzerland)* 8. <https://doi.org/10.3390/w8100450>
- Schwartz, S.E., Harshvardhan, Benkovitz, C.M., 2002. Influence of anthropogenic aerosol on cloud optical depth and albedo shown by satellite measurements and chemical transport modeling. *Proc. Natl. Acad. Sci. U. S. A.* 99, 1784–1789. <https://doi.org/10.1073/pnas.261712099>
- Sen, P.K., 1968. Estimates of the Regression Coefficient Based on Kendall's Tau. *J. Am. Stat. Assoc.* 63, 1379–1389. <https://doi.org/10.2307/2285891>
- Serrano, D., Marín, M.J., Núñez, M., Gandía, S., Utrillas, M.P., Martínez-Lozano, J.A., 2015. Relationship between the effective cloud optical depth and different atmospheric transmission factors. *Atmos. Res.* 160, 50–58. <https://doi.org/10.1016/j.atmosres.2015.03.004>
- Sheffield, J., Goteti, G., Wood, E.F., 2006. Development of a 50-year high-resolution global dataset of meteorological forcings for land surface modeling. *J. Clim.* 19, 3088–3111. <https://doi.org/10.1175/JCLI3790.1>
- Silva, A.S., Justino, F.B., Setzer, A.W., Ávila-Díaz, A.J. Vegetation Fire Activity and the Potential Fire Index (PFIv2) Performance in the Last Two Decades (2001–2016). *Int. J. Climatol.* 55. <https://doi.org/10.1002/joc.6648>
- Silva, V. de P.R. da, Silva, R.A. e., Cavalcanti, E.P., Braga, C.C., Azevedo, P.V. de, Singh, V.P., Pereira, E.R.R., 2010. Trends in solar radiation in NCEP/NCAR database and measurements in northeastern Brazil. *Sol. Energy* 84, 1852–1862. <https://doi.org/10.1016/j.solener.2010.07.011>
- Soden, B.J., Wetherald, R.T., Stenchikov, G.L., Robock, A., 2002. Global Cooling After the

- Eruption of Mount Pinatubo: A Test of Climate Feedback by Water Vapor. *Science* (80-.). 296, 727–730. <https://doi.org/10.1126/science.296.5568.727>
- Soni, V.K., Pandithurai, G., Pai, D.S., 2016. Is there a transition of solar radiation from dimming to brightening over India? *Atmos. Res.* 169, 209–224. <https://doi.org/10.1016/j.atmosres.2015.10.010>
- Stanhill, G., Cohen, S., 2001. Global dimming: a review of the evidence for a widespread and significant reduction in global radiation with discussion of its probable causes and possible agricultural consequences. *Agric. For. Meteorol.* 107, 255–278. [https://doi.org/10.1016/S0168-1923\(00\)00241-0](https://doi.org/10.1016/S0168-1923(00)00241-0)
- Swingedouw, D., Mignot, J., Ortega, P., Khodri, M., Menegoz, M., Cassou, C., Hanquiez, V., 2017. Impact of explosive volcanic eruptions on the main climate variability modes. *Glob. Planet. Change* 150, 24–45. <https://doi.org/10.1016/j.gloplacha.2017.01.006>
- Troy, T.J., Wood, E.F., 2009. Comparison and evaluation of gridded radiation products across northern Eurasia. *Environ. Res. Lett.* 4. <https://doi.org/10.1088/1748-9326/4/4/045008>
- Urraca, R., Huld, T., Gracia-Amillo, A., Martinez-de-Pison, F.J., Kaspar, F., Sanz-Garcia, A., 2018. Evaluation of global horizontal irradiance estimates from ERA5 and COSMO-REA6 reanalyses using ground and satellite-based data. *Sol. Energy* 164, 339–354. <https://doi.org/10.1016/j.solener.2018.02.059>
- Walter-Shea, E.A., Hubbard, K.G., Mesarch, M.A., Roebke, G., 2019. Improving the calibration of silicon photodiode pyranometers. *Meteorol. Atmos. Phys.* 131, 1111–1120. <https://doi.org/10.1007/s00703-018-0624-3>
- Wang, K., Dickinson, R.E., Wild, M., Liang, S., 2010. Evidence for decadal variation in global terrestrial evapotranspiration between 1982 and 2002: 2. Results. *J. Geophys. Res. Atmos.* 115, 1–10. <https://doi.org/10.1029/2010JD013847>
- Wang, K., Ma, Q., Li, Z., Wang, J., 2015. Decadal variability of surface incident solar radiation over China: Observations, satellite retrievals, and reanalyses. *J. Geophys. Res. Atmos.* 120, 6500–6514. <https://doi.org/10.1002/2015JD023420>
- Wang, Y., Le, T., Chen, G., Yung, Y.L., Su, H., Seinfeld, J.H., Jiang, J.H., 2020. Reduced European aerosol emissions suppress winter extremes over northern Eurasia. *Nat. Clim. Chang.* <https://doi.org/10.1038/s41558-020-0693-4>
- Wang, Y.W., Yang, Y.H., 2014. China's dimming and brightening: evidence, causes and hydrological implications. *Ann. Geophys.* 32, 1–6. <https://doi.org/10.5194/angeo-32-1-2014>
- Weedon, G.P., Balsamo, G., Bellouin, N., Gomes, S., Best, M.J., Viterbo, P., 2014. Data methodology applied to ERA-Interim reanalysis data. *Water Resour. Res.* 50, 7505–7514. <https://doi.org/10.1002/2014WR015638>.Received
- Wild, M., 2005. From Dimming to Brightening: Decadal Changes in Solar Radiation at Earth's Surface. *Science* (80-.). 308, 847–850. <https://doi.org/10.1126/science.1103215>
- Wild, M., 2008. Short-wave and long-wave surface radiation budgets in GCMs: A review based on the IPCC-AR4/CMIP3 models. *Tellus, Ser. A Dyn. Meteorol. Oceanogr.* 60, 932–945. <https://doi.org/10.1111/j.1600-0870.2008.00342.x>
- Wild, M., 2009. Global dimming and brightening: A review. *J. Geophys. Res.* 114, 1–31. <https://doi.org/10.1029/2008JD011470>
- Wild, M., 2012. Enlightening global dimming and brightening. *Bull. Am. Meteorol. Soc.* 93, 27–37. <https://doi.org/10.1175/BAMS-D-11-00074.1>
- Wild, M., 2016. Decadal changes in radiative fluxes at land and ocean surfaces and their relevance for global warming. *Wiley Interdiscip. Rev. Clim. Chang.* 7, 91–107. <https://doi.org/10.1002/wcc.372>
- Wild, M., Folini, D., Henschel, F., Fischer, N., Müller, B., 2015. Projections of long-term changes in solar radiation based on CMIP5 climate models and their influence on energy

- yields of photovoltaic systems. *Sol. Energy* 116, 12–24. <https://doi.org/10.1016/j.solener.2015.03.039>
- Wild, M., Hakuba, M.Z., Folini, D., Dörig-Ott, P., Schär, C., Kato, S., Long, C.N., 2018. The cloud-free global energy balance and inferred cloud radiative effects: an assessment based on direct observations and climate models. *Clim. Dyn.* 0, 0. <https://doi.org/10.1007/s00382-018-4413-y>
- Xavier, A.C., King, C.W., Scanlon, B.R., 2016. Daily gridded meteorological variables in Brazil (1980–2013). *Int. J. Climatol.* 36, 2644–2659. <https://doi.org/10.1002/joc.4518>
- Xia, X., Zhu, X., Pan, Y., Zhao, X., Zhang, J., 2019. Calibration and optimization of the Ångström-Prescott coefficients for calculating ET₀ within a year in China: The best corrected data time scale and optimization parameters. *Water (Switzerland)* 11, 1–12. <https://doi.org/10.3390/w11081706>
- Yang, Yang, Anderson, M.C., Gao, F., Wardlow, B., Hain, C.R., Otkin, J.A., Alfieri, J., Yang, Yun, Sun, L., Dulaney, W., 2018. Field-scale mapping of evaporative stress indicators of crop yield: An application over Mead, NE, USA. *Remote Sens. Environ.* 210, 387–402. <https://doi.org/10.1016/j.rse.2018.02.020>
- Zandonadi, L., Acquafredda, F., Fratianni, S., Zavattini, J.A., 2015. Changes in precipitation extremes in Brazil (Paraná River Basin). *Theor. Appl. Climatol.* <https://doi.org/10.1007/s00704-015-1391-4>
- Zhang, H., Xin, X., Li, L., Liu, Q., 2015. Estimating global solar radiation using a hybrid parametric model from MODIS data over the Tibetan Plateau. *Sol. Energy* 112, 373–382. <https://doi.org/10.1016/j.solener.2014.12.015>
- Zhang, X., Liang, S., Wang, G., Yao, Y., Jiang, B., Cheng, J., 2016. Evaluation of the reanalysis surface incident shortwave radiation products from NCEP, ECMWF, GSFC, and JMA using satellite and surface observations. *Remote Sens.* 8. <https://doi.org/10.3390/rs8030225>
- Zhang, J., Zhao, L., Deng, S., Xu, W., Zhang, Y., 2017. A critical review of the models used to estimate solar radiation. *Renew. Sustain. Energy Rev.* 70, 314–329. <https://doi.org/10.1016/j.rser.2016.11.124>

CHAPTER 2. THE CLIMATE CHANGE PERSPECTIVE OF ENERGY PHOTOVOLTAIC POTENTIAL IN BRAZIL

ABSTRACT

Renewable energies, and especially solar energy, are part of the strategies that exist in Brazil to satisfy the population's energy demand in a sustainably and contribute to the reduction of global warming. However, it is still unknown how these renewable energy technologies work in the context of climate change. This study assesses climate change's impact on the photovoltaic power potential (P_{PV}) using a recent set of 47 CMIP6 models under the SPP2-4.5 and SPP5-8.5 scenarios. Changes in the atmospheric variables (RSDS, TAS, CLT and RSDSCS), as well as P_{PV} are calculated for the near-term (2021-2050) and end-of-the-century (2071-2100) future, in relation to the historical period (1981-2010). The ensemble of models with the best performances for the historical period are CIESM (M12), MPI-ESM1-2-LR (M39), EC-Earth3-Veg (M22) and FGOALS-g3 (M25), which adequately captured the spatial distribution and the annual cycle of P_{PV} , with slight overestimation in the northern region of Brazil. For the future, the sign of climate change is consistent in both scenarios, but with more intense magnitudes in the SPP5-8.5 scenario for the end-century, and indicate increases in RSDS (brightening), decrease in CLT and RSDSCS, and warming in almost the whole country. For the near-term future, PP_{PV} projects the maximum increases (2 % - 2.5 %) in the SE region, south of the NE region and north of the N region, under both scenarios. On the other hand, the greatest decreases in P_{PV} are projected for the two scenarios of the end-century future (- 3 %), across the country, except for the north of the SE region. Despite the greater availability of solar energy, the sensitivity to the increase in TAS of current P_{PV} systems' technology would not allow increases in the yield of PV energy production. On the contrary, as TAS increases, solar panels' efficiency decreases, canceling the positive effect of the increase in RSDS.

Keywords: CMIP6 models; solar radiation; cloud cover; SSP, renewable energy.

THE CLIMATE CHANGE PERSPECTIVE OF ENERGY PHOTOVOLTAIC POTENTIAL IN BRAZIL

Cristian Felipe Zuluaga^a, Alvaro Avila-Diaz^a, Flavio B. Justino^a, Aaron B. Wilson^{b,c}

^a Department of Agricultural Engineering, Universidade Federal de Viçosa, Viçosa 36570-900, MG, Brazil

^b Byrd Polar and Climate Research Center, The Ohio State University, Columbus 43210, OH, USA

^c OSU Extension – College of Food, Agricultural, and Environmental Sciences, The Ohio State University, Columbus 43210, OH, USA.

2.1.Introduction

One of humanity's great modern challenges is adapting to global warming. The planet's average temperature has increased by approximately 0.85 °C since the pre-industrial period due to the high emissions of greenhouse gases produced by the use of fossil fuels (IPCC, 2014; Tokarska et al., 2020). All climate change mitigation and temperature reduction targets require the participation of carbon-free renewable energy, such as solar energy (Kang et al., 2020). In this, shortwave solar radiation reaching the surface (RSDS) is converted into electrical energy through photovoltaic systems (PV). Between 2010 and 2019, PV systems' total installed capacity increased by 283%, reaching 629 GW, responsible for generating approximately 3% of the global electricity demand (IEA, 2020).

Additionally to the engineering and infrastructure, PV systems' energy production depends on the amount of RSDS available (Jerez et al., 2015). However, there is strong evidence of decadal RSDS variations, which are not related to external factors such as orbital movements or solar activity (Wild, 2012, 2009). The magnitudes and directions of the RSDS changes in the last 40 years differ widely between regions. For instance, RSDS showed a positive decadal trend (brightening) of approximately 6.6 W/m² over the United States and 2 W/m² in Europe (Augustine and Dutton, 2013; Sanchez-Lorenzo et al., 2017). Since 2005, China also showed a brightening of 7.9 W/m² per decade (Li et al., 2018; Zhou et al., 2019), after thirty years of negative trends (dimming) of 2.9 W/m² per decade (Wang et al., 2015). However, over India and Iran, RSDS exhibited average dimming of 3W/m² per decade (Jahani et al., 2018; Soni et al., 2016). The causes of these trends were attributed to two factors, atmospheric aerosol loading

and cloud cover changes. While in the United States and China, brightening was associated with cloud cover decrease, in Europe brightening was caused by aerosol loading reduction. Simultaneously, dimming in the rest of Asia has been linked to the increase in anthropogenic aerosol emissions. However, there are still many uncertainties about how RSDS variability is influenced by cloud-aerosol interaction, different types of clouds and aerosols, and missing *in-situ* observations, among others (Wild, 2016b; Zhou et al., 2019).

It should be stressed that the Earth System Models (ESMs) play an important role in understanding the interactions between RSDS, clouds and aerosols, and estimating possible future changes in these variables (Huber et al., 2016). ESMs have become a useful tool to study the historical and future climate change under different scenarios over the 21st century since they allow understanding each variable's role in the climate system (Wild et al., 2015) separately. The Intergovernmental Panel on Climate Change (IPCC) lead the Coupled Model Intercomparison Project (CMIP) from different research institutes since 1995, which have become the basis for meteorological studies and projection of solar energy resources in various places around the world (Covey et al., 2003).

Wild et al. (2015) used the projections from ESMs from CMIP5 to determine possible RSDS changes by 2050, and their impact on PV systems' global energy production. They found reductions of 1% per year in PV systems potential in most parts of the world except Germany and Spain, which projected an increase in RSDS associated with decreased cloud cover. Zou et al. (2019) analyzed RSDS historical (1985 - 2005) and the projections of PV energy production (2006 - 2100) from 36 ESMs from CMIP5. They determined that, on average, the world would experience a decrease in RSDS of 0.67 kWh/m² per year, highlighting that PV energy installations' efficiency must be improved. Yang et al. (2018) used ESMs from CMIP5 to project possible RSDS and cloud cover changes between 2006 and 2049 over China, and their influence on PV power generation. The results showed that in most of China, the RSDS decreases, reducing PV energy production by approximately 0.04% per year. Müller et al. (2019) quantified the energy yield variations of PV systems expected for the 2060-2080 years using 23 ESMs from CMIP5. They concluded that PV power systems are an attractive investment in Europe under all future climate change scenarios, due to stability in the RSDS values over time.

In Brazil, between 69 and 84% of the electricity consumed is generated by hydroelectric plants (Schmidt et al., 2016). However, the historical and projected variations in precipitation (Avila-Diaz et al., 2020a, 2020b) put at risk the energy supply in the country, making it necessary to seek other sources of electrical energy, such as energy from PV systems, which currently represents 0.02% of the Brazilian electrical matrix (Pereira et al., 2017). Like elsewhere in the world, RSDS over Brazil presents temporal variations. Zuluaga et al. (2021) showed that the RSDS in almost all of Brazil increased (brightening) by approximately 3.2 W/m² per decade during the period 1980-2016. The decrease in cloud cover largely explained this brightening. Jong et al. (2019), using three different downscaled ESMs from CMIP5, found an increase of the RSDS at the northeast and southeast regions of Brazil, between 2030 and 2080, under a high greenhouse gas emissions scenario. Both studies reveal Brazil's potential to generate electricity from PV systems due to the amount of RSDS available. However, some questions still remain, such as the influence of aerosols and cloud-aerosol interaction on the seasonal variability of RSDS, as well as extended projections of these variables throughout the 21st century under different scenarios of climate change based on recent climate models.

Considering that previous studies on this topic were done using CMIP5 future climate projections, the present work evaluates the future solar resource for energy production from PV systems in climate change scenarios using the latest ESMs from CMIP6, which will provide the basis for the IPCC's sixth assessment report (AR6) (Eyring et al., 2016). The first objective of this work is to evaluate how the ESMs from CMIP6 estimate the RSDS spatiotemporal variability and its causes over Brazil in the 1981-2010 historical period. Additionally, using the best models, the second objective is to estimate how the future changes (2015-2100) of RSDS, under two different Shared Socioeconomic Pathways (SSP) scenarios (SSP2-4.5 and SSP5-8.5), would affect the future electricity generation of PV systems in the Brazilian territory.

2.2.Data and methodology

2.2.1. Reference dataset

The ESMs capacity to estimate RSDS over Brazil was examined by comparing ESMs outputs with the fifth generation reanalysis of the European Center for Medium-Range Weather Forecast (ERA5) during the period 1981-2010 (historical period). We assumed the ERA5 reanalysis as reference datasets because it delivered the best performance (with values close to

the observations) in representing the climate variables (e.g., precipitation, temperature and solar radiation) over Brazil during the last fourth decades (Avila-Diaz et al., 2020b; Zuluaga et al., 2021). The RSDS under clear sky (RSDSCS), cloud cover percentage (CLT) and the air temperature (TAS) were also evaluated since these are variables associated with RSDS spatiotemporal changes and PV systems production (Sawadogo et al., 2020a; Zou et al., 2019). The ERA5 dataset has a horizontal spatial resolution of $0.25^\circ \times 0.25^\circ$, hourly time frequency, and covers the period from 1979 to the present (Hersbach et al., 2020).

2.2.2. ESMs from CMIP6

The RSDS, RSDSCS, CLT and TAS have been assessed for both history and the future. We used outputs from 47 ESMs belonging to the Coupled Model Intercomparison Project Phase 6 (CMIP6). The models used here were selected based on the availability of the RSDS, RSDSCS and CLT and TAS variables (see list of models in Table S1). Models were downloaded from <https://esgf-node.llnl.gov/search/cmip6/>.

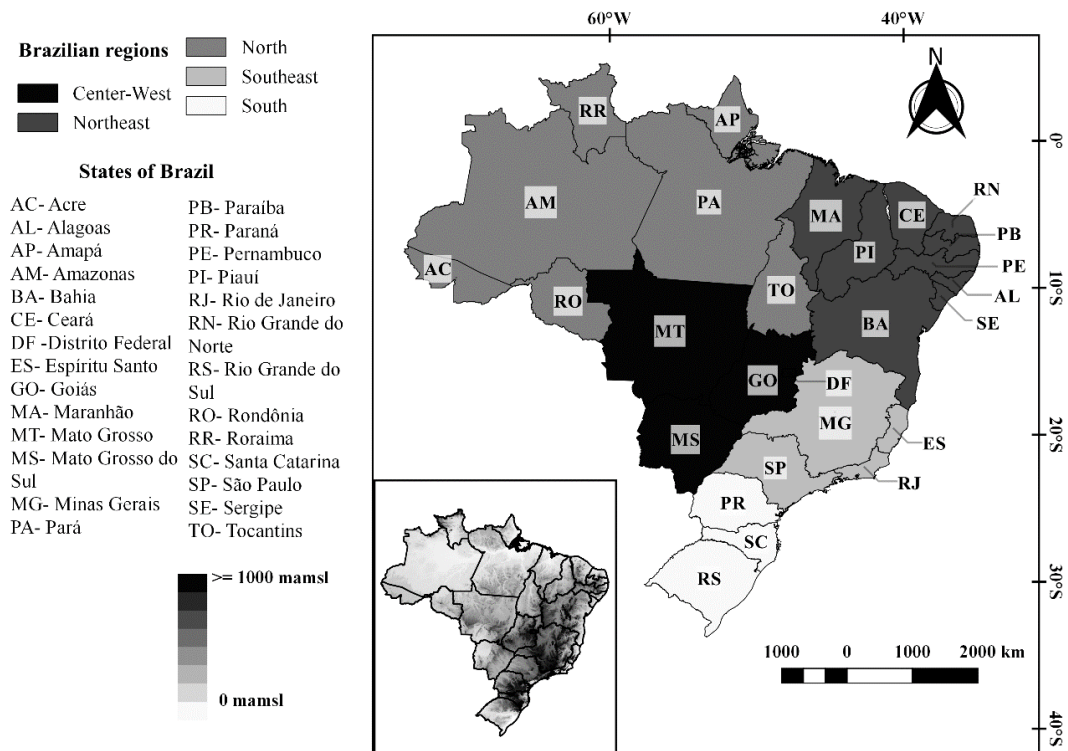
For the historical period, these variables were obtained from the “CMIP6 historical simulations” experiment, defined for the 1850-2014 period, which uses forced simulations by evolving, externally imposed forcings such as solar variability, volcanic aerosols, and changes in atmospheric composition (greenhouse gases and aerosols) caused by human activities (Eyring et al., 2016).

For future climate change projections, CMIP6 developed the Scenario Model Intercomparison Project (ScenarioMIP), run for the 2015-2100 period. The ScenarioMIP experiment consists of a set of pathways driven by a new set of emissions and land use scenarios produced with integrated assessment models (IAMs) based on new future pathways of societal development, namely Shared Socioeconomic Pathways (SSPs), which represents the radiative forcing at the end of the century. There are five SSPs categories: sustainability (SSP1), middle of the road (SSP2), regional rivalry (SSP3) inequality (SSP4) and fossil-fueled development (SSP5); and seven RCPs: 1.9 W/m², 2.6 W/m², 3.4 W/m², 4.5 W/m², 6.0 W/m², 7.0 W/m² e 8.5 W/m² (Keeble et al., 2020; O’Neill et al., 2016). In this work, we focused on the 1981–2010 period as present-day reference conditions common to two future periods, 2021–2050 (near-term) and 2071–2100 (end-century). Each period was studied under two SSPs scenarios: 1) SSP2-4.5 (or RCP 4.5 W/m²) that represents a combination of social vulnerability with an

intermediate level of forcing, and seems to be more consistent with reality, producing a radiative force of 4.5 W/m^2 during the 21st century. 2) SSP5-8.5 (or RCP 8.5 W/m^2) that represents the most pessimistic and catastrophic scenario on climate change in the literature, with emissions high enough to produce a radiative force of 8.5 W/m^2 in 2100. More details about the ScenarioMIP and SSP scenarios can be found in O'Neill et al. (O'Neill et al., 2016).

2.2.3. Ranking of the ESMs performance.

To facilitate the intercomparison between ESMs and reference datasets, all variables were regridded to a common spatial horizontal resolution of 1° by bilinear interpolation, to maintain homogeneity in all data sets. The Multi-Model Ensemble (MME; ID: M48) was also evaluated to reduce individuals ESM variability. The results presented in this study are based on annual, seasonal and monthly averages, and were analyzed for North (N), Northeast (NE), Center-West (CW), Southeast (SE) and South (S) regions, as shown in Figure 1. The seasons for the analysis are autumn (March – May; MAM), winter (June – August; JJA), spring (September – November; SON) and summer (December – February; DJF).



The performance of the models was determined using the Kling-Gupta Efficiency (KGE) metric (Eq. 1), which is a combination of three components: the correlation coefficient (r ; Eq. 2), the bias ratio (β ; Eq. 3) and the variability ratio (γ ; Eq. 4).

$$KGE = 1 - \sqrt{(r - 1)^2 + (\beta - 1)^2 + (\gamma - 1)^2} \quad (1)$$

$$r = \frac{\sum_{i=1}^N (O_i - \bar{O})(P_i - \bar{P})}{\sqrt{\sum_{i=1}^N (O_i - \bar{O})^2} \sqrt{\sum_{i=1}^N (P_i - \bar{P})^2}} \quad (2)$$

$$\beta = \frac{\mu_P}{\mu_O} \quad (3)$$

$$\gamma = \frac{CV_P}{CV_O} \quad (4)$$

where P is the modeled value, O is the reference value, N is the number of observations, μ is the mean value and CV is the coefficient of variation. KGE and its components close to one (+1.0) indicate higher simulation ability of the models.

Once the metrics of statistical performance were obtained, the ESMs were classified according to a comprehensive ranking, which classifies the models from the best (1) to the worst (47) based on the KGE values (and its components) accumulated for each region and each variable.

2.2.4. Projections of PV power potential

In this section, we used the methodology proposed by Crook et al. (2011), in which PV energy systems generation fundamentally depends on battery materials, sunshine and ambient temperature. This methodology is widely used in studies about PV systems potential (Bazyomo et al., 2016; Jerez et al., 2015; Wild et al., 2015; L. Yang et al., 2018; Zou et al., 2019). This approach estimates changes in PV energy systems generation due to changes in RSDS and in TAS. According to Wild et al. (2015), it is a simplistic approach. Still, it provides a good approximation of the order of magnitude of the impact of the projected changes in solar radiation and temperature on PV systems' potential.

The PV energy potential (P_{pv}) can be obtained as follows:

$$P_{pv} = RSDS \times n_{ef} \quad (5)$$

Where n_{ef} is the efficiency of the PV panel and is calculated as follows:

$$n_{ef} = 1 + \gamma (T_{cell} - T_{ref}) \quad (6)$$

Where γ is a constant that depends on the panel material and structure. T_{cell} and T_{ref} are the cell and the reference temperatures. According to previous studies (Sawadogo et al., 2020b; Wild et al., 2015; L. Yang et al., 2018; Zou et al., 2019) for monocrystalline silicon modules, $T_{ref} = 25^\circ\text{C}$ and $\gamma = -0.005$. Cell temperature may be expressed as:

$$T_{cell} = c_1 + c_2 T_{as} + c_3 RSDS \quad (7)$$

Where $c_1 = -3.75^\circ\text{C}$, $c_2 = 1.14$ and $c_3 = 0.0175^\circ\text{Cm}^2/\text{W}$ for monocrystalline silicon module.

The photovoltaic energy potential (P_{PV}) was calculated using the ensemble of the four best-performing models. Like the atmospheric variables, P_{PV} was calculated for the historical period and for the near-term and end-century periods under the 2-4.5 and 5-8.5 SSPs. Projected changes were determined using the difference between the future and historical periods, expressed in absolute values (for atmospheric variables) and percentages of the reference values (PV energy potential). The statistical significance of the simulated changes was assessed at the 95% confidence level based on a student t-test.

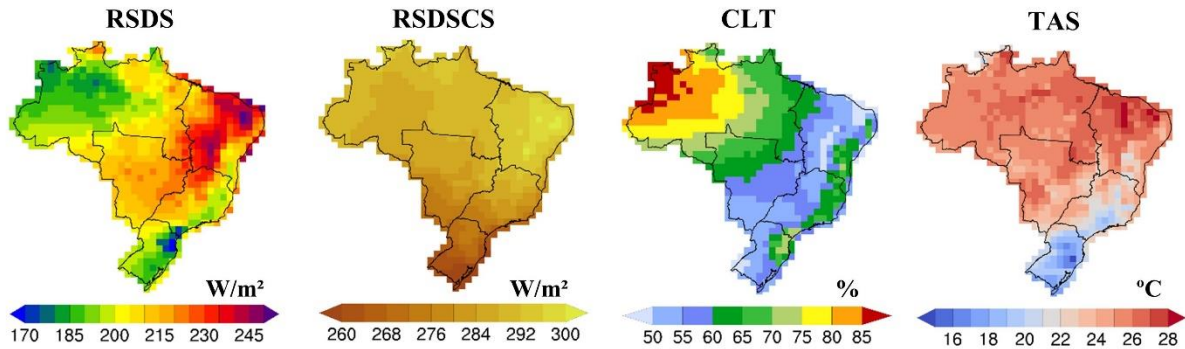
2.3.Results

2.3.1. Climatology and observed trends of atmospheric variables

Fig. 2 presents the mean annual climatology values and the decadal trends of RSDS, RSDSCS, CLT and TAS, delivered by ERA5 during the 1981-2010 period. As a complement

to the previous one, Fig. S1 and S2 show the climatologies and decadal trends on the seasonal scale of the same atmospheric variables as in Fig. 2

a) Climatology



b) Decadal Trends

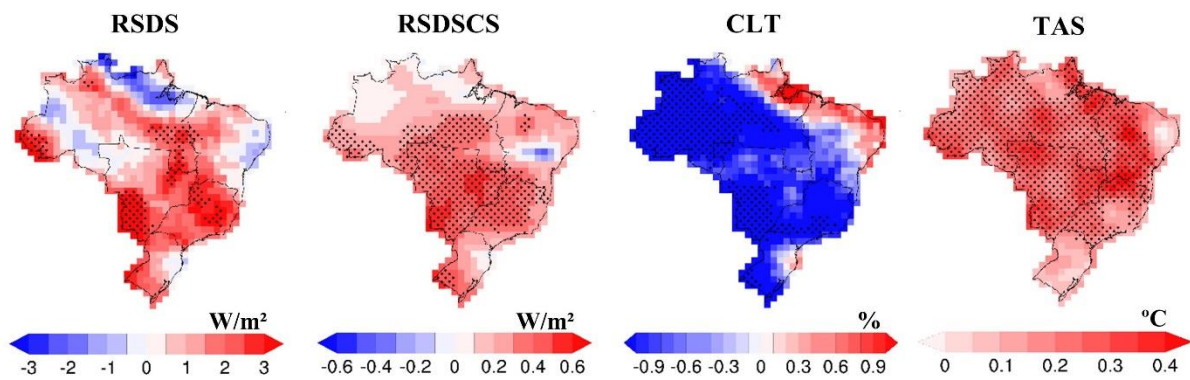


Figure 2. a) Annual mean climatology and b) decadal trends of the RSDS, RSDSCS, CLT and TAS over Brazil during the historical period (1981 – 2010). In trend maps, dots indicate statistical significance at the 95% level. Reference dataset: ERA5.

RSDS displays the highest annual values in the NE region ($> 220 \text{ W/m}^2$, Fig. 2a), with maximum seasonal values (280 W/m^2), and minimum values (180 W/m^2) during JJA (Fig. S1a). The N region has RSDS values that range from the East (210 W/m^2) to the West end (180 W/m^2). In the N region, the period with the highest RSDS value corresponds to JJA and SON seasons (Fig. S1a). The CW region shows a more homogeneous RSDS distribution, with an average annual value of 215 W/m^2 (Fig. 2a). The topography of the SE region clearly marks a spatial gradient of RSDS between the east side and the west side of the mountains (from 190 to 240 W/m^2 , Fig. 2a). The lowest RSDS values in Brazil correspond to the S region ($< 200 \text{ W/m}^2$, Fig. 2a). The seasonality of RSDS in the CW, SE and S regions is very similar, with the highest values in DJF and the lowest in JJA (Fig. S1a). Regarding RSDS trends (Fig. 2b) – except for

the north and west of the N region, and the coast of the NE region - Brazil (especially over the SE region) experiences an increase (brightening) that varies between 2 - 3 W/m² per decade. Brightening is mainly strong during JJA and SON (Fig. S3a).

RSDSCS is modulated mainly by water vapor and aerosols, which can absorb and/or spread atmospheric radiation, and consequently modify RSDS (Zhang and Ma, 2020). In conditions of low concentration of aerosols and water vapor, RSDSCS depends mainly on seasonal variations caused by changes in the zenith angle and solar declination (Hogan and Hirahara, 2016). This is the case in Brazil, where the RSDSCS values range from 260 W/m² over S region to 300 W/m² over NE region (Fig. 2b); with maximum values during summer and minimums in winter (Fig. S1b). Fig. 2b shows positive trends of RSDSCS for the whole country, suggesting that aerosols have a low impact on the radiation spread/absorption in Brazil.

Fig. 2a also shows that CLT over Brazil is mainly concentrated in the N region and in the north of the CW region, with values above 70%. There is a band of low cloud cover (< 50 %) that covers the southeast of the CW region and the total of the NE, SE and S regions (except for mountain areas). The CLT seasonality (Fig. S1c) shows that DJF is the period of greatest cloudiness in most of Brazil, related to the South Atlantic Convergence Zone (SACZ) that begins in the Amazon region and spreads towards the CW, SE and S during the southern summer (Kodama et al., 2012). In contrast, in JJA the clear sky predominates. In general, CLT decreases throughout the Brazilian territory (except on the NE coast, Fig. 2b), which explains the generalized increase in RSDS. It is noteworthy that only at the MAM season there is an increase in CLT over the border of the N, NE, CW and SE regions, suggesting a possible increase in precipitation (Fig. S2c).

TAS presents average annual values between 25 and 29 °C in the N, NE and CW regions (Fig. 2a) with low seasonal variability (Fig. S1d). In the S (SE) region, TAS shows an average value of 18 °C (24 °C) (Fig. 2a), with a strong seasonal variation ranging from 12 °C (18 °C) in the JJA, to 26 °C (28 °C) during DJF (Fig. S1d). There is a statistically significant decadal increase in the average annual temperature across the country, which varies between 0.1 and 0.4 °C, with the main emphasis on the CW and N regions (Fig. 2b). This warming takes place mainly at JJA and SON seasons (Fig. S2d).

2.3.2. Performance of CMIP6 models

The performance of ESMs from CMIP6 in representing the annual average values of RSDS, RSDSCS, CLT and TAS, in relation to ERA5 in the period 1981–2010, is summarized by the statistical metrics of Fig. 3. Figures S3 to S6 are presented the same statistical metrics, but on a seasonal scale.

Regarding RSDS estimates, KGE values can be considered low (< 0.5 , Fig. 3a). In general, the models perform better in the SE region with 0.44 (M22) $> KGE > -0.49$ (M8), and the worst performances in the N region with 0.24 (M46) $> KGE > -0.44$ (M10). Although the models exhibit a wide variability of performances between regions, M22 (EC-Earth3-Veg) has the best KGE five regions average (0.15), with the highest value in the CW (0.47) and the lowest in the S (-0.20). The low KGE values can be explained in large part by the low correlations ($r < 0.5$) between observed and modeled RSDS (Fig. 3b). In general, the r values were negative and very close to zero, which indicates opposite trends and discrepancies in the extreme values, respectively. In addition to the previous one, the highest r values coincide with the best KGE performances, with M22 standing out in the average of the five regions ($r = 0.17$), with the highest value in the CW region (0.48 - statistically significant) and the lowest in the S region (-0.20). The bias ratio (Fig. 3c) shows a slight overestimation of most models in all regions, but still very close to one, demonstrating the models' good ability to estimate average annual values of RSDS. The highest overestimation (underestimation) of RSDS is shown by M4 (M7) in the N (SE) region with $\beta = 1.26$ ($\beta = 8.30$). In terms of variability (γ , Fig. 3d) the EMSs show, in general, less mean annual RSDS variability of than the observations ($\gamma < 0.8$), except for models 44, 43 and 44 that reach the ideal value ($\gamma < 1.0$) in at least 3 regions each. Analyzing on a seasonal scale (Fig. S3 - S6) it is noted that KGE values are mainly affected by an underestimation during DJF ($\beta < 1.00$) and a marked overestimation ($\beta > 1.00$) during JJA and SON. In addition to the previous one, there is a predominance of weak (negative) correlations in MAM (JJA). It is interesting to note that the Multi-Model-Ensemble (M48) exhibits the worst results in all statistical metrics over all regions, showing a greater weight of poor performance models and clarifying the need to classify and select only the best models.

In the case of the RSDSCS annual average estimates, there are strong performance contrasts between the models (Fig. 3a), with KGE values ranging from 0.89 in the N (M4) to -2.20 in the CW (M34). The worst performances of the models ($KGE < 0$) are concentrated in JJA and SON (Fig. S3), probably associated with the season of high aerosol emissions due to

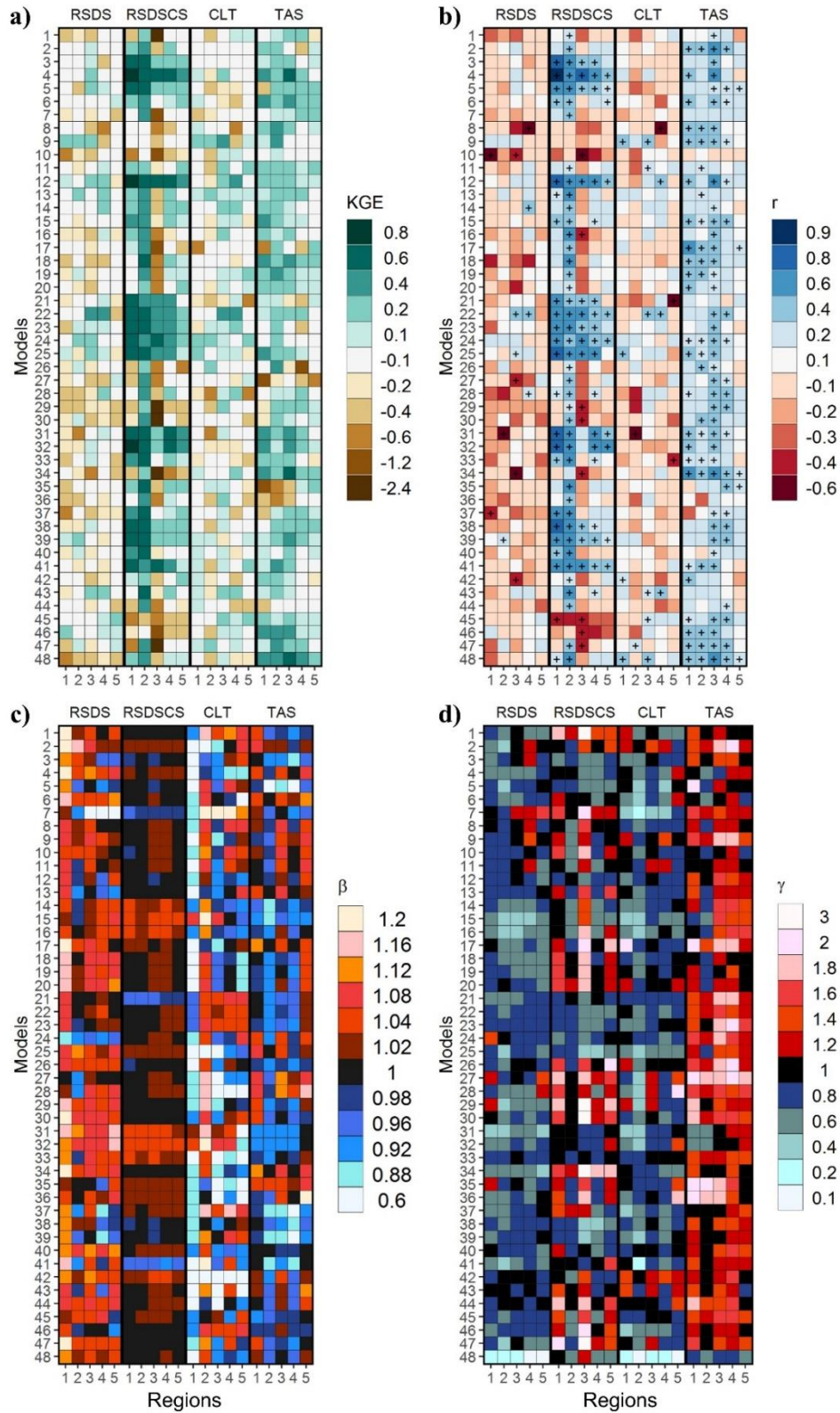


Figure 3. Statistical performance for RSDS, RSDSCS, CLT and TAS for 47 ESMs from CMIP6 and a Multi-model-ensemble (M48), during the historical period (1981 – 2010) over Brazil. a) KGE, b) Correlation coefficient (r), c) Bias ratio (β) and d) Variability ratio (γ). Lower horizontal axis represents the North (1), Northeast (2), Center-West (3), Southeast (4) and South (5) regions. Left vertical axis shows the ESMs. Crosses indicate statistically significant correlations at the 95% level.

the burning of vegetation in the N and CW regions (Reis et al., 2018; Silva et al., 2020), which affects atmospheric transparency in other regions of the country and consequently the RSDSCS values. The consistency of the ESMs in the estimation of RSDSCS stands out, since those models with good performance are able to maintain this pattern for all regions (e.g., M4, M12). Analyzing the components r , β and γ (Fig. 3b-d), it is observed that the factor that weighed more for the best models did not reach ideal KGE value, was their inability to simulate the variability of RSDSCS (Fig. 3d) underestimating it during DJF-MAM and overestimating it during JJA-SON (Fig. S6). On the other hand, most models with poor performance show a combination of $r < 0.1$ and $\gamma > 1$ values (Fig. 3b and d). M48 shows better results in KGE compared to RSDS; however, there is still a very large weight in the drop in performance due to the worst models (e.g., CW region).

The KGE values in the CLT's simulation (Fig. 3a) are similar to the findings in the RSDS's simulation, showing the strong relationship between these two variables. The SE region presents better performance of the models with $0.47 \text{ (M22)} > \text{KGE} > -0.17 \text{ (M5)}$. The M9 (CESM2-FV2) has the best KGE average of the five regions (0.20), with the highest value in CW (0.45) and the lowest in S (-0.23). The predominance of values of $r < 0.20$ (Fig. 3b) is essential to understand the weak statistical performances, since the worst KGE values coincide with the values of r furthest from 1 (e.g., M21 in S, M31 in NE). On the other hand, the CLT underestimation ($\beta < 1$, Fig. 3c) explains the overestimation of the RSDS values described above, and may indicate an underestimation of precipitation by the models, which has already been found in other studies that used models derived from the CMIP5 (Avila-Diaz et al., 2020a; Díaz and Vera, 2017; Vasconcellos et al., 2020). Seasonally, the underestimation of CLT is strongly marked during JJA and SON (Fig. S5). The γ values show that the models underestimate the CLT variability (Fig. 3d) mainly during DJF, a period that corresponds to the highest activity of the SACZ. According to Vasconcellos et al. (2020), underestimation of CLT by EMSs is usually associated with incorrect representations of availability of moisture for convection, which, in turn, are linked to a negative bias in sea surface temperature (SST) in the Atlantic Tropical north, inducing changes in the strongest trade winds.

In general, the EMSs present acceptable performances in estimating TAS in all regions of the country ($\text{KGE} > 0.10$, Fig. 3a), with the exception of M26 in SE ($\text{KGE} = -0.62$); M27 in N ($\text{KGE} = -0.69$) and S ($\text{KGE} = -0.44$), and M35-36 in the N ($\text{KGE} < -0.40$), NE ($\text{KGE} < -0.54$) and CW ($\text{KGE} < -0.24$) regions. The models that exhibit the highest KGE values are M15 in N

(0.55), M19 in NE (0.58), M34 in CW (0.65) and SE (0.40), and M5 in S (0.36). Seasonally (Fig. S3), the worst performances are observed during the autumn season (MAM) in the CW, SE and S regions. KGE values are mainly affected by a slight cold trend in the models associated with underestimations ($\beta < 1$, Fig. 3c) and a considerable overestimation of the variability in relation to the observations ($\gamma > 1.0$). In this one-off case, M48 shows robust and consistent simulations over all regions, compared to individual models, especially at JJA and SON stations (Fig. S3-S6).

2.3.3. Classification of EMSs

Considering the wide variety of performances between the EMSs over the different regions - reflected in the low KGE of M48 - as well as the low consistency between the estimates of the atmospheric variables, we adopted a comprehensive ranking that allows to choose the appropriate models for our analyzes. Fig. 4 presents the results of the model ranking that covers the four variables analyzed in the previous section, for all of Brazil. Each model is rated from 1 (best) to 47 (worst) based on the KGE results. A cumulative classification score for the four atmospheric variables (RSDS, RSDSCS, CLT and TAS) is calculated and represented in columns of different lengths, where the shorter ones mean lower cumulative classification and, therefore, better performance of the model. The classification is made for each region of the country (Fig. S7) and based on these, a ranking for the whole of Brazil is constructed (Fig. 4).

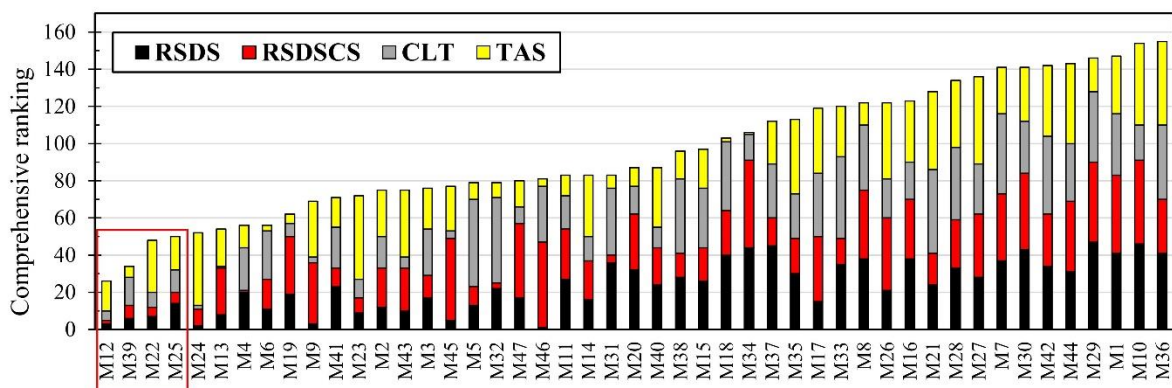


Figure 4. Comprehensive ranking based on KGE performance of ESMs calculating RSDS, RSDSCS, CLT and TAS. The y-axis represents the accumulation of ESMs ranking for the atmospheric variables. The first four ESMs are inside the red rectangle

Analyzing the proportional magnitude of each variable, the first four models in the ranking are selected: M12 (CIESM), M39 (MPI-ESM1-2-LR), M22 (EC-Earth3-Veg) and M25 (FGOALS -g3). It is observed that at least one of the four models appears among the top three classified in each region (Fig. S7). Additionally, our results show that the spatial resolution is not a good indicator of the model's performance, since no model is consistent across all regions or all variables. The previous one agrees with the findings by Akinsanola et al. (2020).

2.3.4. PV power potential (P_{PV}) during the historical period

Fig. 5 shows the P_{PV} potential in Brazil for the historical period calculated from the ERA5 reanalysis and the CMIP6 models. For the latter, the Optimal Model Ensemble (OME, hereafter) is used, composed of the four best ESMs, selected in the previous section.

The N region exhibits values that vary between 1270 kWh/m² year in the West (State of AM) and 1420 kWh/m² year in the East (the States of PA and TO; Fig. 5). These values follow the CLT distribution, which has high values over the Amazon basin, associated with biome's high evapotranspiration (Angelini et al., 2011). The annual cycle per month (Fig. 5b) shows a strong variability linked to the distribution of annual rainfall in the region (Alves et al., 2017), with low P_{PV} values (≈ 105 kWh/m² month) during the wet season (Jan-Jun) and high P_{PV} values (≈ 120 kWh/m² month) during the dry season (Jul–Dec). The NE region has the highest P_{PV} in the entire country during the historical period, with values above 1450 in the entire region, concentrated mainly in the states of CE, PI and BA (Fig. 5a). In the annual cycle (Fig. 5c), the highest values correspond to June (110 kWh/m²) and the lowest to October (137 kWh/m²). The second region with the greatest P_{PV} is CW, with annual values of up to 1500 kWh/m² year in the state of GO (Fig. 5a). The maximum values (Fig. 5d) occur during SON and DJF (≈ 127 kWh/m² month) and the weakest during MAM and JJA (≈ 114 kWh/m² month). In the SE region, the P_{PV} distribution is defined by the topography (Fig. 5a), with the minimum values (< 1350 kWh/m² year) located on the east side of the mountain region, and the maximum values (> 1450 kWh/m² year) in the west. In this region, in the middle of summer (February), the highest P_{PV} value (134 kWh/m²) appears, while the minimum value occurs in June (97 kWh / m²; Fig. 5e), during winter. Along with the N region, the extreme south of Brazil - the S region - has the lowest P_{PV} values (< 1250 kWh/m² year) in the state of SC and east of PR (Fig. 5a). This region experiences the greatest amplitude of the seasonal cycle (Fig. 5f), with maximum during DJF (141 kWh/m² month) and minimum during JJA (84 kWh/m² month).

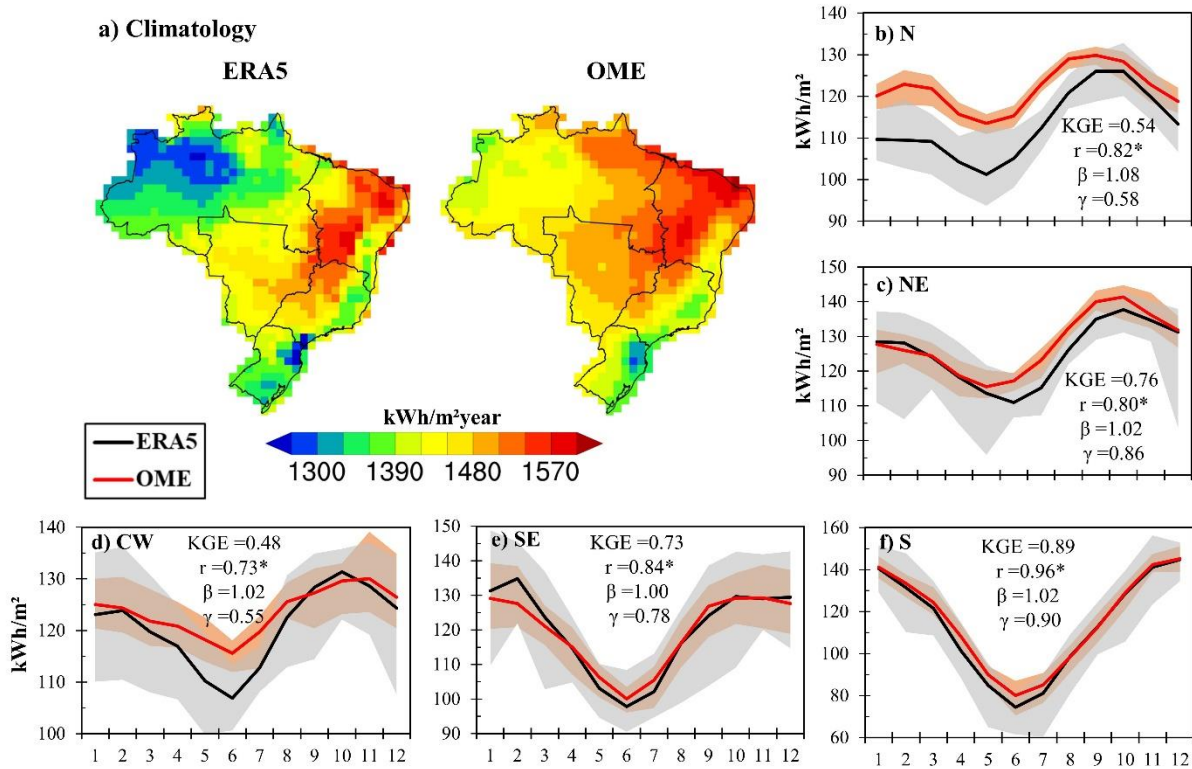


Figure 5. Climatology of annual potential PV systems (a), and mean annual PV potential generation cycle by month for the b) N, c) NE, d) CW, e) SE and f) S regions, from ERA5 and OME over Brazil during the historical period (1981 – 2010).

As far as simulated values are concerned, in general OME exhibits a spatial distribution of P_{PV} very close to that from ERA5, with the exception of overestimations in the west of the N region, and in the north of the CW region (Fig. 5a). In the case of region N, overestimation of P_{PV} persists throughout the annual cycle (Fig. 5b), with a greater bias during the wet season (≈ 11 kWh/m² month) than in the dry season (≈ 6 kWh/m² month). In the CW region, overestimation occurs between the months of March and August with an average bias of 5 kWh/m² month. This is reflected in the performance of OME in the N and CW regions, with KGE values below 0.55. In general, OME underestimates the P_{PV} variability ($\gamma < 1$) in all regions. In the NE, SE and S regions, OME performs well ($KGE > 0.75$), confirming that the conformation of an ensemble with only the best models was a correct decision. The P_{PV} distribution values found in this study (ERA5 and OME) are very close to those delivered by the Solargis platform for Brazil (<https://solargis.com/maps-and-gis-data/download/brazil>) which it provides solar radiation data since 2010, and is widely used for P_{PV} studies.

2.3.5. Projected changes and climate scenarios

Although we consider two future periods, in the main body of this work, we focus on the near-term future (2021-2050) for two reasons: 1) the uncertainties of climate projections increase as they approach the end of the century, as the model errors accumulate during the simulation years. 2) We consider it very likely that the P_{PV} technology will continue until 2050 and, therefore, the constants assumed in section 2.4 fit into a realistic approach. On the other hand, it is unlikely that this same technology will be maintained until the end of the century.

2.3.5.1. Atmospheric variables

Figs. 6 and 7 illustrate the projected annual and seasonal changes in the variables RSDS, CLT, TAS and RSDSCS for the near-term future (2021 - 2050) in relation to the base period (1981–2010) under the SSP2.4-5 and SSP5-8.5 scenarios. The changes projected for the end-century future (2081–2100) are in the Supplementary Material (Figs. S8 and S9).

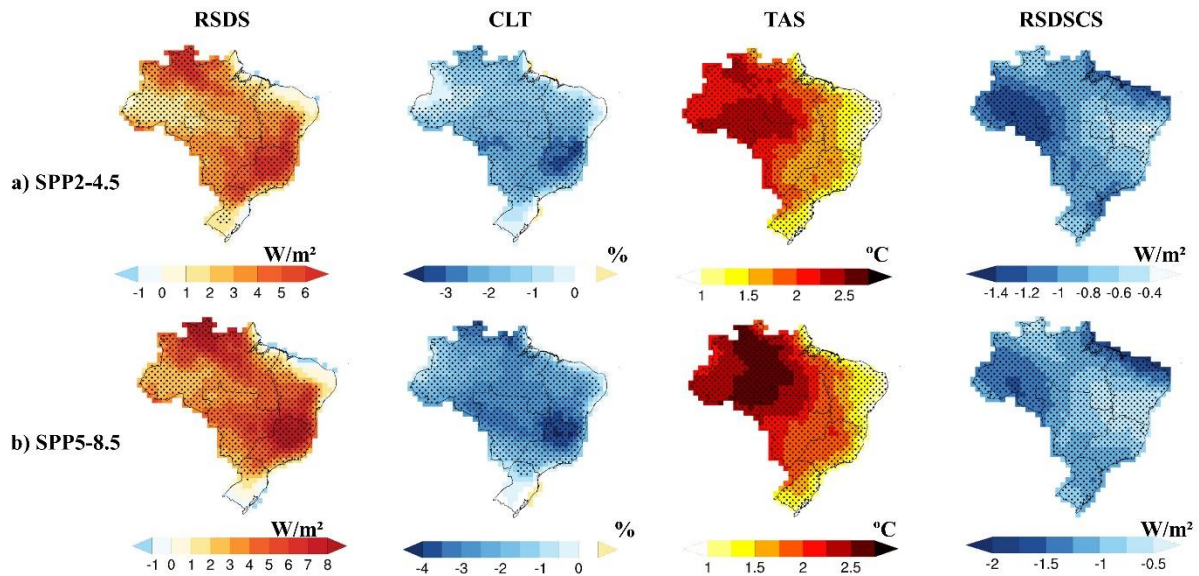


Figure 6. Projected changes from OME in the annual mean of RSDS, CLT, TAS and RSDSCS for the near-term future (2021 – 2050) relative to the historical period (1981 – 2010), under a) SSP2-4.5 and b) SSP5-8.5 scenarios. Significant differences at the 95% level of changes are dotted.

In Fig. 6a, the OME projects a statistically significant increase in RSDS (brightening) in most of the country, with the exception of the north coast of the NE region, with a decrease of up to 1 W/m² (States of CE, RN, PA and PE) and the extreme south of Brazil (unchanged).

The most notable increases in RSDS ($> 6 \text{ W/m}^2$) are in the north of the N region (state of RR), south of the NE region and in the SE region. Under the SSP5-8.5 scenario (Fig. 6b) the same brightening pattern is maintained, but with values that exceed 8 W/m^2 . The projected increases in RSDS under both scenarios are clearly related to the decrease in CLT in the Brazilian territory, mainly concentrated in the SE and northern N regions, with reductions of over 4%. On the other hand, slight or nonexistent increases (west of the N region and south of S) or decreases in RSDS, are related to drastic reductions in RSDSCS, probably explained by the increase in aerosols from biomass burning (region N), marine (region NE) and urbanization (region S). In addition, there is a general warming throughout the country that increases from the coast towards to the interior. The biggest warms are in the N region with 2°C and 2.5°C under SSP2-4.5 and SSP5-8.5, respectively. The temperature results are in agreement with those found by (Avila-Diaz et al., 2020b). For the end of the century (Fig. S8), there is an amplification of the magnitudes of the trends found in the period 2021-2050, however, TAS shows a very large warming focus in the west of the region N under the SSP2-4.5 scenario, while under SSP5-8.5, heating is more distributed in this region, and in general, throughout Brazil.

Fig. 7 shows when the changes in the atmospheric variables described in Fig. 6 were most accentuated in the annual cycle. In the N region, it can be seen that the largest increases (decreases) in RSDS (CLT) occur during the wet season (Jan-Jun), which may suggest a change in the rainy season. RSDSCS exhibits the greatest reductions in September and October, when biomass burns occurs in the region, which generate aerosol emissions (Pivello, 2011), when TAS also presents the largest increments. Reductions in RSDS over the coast of NE region occur in the first quarter of the year, associated with the increase in CLT and large decreases in RSDSCS. The CW region exhibits the greatest reduction in CLT between August and October, which coincides with an increase in RSDS and TAS in this period. During SON and DJF there are increases (decreases) of RSDS (CLT) in the SE region, which may indicate changes in the behavior of the SACZ, the main responsible for precipitation during this time in the region. The reductions (increments) of RSDS in the S region occur during winter (summer), showing an increase in the amplitude of the seasonal cycle. In general, warming is constant throughout the year in all regions ($\approx 2^\circ\text{C}$). The SSP2-4.5 and SSP 5-8.5 scenarios (in both futures) show the same sign, only differing in magnitudes for all variables.

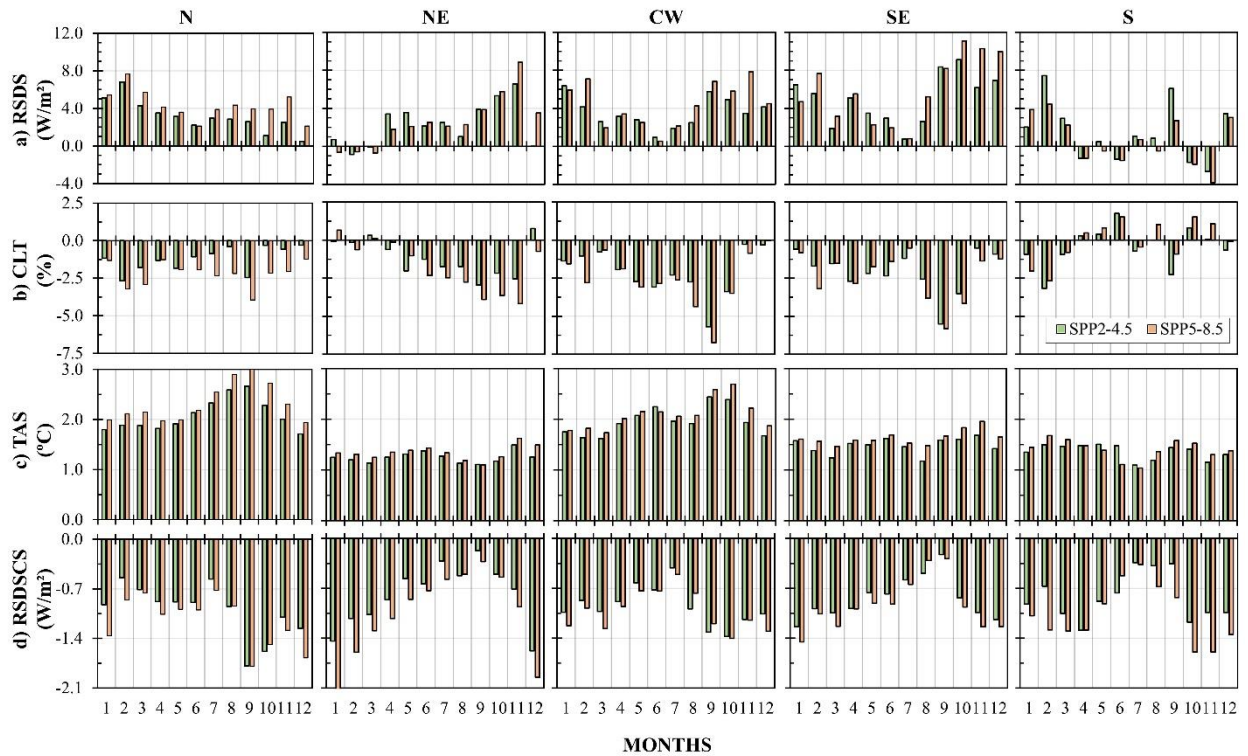


Figure 7. Projected changes to the near-term future (2021-2050 versus 1981-2010) from OME in the annual cycle by month of a) RSDS, b) CLT, c) TAS and d) RSDSCS over five Brazilian regions under SSP2-4.5 (green) and SSP5-8.5 (orange) scenarios

2.3.5.2. PV power potential

Fig. 8 illustrates the annual and monthly changes in PV power potential in Brazil under the SSP2-4.5 and SSP 5-8.5 scenarios in the near-term future compared to the historical period. Similar to the observed pattern in the atmospheric variables, both scenarios present the same general P_{PV} distribution pattern, with differences only in its magnitudes.

In Fig. 8a, the country presents two contrasting projections for the period 2021-2050 in both scenarios, with positive changes (2 - 2.5%) in the north of N, south of NE, and SE; and negative changes in the south of N, north coast of NE and extreme south of the country. On the one hand, the increases in P_{PV} are due to increases in RSDS (Fig. 6a) in the States of RR (N region), BA (NE region), MG, ES, RJ and north of SP (SE region). On the other hand, the decreases in P_{PV} can be explained by the significant warming and reduction of RSDSCS projected in the States of AC, RO and south of AM and PA (Fig. 6a); and the decrease in RSDS on the coast of the NE and in the extreme south of Brazil (Fig. 6a). Positive changes in the N region (Fig. 8b) occur

during the first quarter of the year, while negative changes occur in the second half, unlike in the NE region (Fig. 8c). The SE region shows positive changes throughout the year (except in July) that reach values of up to 2.5% during SON (Fig. 8e) when CLT shows the maximum reductions (Fig. 7b). Although the S region shows a general reduction in PV power potential, during February (summer) and September (spring) it projects increases of 1% and 2% respectively (Fig. 8f) under the SSP2-4.5 scenario, located in the state of PR (Fig. 8a). For the end-of-the-century future (2071 - 2100), the generalized reduction of the P_{PV} (Fig. S10a) shows the negative sensitivity of the technology of the PV generation systems to the increase in TAS, including over the influence of the increase in RSDS. By the end-of-the-century, the reductions in the N, NE and S regions have intensified, reaching values above 3%. The increases in P_{PV} ($\approx 1.5\%$) in the SE region are only concentrated in a reduced part of the state of MG during SON and DJF, under the SSP5-8.5 scenario (Fig. S10e).

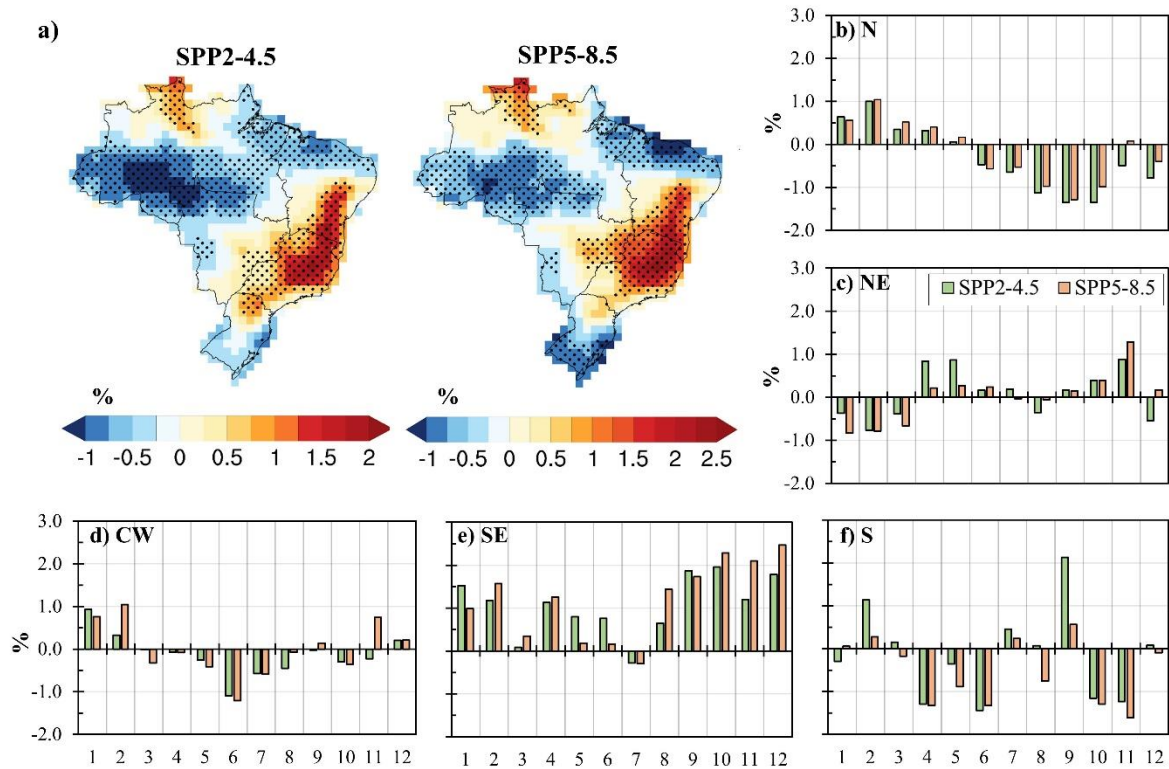


Figure 8. Projected changes in annual potential PV systems (a), and in PV potential generation cycle by month for the b) N, c) NE, d) CW, e) SE and f) S regions, to the near-term future (2021-2050 versus 1981-2010) from OME under SSP2-4.5 (green) and SSP5-8.5 (orange) scenarios. In maps (a), significant differences at the 95% level of changes are dotted.

2.3.5.3. Contribution of RSDS and TAS to projected P_{PV} changes

To better understand the role that TAS and RSDS play in the projections of the P_{PV} changes, it is necessary to separate the isolated contribution of each variable. For this, the P_{PV} is recalculated for two conditions:

1) $P_{pv}(\Delta RSDS)$: Estimates the P_{PV} , maintaining the historical values of TAS and varying only RSDS under the two SSPs.

2) $P_{pv}(\Delta TAS)$: It conserves the historical values of RSDS and varies TAS to compute P_{PV} under the two SSPs.

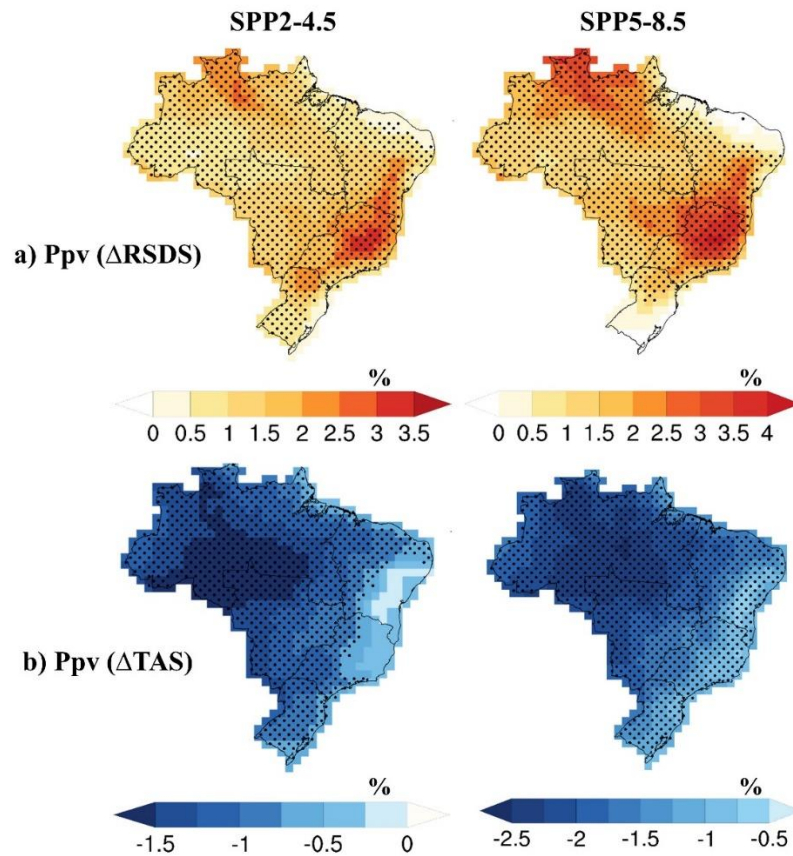


Figure 9. Projected changes in potential PV generation by a) isolated variation of RSDS ($P_{pv}(\Delta RSDS)$) and b) Isolated variation of TAS ($P_{pv}(\Delta TAS)$) for the near-term future (2021-2050 versus 1981-2010) from OME under SSP2-4.5 and SSP5-8.5 scenarios. Dots indicate significant differences at the 95% level.

Fig. 9 shows the results of individual contributions from RSDS and TAS in the P_{PV} changes projections for the 2021 - 2050 period under the scenarios SSP2-4.5 and SSP5-8.5. The

results for the 2071 - 2100 period are shown in Fig. S11. If TAS remains constant, the projections of the P_{PV} show an increase in almost the whole country ($> 1\%$, Fig. 9a) due to the RSDS increments (Fig. 6). For example, in the SE region, RSDS contributes to P_{PV} growth of up to 3.5% (SSP2-4.5) and 4% (SSP5-8.5). The only places that do not change are the NE coast (under the two SSPs) and the extreme south of the country (under SSP5-8.5). Figs 9b and S11b show that TAS makes a negative contribution to the P_{PV} , which increases as the warming level increases. Thus, it is observed that the N and CW regions suffer the greatest reductions in P_{PV} , with up to -1.5% (SSP2-4.5) and -2.5% (SSP5-8.5) for the near-term future, and lower to -9% for the end-of-the-century future. In the case of NE and SE regions - with high PV power potential - it can be seen that the increases in TAS cancel the positive influence of the increase in RSDS under all scenarios. Our results are in agreement with many others studies (Crook et al., 2011; Jerez et al., 2015; Müller et al., 2019; Sawadogo et al., 2020a, 2020b; Zou et al., 2019) that show that the heating of the ambient temperature (increase of TAS) decreases the efficiency of the solar cells; and consequently the P_{PV} .

2.4. Discussion and conclusions

This study estimated the potential impacts of climate change on the photovoltaic power potential under the climate change scenarios SSP2-4.5 and SSP5-8.5 to better understand the strengths/weaknesses of using solar energy in the coming years in Brazil. Four atmospheric variables that determine the efficiency of the PV systems (RSDS, CLT, TAS and RSDSCS) from 47 ESMs from CMIP6 - with different spatial resolutions - were evaluated compared to the ERA5 reanalysis during the historical period (1981-2010). The KGE statistical performance indicator for the model set was analyzed on annual and seasonal scales for five Brazil regions.

The statistical evaluation showed that, in this case, the spatial resolution is not a good indicator of the models' performance. Overall, ESMs showed good consistency across regions for TAS and RSDSCS. For RSDS and CLT (closely linked variables) the performances of the ESMs were very heterogeneous between the regions, with the best results in the SE and NE regions, and the worst in the N and S regions. The limitations were mainly related to the underestimation of variability, biases positive and weak correlations. Two rankings were built from the statistical results covering the models' performance in the simulation of the four atmospheric variables – one for each region and another for the whole country. These rankings

concluded that the four best models were CIESM (M12), MPI-ESM1-2-LR (M39), EC-Earth3-Veg (M22) and FGOALS- g3 (M25).

An Optimal Model Ensemble (OME) was calculated from the best four models, used to estimate the historical P_{PV} and for two future periods: near-term (2021-2050) and end-of-the-century (2071-2100) under the SSP2-4.5 and SSP5-8.5 scenarios. The regions with the highest annual P_{PV} are NE, CW and SE ($> 1400 \text{ kWh/m}^2 \text{ year}$), mainly between July and January ($> 110 \text{ kWh/m}^2 \text{ month}$).

Future climate projections showed the same sign in all scenarios and periods, but with different magnitudes in the RSDS increments (brightening) throughout the Brazilian territory (except the northern NE and southern coast of the country), decrease in CLT and RSDSCS, and warming throughout Brazil, concentrated in the N and CW regions. P_{PV} showed slight increases only in the north of the N region, south of the NE region, and in the SE region in all scenarios and periods, with maximum growth values of 2.5 % under SSP5-8.5 for the near-term future. Despite the greater availability of solar energy, the sensitivity to the increase in TAS of the technology of current PV systems would not allow increases in the yield of PV energy production. On the contrary, as TAS increases, the efficiency of solar panels decreases, canceling the positive effect of the increase in RSDS.

This is the first work that assesses the impacts of climate change on P_{PV} in Brazil and provides a valuable reference for the rational and efficient use of renewable and sustainable solar energy. Based on these results, several strategies can be adopted, such as installations in certain regions and / or months of maximum use of solar energy. In addition to the above, Brazil should consider aspects of the life and prices of PV panels, as well as appropriate policies to support the implementation of PV systems, to plan an efficient expansion of its energy matrix. These results can be improved by using regional models with higher spatial resolution, and / or outputs of models with higher temporal resolution (e.g., hourly).

2.5. Acknowledgments

We acknowledge the Coordination for the Improvement of Higher Education Personnel (CAPES) for supporting this research. We acknowledge all the Institutions that make their datasets available, especially the Couple Model Intercomparison Project (CMIP). The author thanks the graduate program in Applied Meteorology at the Universidade Federal de Viçosa.

2.6. Supplementary material

Table S1. ESMs from CMIP6 used in this study.

ID	Model	Institution - Country	Resolution (lat x lon)
1	ACCESS-CM2	Commonwealth Scientific and Industrial Research Organization (CSIRO), ARC Centre of Excellence for Climate System Science (ARCCSS) - Australia	1.25° x 1.87°
2	ACCESS-ESM1-5	Commonwealth Scientific and Industrial Research Organization (CSIRO) - Australia	1.25° x 1.87°
3	AWI-CM-1-1-MR	Alfred Wegener Institute Helmholtz Centre for Polar and Marine Research (AWI) - Germany	0.93° x 0.93°
4	AWI-ESM-1-1-LR		1.87° x 1.87°
5	BCC-CSM2-MR	Beijing Climate Center (BCC), China Meteorological Administration - China	1.12° x 1.12°
6	BCC-ESM1		2.81° x 2.81°
7	CAS-ESM2-0	Institute of Atmospheric Physics (IAP), Chinese Academy of Sciences (CAS) - China	1.40° x 1.40°
8	CESM2	National Center for Atmospheric Research (NCAR) - United States	0.93° x 1.25°
9	CESM2-FV2		1.87° x 2.50°
10	CESM2-WACCM		0.93° x 1.25°
11	CESM2-WACCM-FV2		1.87° x 2.50°
12	CIESM	Tsinghua University (THU) - China	0.93° x 1.25°
13	CMCC-CM2-SR5	Euro-Mediterranean Center on Climate Change (CMCC) - Italia	0.93° x 1.25°
14	CNRM-CM6-1	Centre National de Recherches Météorologiques, Centre Européen de Recherche et Formation Avancée en Calcul Scientifique (CNRM- CERFACS) - France	1.40° x 1.40°
15	CNRM-CM6-1-HR		0.50° x 0.50°
16	CNRM-ESM2-1		1.40° x 1.40°
17	CanESM5	Canadian Centre for Climate Modelling and Analysis (CCCma) - Canada	2.81° x 2.81°
18	E3SM-1-0	The Energy Exascale Earth System Modeling (E3SM) project, U.S. Department of Energy (DOE) - United States	1.00° x 1.00°

19	E3SM-1-1		1.00° x 1.00°
20	E3SM-1-1-ECA		1.00° x 1.00°
21	EC-Earth3		0.70° x 0.70°
22	EC-Earth3-Veg	EC-Earth-Consortium - 10 European countries	0.70° x 0.70°
23	EC-Earth3-Veg-LR		1.12° x 1.12°
24	FGOALS-f3-L	Institute of Atmospheric Physics (IAP), Chinese Academy of Sciences (CAS) - China	1.00° x 1.25°
25	FGOALS-g3		2.25° x 2.00°
26	GFDL-ESM4	Geophysical Fluid Dynamics Laboratory (GFDL) of National Oceanic and Atmospheric Administration (NOAA) - United States	1.00° x 1.25°
27	GISS-E2-1-G	National Aeronautics and Space Administration (NASA) - United States	2.00° x 2.50°
28	GISS-E2-1-H		2.00° x 2.50°
29	HadGEM3-GC31-LL	Met Office Hadley Centre (MOHC) - United Kingdom	1.25° x 1.87°
30	HadGEM3-GC31-MM		0.55° x 0.83°
31	INM-CM4-8	Institute for Numerical Mathematics (INM) - Russia	1.50° x 2.00°
32	INM-CM5-0		1.50° x 2.00°
33	IPSL-CM6A-LR	Institut Pierre-Simon Laplace (IPSL) - France	1.25° x 2.50°
34	KACE-1-0-G	National Institute of Meteorological Sciences/Korea Meteorological Administration (NIMS/KMA) - Korea	1.25° x 1.87°
35	MIROC6	Atmosphere and Ocean Research Institute (The University of Tokyo), National Institute for Environmental Studies, and Japan Agency for Marine-Earth Science and Technology - Japan	1.40° x 1.40°
36	MIROC-ES2L		2.81° x 2.81°
37	MPI-ESM-1-2-HAM	HAMMOZ-Consortium - 7 european agencies	1.87° x 1.87°
38	MPI-ESM1-2-HR	Max Planck Institute Earth System Model - Germany	0.93° x 0.93°
39	MPI-ESM1-2-LR		1.87° x 1.87°

40	MRI-ESM2-0	Meteorological Research Institute (MRI) - Japan	1.12° x 1.12°
41	NESM3	Nanjing University of Information Science and Technology (NUIST) - China	1.87° x 1.87°
42	NorCPM1		1.87° x 2.50°
43	NorESM2-LM	Norwegian Climate Center (NCC) - Norway	1.87° x 2.50°
44	NorESM2-MM		0.93° x 1.25°
45	SAM0-UNICON	Seoul National University (SNU) - South Korea	0.93° x 1.25°
46	TaiESM1	Research Center for Environmental Changes (RCEC) of Academia Sinica (AS) - Taiwan	0.93° x 1.25°
47	UKESM1-0-LL	Met Office Hadley Centre (MOHC) - United Kingdom	1.25° x 1.87°

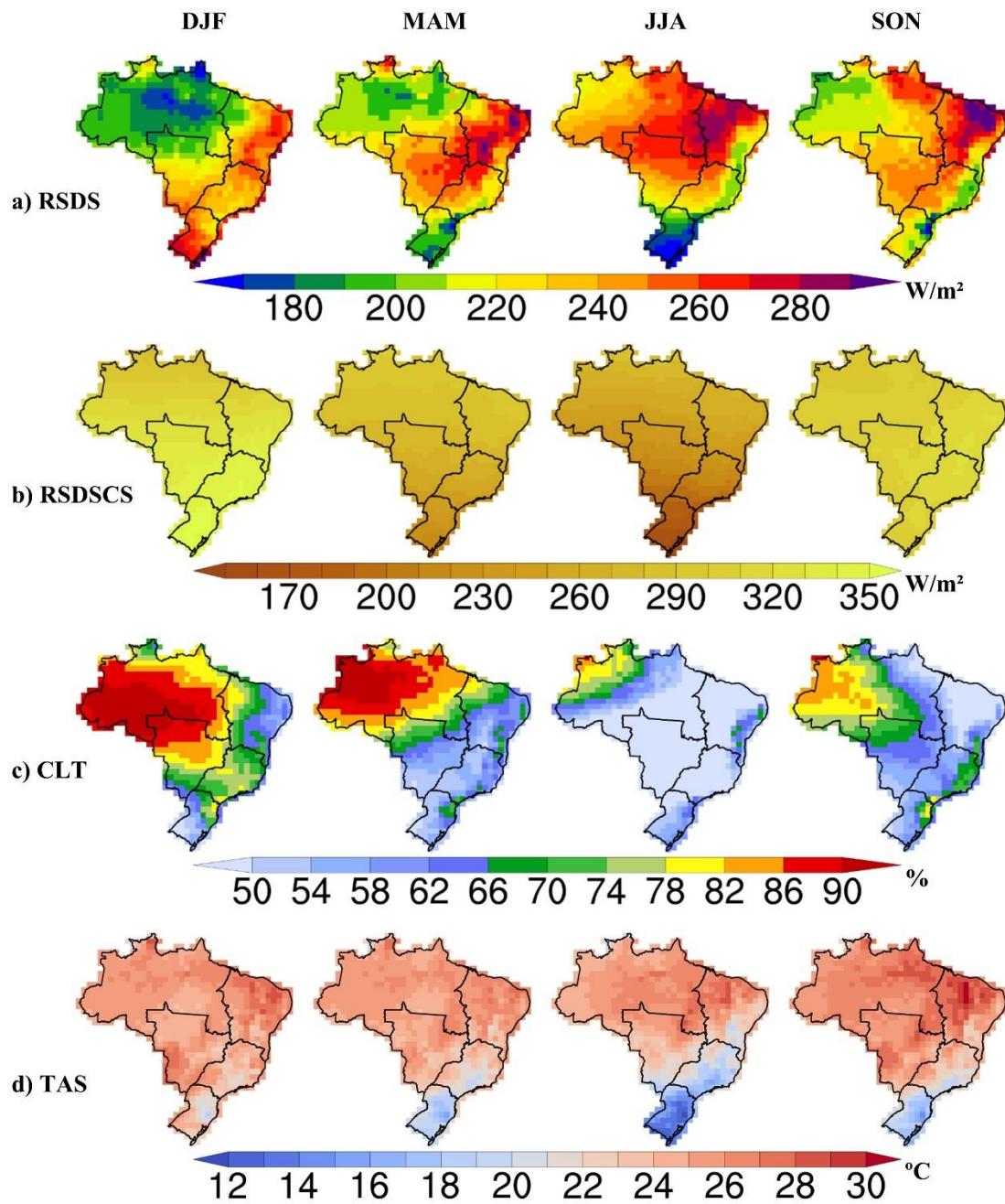


Figure S1. Seasonal mean climatologies of the a) RSDS, b) RSDSCS, c) CLT and d) TAS over Brazil during the historical period (1981 – 2010). The seasons are summer (DJF), autumn (MAM), winter (JJA) and spring (SON). Dataset: ERA5.

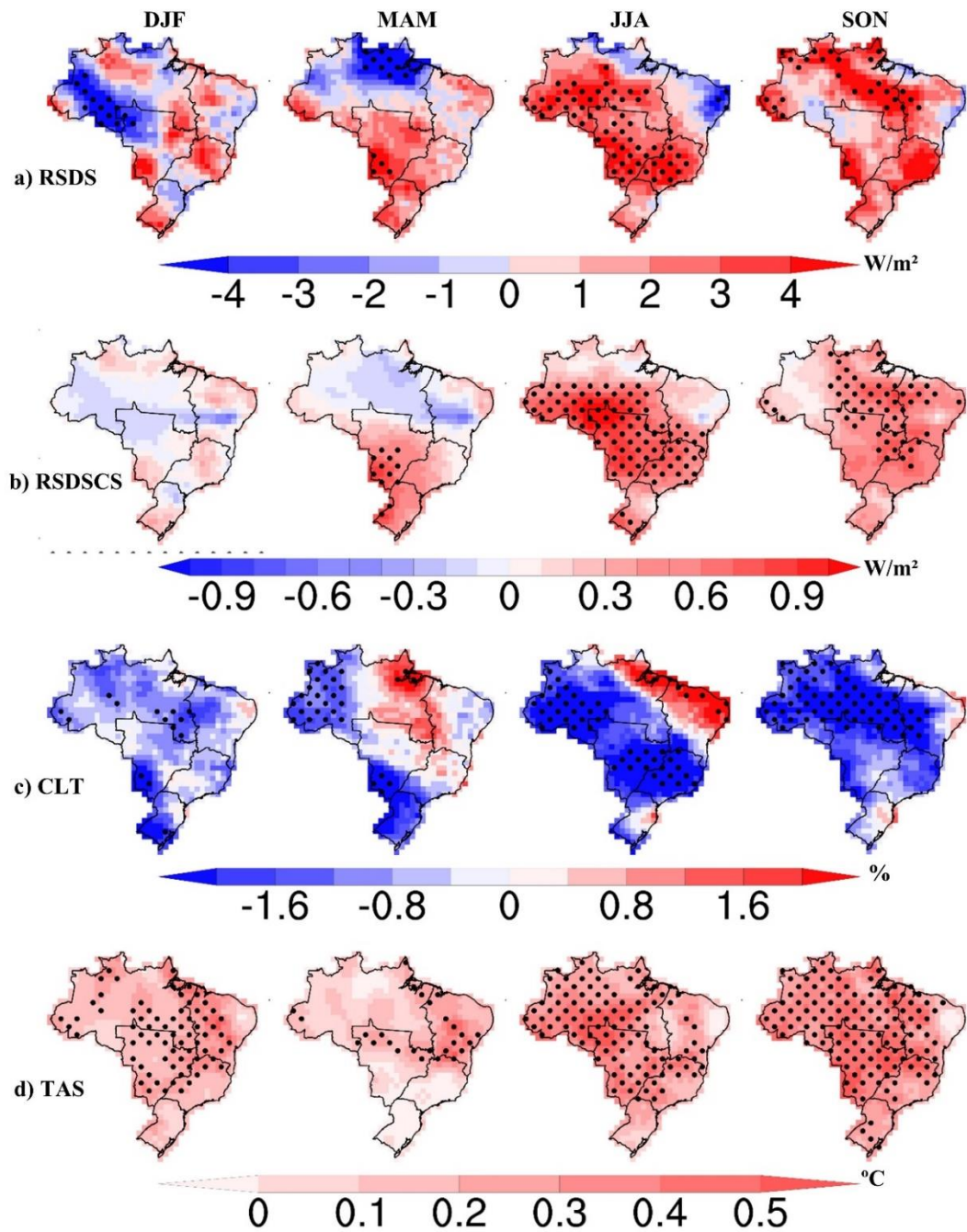


Figure S2. Seasonal trends per decade of the a) RSDS, b) RSDSCS, c) CLT and d) TAS over Brazil during the historical period (1981 – 2010). The seasons are summer (DJF), autumn (MAM), winter (JJA) and spring (SON). Dots indicate statistical significance at the 95% level Dataset: ERA5.

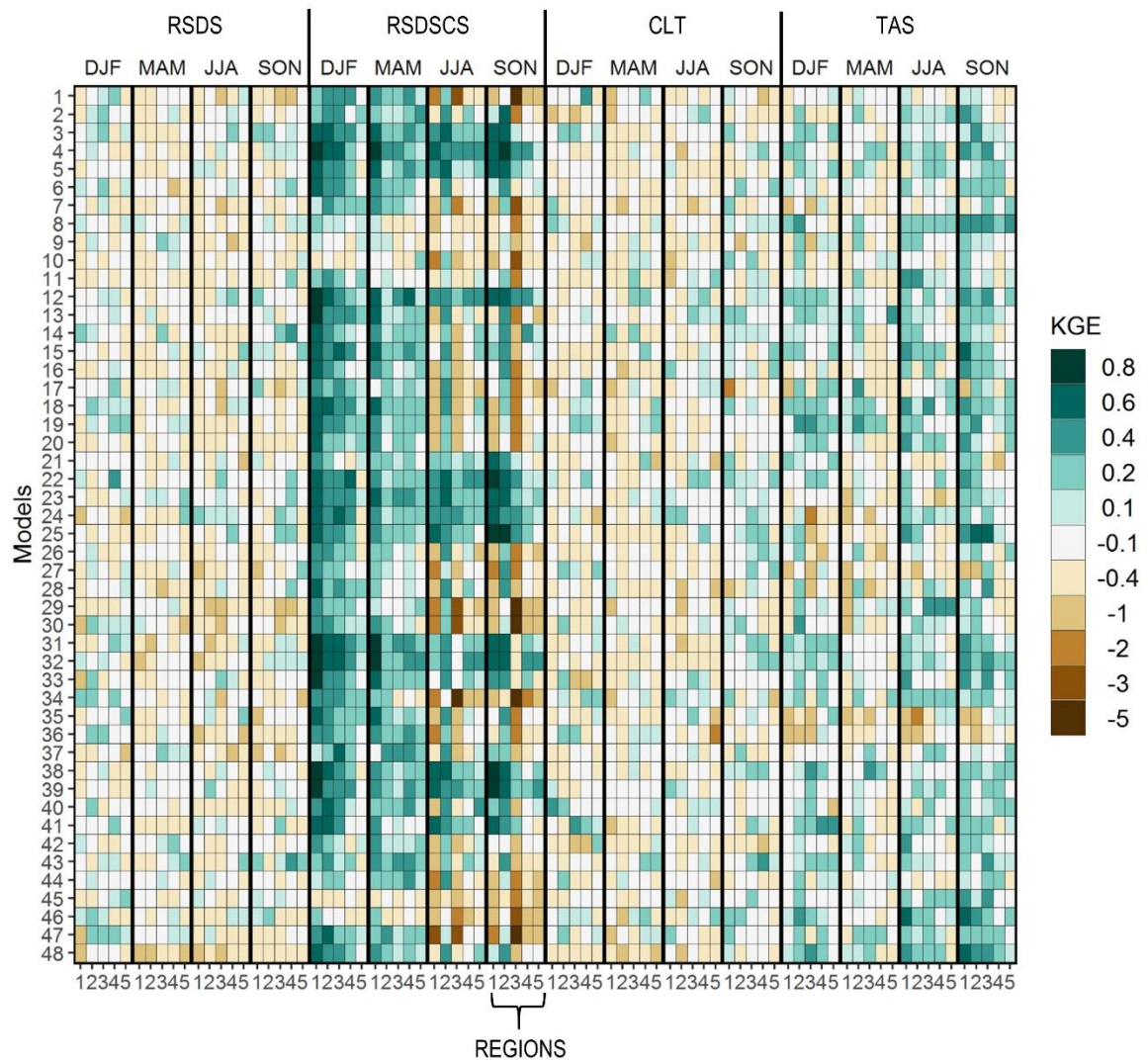


Figure S3. Seasonal KGE values for RSDS, RSDSCS, CLT and TAS for 47 ESMs from CMIP6 and a Multi-model-ensemble (M48), during the historical period (1981 – 2010) over Brazil. Lower horizontal axis represents the North (1), Northeast (2), Center-West (3), Southeast (4) and South (5) regions. Left vertical axis shows the ESMs.

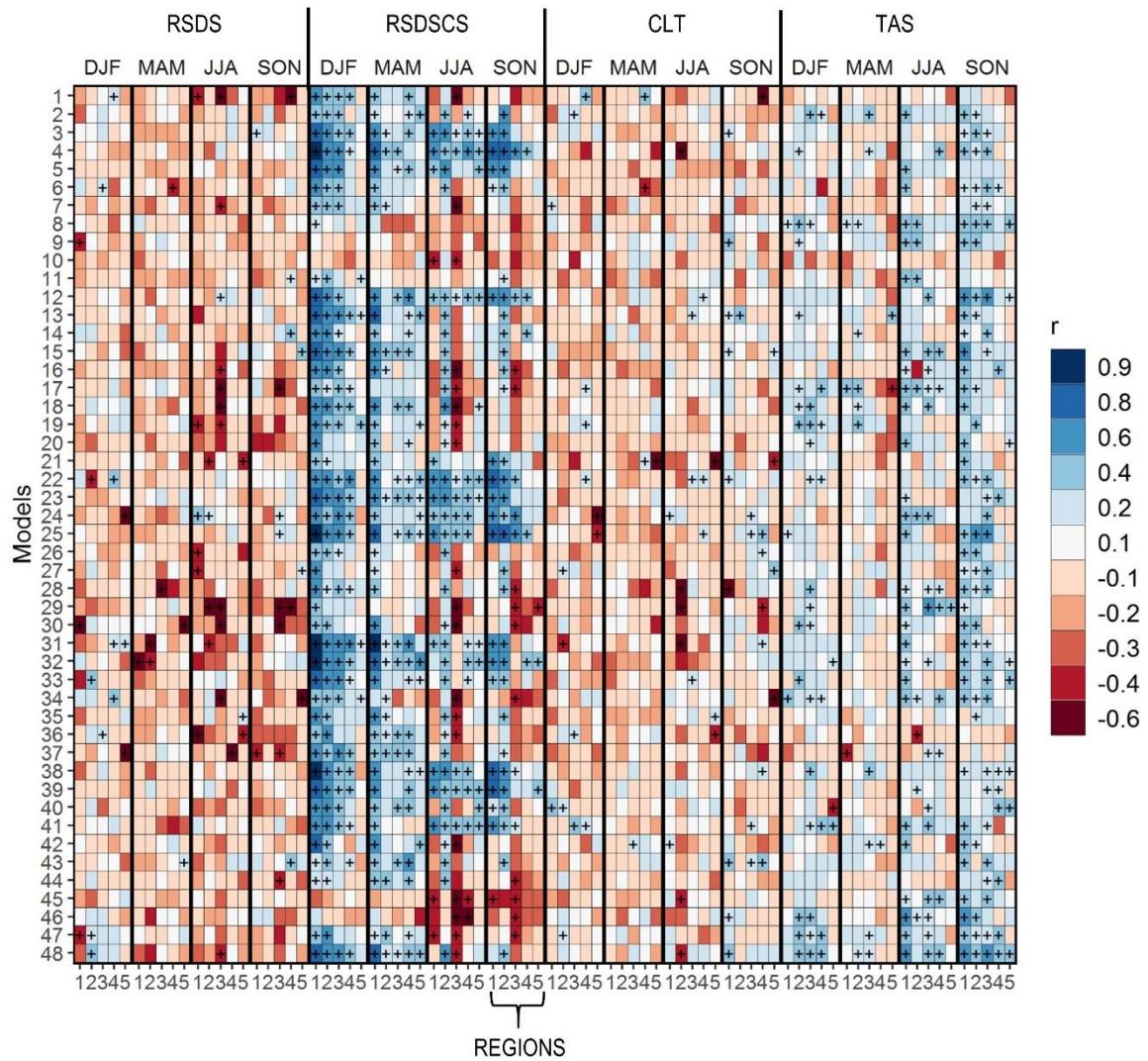


Figure S4. Similar to Fig. S3, but for the correlation (r) values. Crosses indicate statistically significant correlations at the 95% level.

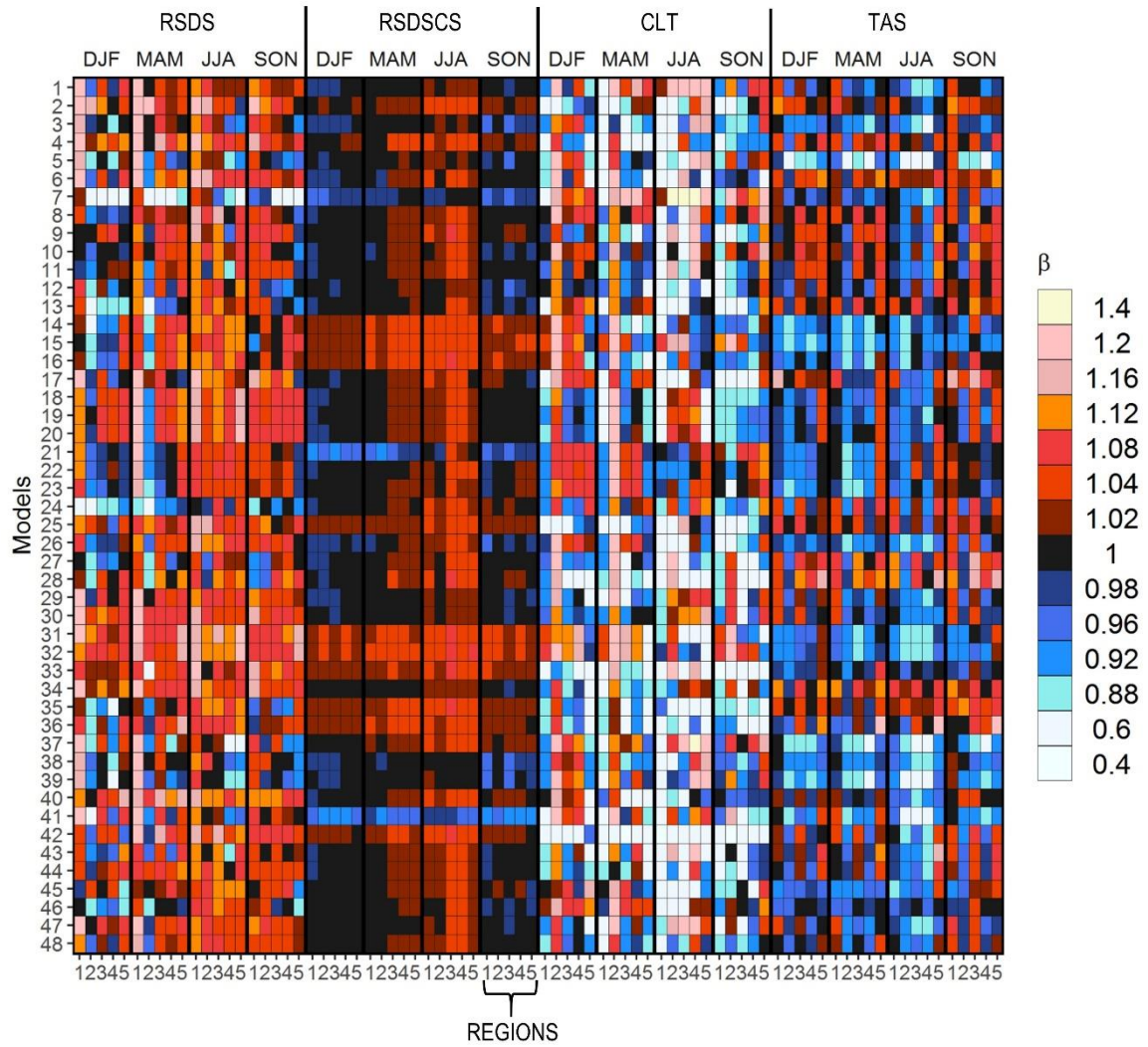


Figure S5. Similar to Fig. S3, but for the bias ratio (β) values.

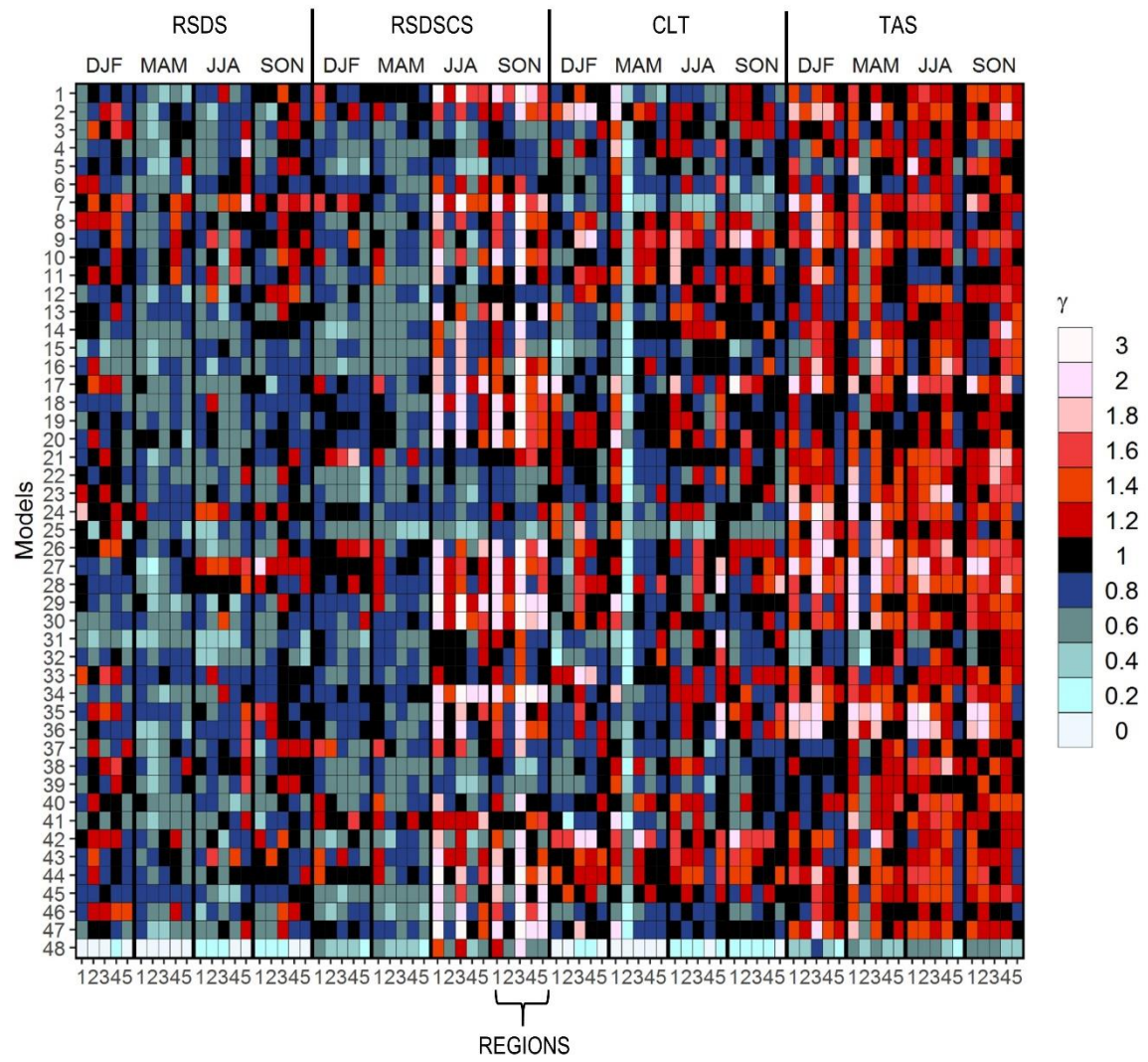


Figure S6. Similar to Fig. S3, but for the variability ratio (γ) values.

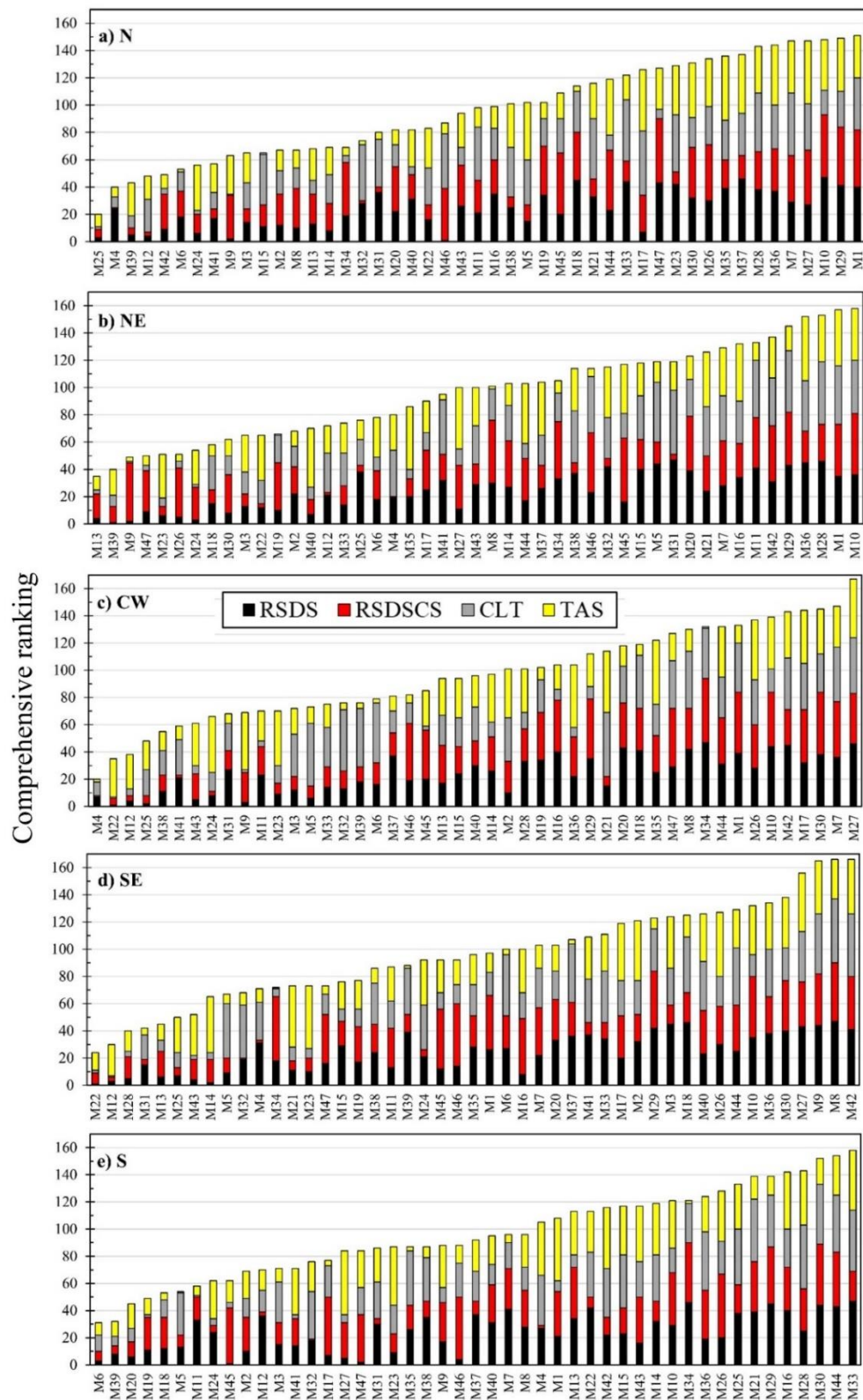


Figure S7. Comprehensive ranking based on KGE performance of ESMs calculating RSDS, RSDSCS, CLT and TAS for the a) N, b) NE, c) CW, d) SE and e) S regions. The y-axis represents the accumulation of ESMs ranking for the atmospheric variables.

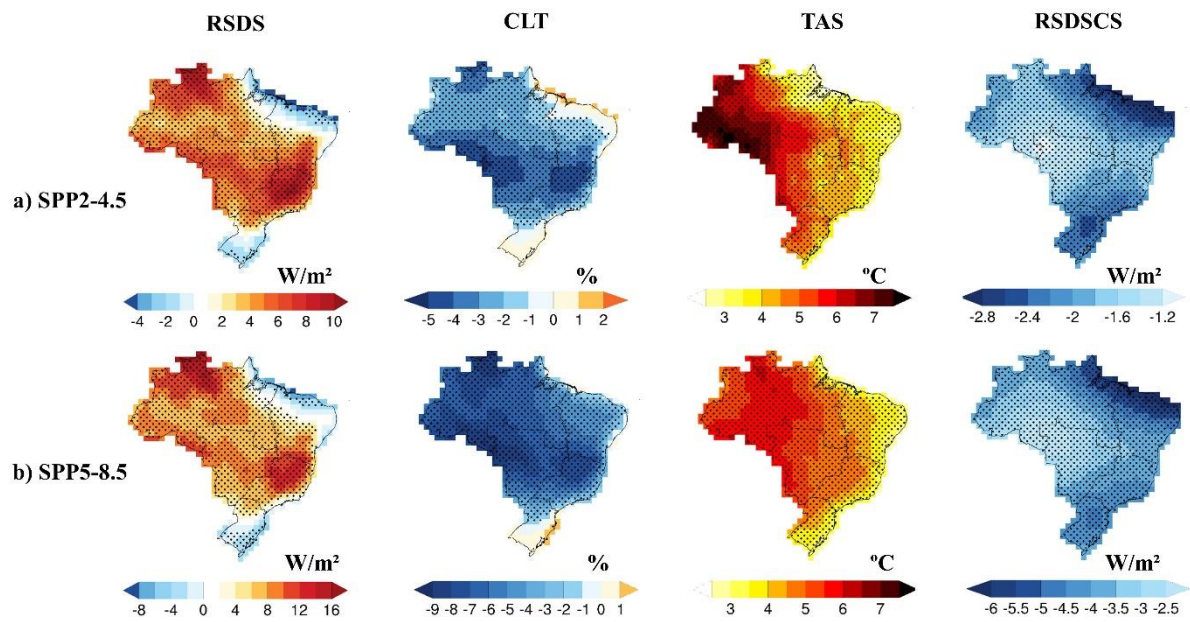


Figure S8. Projected changes from OME in the annual mean of RSDS, CLT, TAS and RSDSCS for the end-century future (2071 – 2100) relative to the historical period (1981 – 2010), under a) SSP2-4.5 and b) SSP5-8.5 scenarios. Significant differences at the 95% level of changes are dotted.

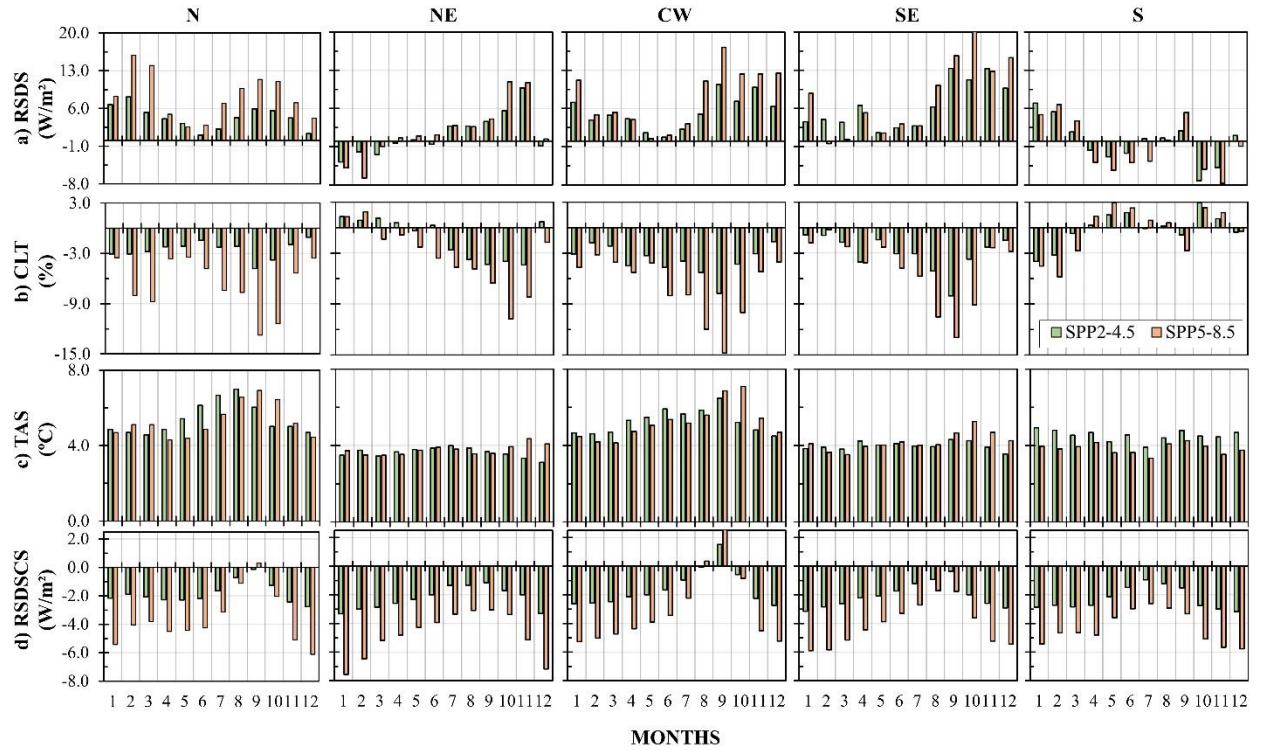


Figure S9. Projected changes to the end-century future (2071-2100 versus 1981-2010) from OME in the annual cycle by month of a) RSDS, b) CLT, c) TAS and d) RSDSCS over five Brazilian regions under SSP2-4.5 (green) and SSP5-8.5 (orange) scenarios.

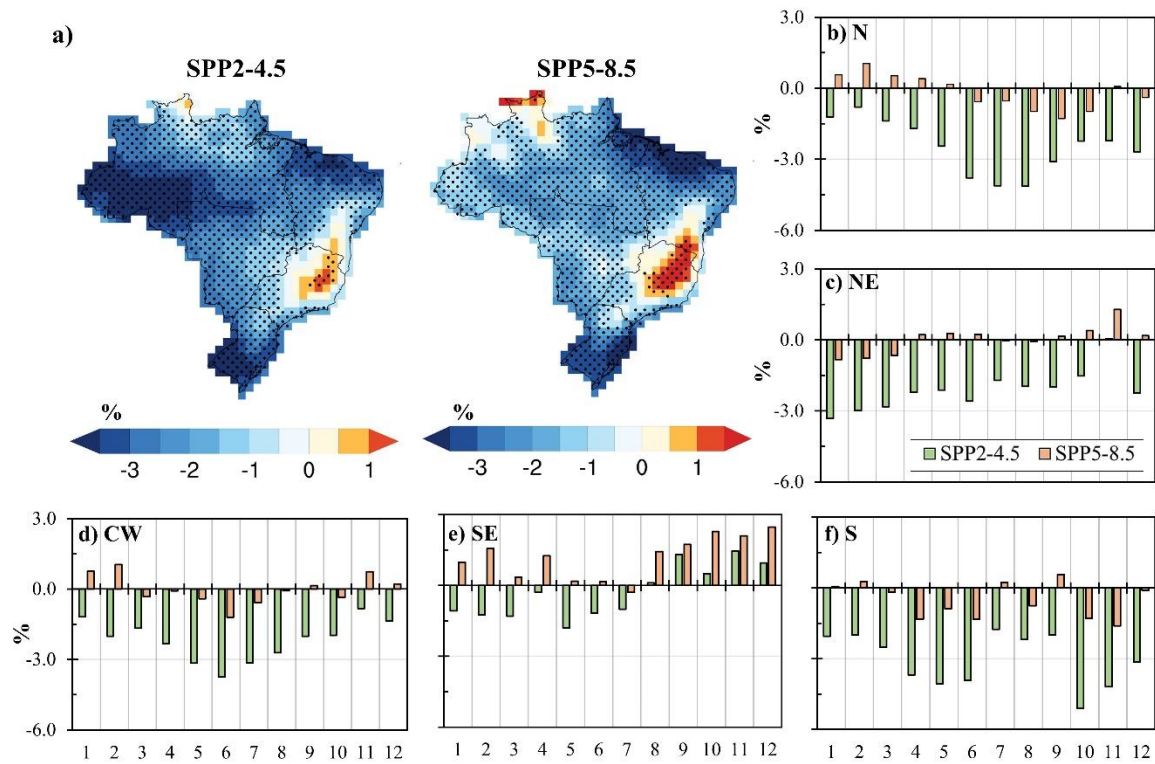


Figure S10. Projected changes in annual potential PV generation (a), and in PV potential generation cycle by month for the b) N, c) NE, d) CW, e) SE and f) S regions, to the end-century future (2071-2100 versus 1981-2010) from OME under SSP2-4.5 (green) and SSP5-8.5 (orange) scenarios. In maps (a), significant differences at the 95% level of changes are dotted.

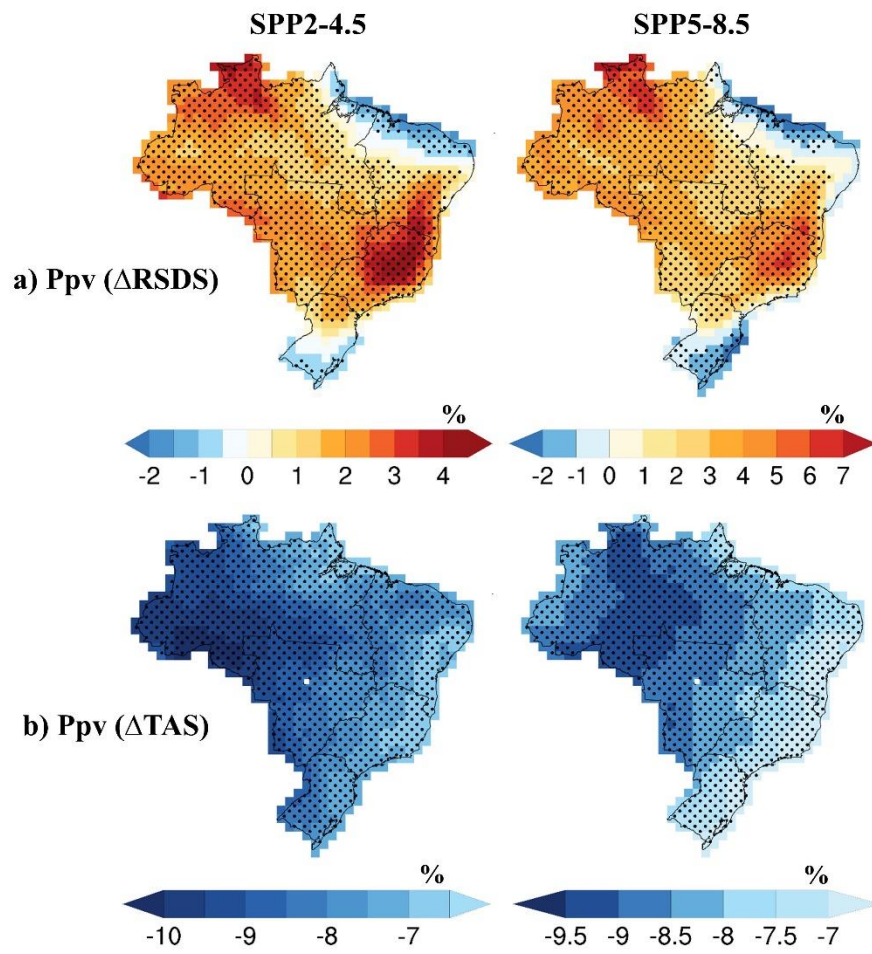


Figure S11. Projected changes in potential PV generation by a) isolated variation of RSDS ($P_{pv}(\Delta RSDS)$) and b) Isolated variation of TAS ($P_{pv}(\Delta TAS)$) for the end-century future (2071-2100 versus 1981-2010) from OME under SSP2-4.5 and SSP5-8.5 scenarios. Dots indicate significant differences at the 95% level.

2.7. References

- Akinsanola, A., Kooperman, K., Pendergrass, P., Hannah, H., Reed, R., 2020. Seasonal representation of extreme precipitation indices over the United States in CMIP6 present-day simulations. *Environ. Res. Lett.* 15. <https://doi.org/10.1088/1748-9326/ab92c1>
- Alves, L.M., Marengo, J.A., Fu, R., Bombardi, R.J., 2017. Sensitivity of Amazon Regional Climate to Deforestation. *Am. J. Clim. Chang.* 06, 75–98. <https://doi.org/10.4236/ajcc.2017.61005>
- Angelini, I.M., Garstang, M., Davis, R.E., Hayden, B., Fitzjarrald, D.R., Legates, D.R., Greco, S., Macko, S., Connors, V., 2011. On the coupling between vegetation and the atmosphere. *Theor. Appl. Climatol.* 105, 243–261. <https://doi.org/10.1007/s00704-010-0377-5>
- Augustine, J.A., Dutton, E.G., 2013. Variability of the surface radiation budget over the United States from 1996 through 2011 from high-quality measurements. *J. Geophys. Res. Atmos.* 118, 43–53. <https://doi.org/10.1029/2012JD018551>
- Avila-Diaz, A., Abrahão, G., Justino, F., Torres, R., Wilson, A., 2020a. Extreme climate indices in Brazil: evaluation of downscaled earth system models at high horizontal resolution. *Clim. Dyn.* 54, 5065–5088. <https://doi.org/10.1007/s00382-020-05272-9>
- Avila-Diaz, A., Benezoli, V., Justino, F., Torres, R., Wilson, A., 2020b. Assessing current and future trends of climate extremes across Brazil based on reanalyses and earth system model projections. *Clim. Dyn.* 55, 1403–1426. <https://doi.org/10.1007/s00382-020-05333-z>
- Bazyomo, S.D.Y.B., Lawin, E.A., Coulibaly, O., Ouedraogo, A., 2016. Forecasted changes in West Africa photovoltaic energy output by 2045. *Climate* 4, 1–15. <https://doi.org/10.3390/cli4040053>
- Covey, C., AchutaRao, K.M., Cubasch, U., Jones, P., Lambert, S.J., Mann, M.E., Phillips, T.J., Taylor, K.E., 2003. An overview of results from the Coupled Model Intercomparison Project. *Glob. Planet. Change* 37, 103–133. [https://doi.org/10.1016/S0921-8181\(02\)00193-5](https://doi.org/10.1016/S0921-8181(02)00193-5)
- Crook, J.A., Jones, L.A., Forster, P.M., Crook, R., 2011. Climate change impacts on future photovoltaic and concentrated solar power energy output. *Energy Environ. Sci.* 4, 3101–3109. <https://doi.org/10.1039/c1ee01495a>
- de Jong, P., Barreto, T.B., Tanajura, C.A.S., Kouloukoui, D., Oliveira-Esquerre, K.P., Kiperstok, A., Torres, E.A., 2019. Estimating the impact of climate change on wind and solar energy in Brazil using a South American regional climate model. *Renew. Energy* 141, 390–401. <https://doi.org/10.1016/j.renene.2019.03.086>
- Díaz, L.B., Vera, C.S., 2017. Austral summer precipitation interannual variability and trends over Southeastern South America in CMIP5 models. *Int. J. Climatol.* 37, 681–695. <https://doi.org/10.1002/joc.5031>
- Eyring, V., Bony, S., Meehl, G.A., Senior, C.A., Stevens, B., Stouffer, R.J., Taylor, K.E., 2016. Overview of the Coupled Model Intercomparison Project Phase 6 (CMIP6) experimental design and organization. *Geosci. Model Dev.* 9, 1937–1958. <https://doi.org/10.5194/gmd-9-1937-2016>
- Hersbach, H., Bell, B., Berrisford, P., Hirahara, S., Horányi, A., Muñoz-Sabater, J., Nicolas, J., Peubey, C., Radu, R., Schepers, D., Simmons, A., Soci, C., Abdalla, S., Abellan, X., Balsamo, G., Bechtold, P., Biavati, G., Bidlot, J., Bonavita, M., Chiara, G., Dahlgren, P., Dee, D., Diamantakis, M., Dragani, R., Flemming, J., Forbes, R., Fuentes, M., Geer, A., Haimberger, L., Healy, S., Hogan, R.J., Hólm, E., Janisková, M., Keeley, S., Laloyaux, P., Lopez, P., Lupu, C., Radnoti, G., Rosnay, P., Rozum, I., Vamborg, F., Villaume, S., Thépaut, J., 2020. The ERA5 global reanalysis. *Q. J. R. Meteorol. Soc.* 146, 1999–2049. <https://doi.org/10.1002/qj.3803>
- Hogan, R.J., Hirahara, S., 2016. Effect of solar zenith angle specification in models on mean

- shortwave fluxes and stratospheric temperatures. *Geophys. Res. Lett.* 43, 482–488. <https://doi.org/10.1002/2015GL066868>
- Huber, I., Bugliaro, L., Ponater, M., Garny, H., Emde, C., Mayer, B., 2016. Do climate models project changes in solar resources? *Sol. Energy* 129, 65–84. <https://doi.org/10.1016/j.solener.2015.12.016>
- International Energy Agency: Photovoltaic Power Systems Programme. Snapshot of Global PV Markets, 2020.
- IPCC, 2014. Climate Change 2014: Synthesis Report. Contribution of Working Groups I, II and III to the Fifth Assessment Report of the Intergovernmental Panel on Climate Change. Geneva, Switzerland.
- Jahani, B., Dinpashoh, Y., Wild, M., 2018. Dimming in Iran since the 2000s and the potential underlying causes. *Int. J. Climatol.* 38, 1543–1559. <https://doi.org/10.1002/joc.5265>
- Jerez, S., Tobin, I., Vautard, R., Montávez, J.P., López-Romero, J.M., Thais, F., Bartok, B., Christensen, O.B., Colette, A., Déqué, M., Nikulin, G., Kotlarski, S., Van Meijgaard, E., Teichmann, C., Wild, M., 2015. The impact of climate change on photovoltaic power generation in Europe. *Nat. Commun.* 6. <https://doi.org/10.1038/ncomms10014>
- Kang, J.N., Wei, Y.M., Liu, L.C., Han, R., Yu, B.Y., Wang, J.W., 2020. Energy systems for climate change mitigation: A systematic review. *Appl. Energy* 263. <https://doi.org/10.1016/j.apenergy.2020.114602>
- Keeble, J., Hassler, B., Banerjee, A., Checa-Garcia, R., Chiodo, G., Davis, S., Eyring, V., Griffiths, P., Morgenstern, O., Nowack, P., Zeng, G., Zhang, J., Bodeker, G., Cugnet, D., Danabasoglu, G., Deushi, M., Horowitz, L., Li, L., Michou, M., Mills, M., Nabat, P., Park, S., Wu, T., 2020. Evaluating stratospheric ozone and water vapor changes in CMIP6 models from 1850–2100. *Atmos. Chem. Phys. Discuss.* 1–68. <https://doi.org/10.5194/acp-2019-1202>
- Kodama, Y.M., Sagawa, T., Ishida, S., Yoshikane, T., 2012. Roles of the Brazilian plateau in the formation of the SACZ. *J. Clim.* 25, 1745–1758. <https://doi.org/10.1175/2011JCLI3785.1>
- Li, J., Jiang, Y., Xia, X., Hu, Y., 2018. Increase of surface solar irradiance across East China related to changes in aerosol properties during the past decade. *Environ. Res. Lett.* 13. <https://doi.org/10.1088/1748-9326/aaa35a>
- Müller, J., Folini, D., Wild, M., Pfenninger, S., 2019. CMIP-5 models project photovoltaics are a no-regrets investment in Europe irrespective of climate change. *Energy* 171, 135–148. <https://doi.org/10.1016/j.energy.2018.12.139>
- O'Neill, B.C., Tebaldi, C., Van Vuuren, D.P., Eyring, V., Friedlingstein, P., Hurtt, G., Knutti, R., Kriegler, E., Lamarque, J.F., Lowe, J., Meehl, G.A., Moss, R., Riahi, K., Sanderson, B.M., 2016. The Scenario Model Intercomparison Project (ScenarioMIP) for CMIP6. *Geosci. Model Dev.* 9, 3461–3482. <https://doi.org/10.5194/gmd-9-3461-2016>
- Pereira, E.B., Martins, F.R., Gonçalves, A.R., Lima, F.J.L. de, Rüther, R., Abreu, S.L., Tiepolo, G.M., Pereira, S.V., Souza, J.G. de, 2017. Atlas Brasileiro de Energia Solar, 2. ed. ed. INPE, São José dos Campos.
- Pivello, V.R., 2011. The use of fire in the cerrado and Amazonian rainforests of Brazil: Past and present. *Fire Ecol.* 7, 24–39. <https://doi.org/10.4996/fireecology.0701024>
- Reis, S.M., Marimon, B.S., Marimon Junior, B.H., Morandi, P.S., de Oliveira, E.A., Elias, F., Das Neves, E.C., de Oliveira, B., Nogueira, D. da S., Umetsu, R.K., Feldpausch, T.R., Phillips, O.L., 2018. Climate and fragmentation affect forest structure at the southern border of amazonia. *Plant Ecol. Divers.* 11, 13–25. <https://doi.org/10.1080/17550874.2018.1455230>
- Sanchez-Lorenzo, A., Enriquez-Alonso, A., Wild, M., Trentmann, J., Vicente-Serrano, S.M., Sanchez-Romero, A., Posselt, R., Hakuba, M.Z., 2017. Trends in downward surface solar

- radiation from satellites and ground observations over Europe during 1983–2010. *Remote Sens. Environ.* 189, 108–117. <https://doi.org/10.1016/j.rse.2016.11.018>
- Sawadogo, W., Abiodun, B.J., Okogbue, E.C., 2020a. Impacts of global warming on photovoltaic power generation over West Africa. *Renew. Energy* 151, 263–277. <https://doi.org/10.1016/j.renene.2019.11.032>
- Sawadogo, W., Reboita, M.S., Faye, A., da Rocha, R.P., Odoulami, R.C., Olusegun, C.F., Adeniyi, M.O., Abiodun, B.J., Sylla, M.B., Diallo, I., Coppola, E., Giorgi, F., 2020b. Current and future potential of solar and wind energy over Africa using the RegCM4 CORDEX-CORE ensemble. *Clim. Dyn.* <https://doi.org/10.1007/s00382-020-05377-1>
- Schmidt, J., Cancellà, R., Pereira, A.O., 2016. An optimal mix of solar PV, wind and hydro power for a low-carbon electricity supply in Brazil. *Renew. Energy* 85, 137–147. <https://doi.org/10.1016/j.renene.2015.06.010>
- Silva, A.S., Justino, F., Setzer, A.W., Avila-Diaz, A., 2020. Vegetation fire activity and the Potential Fire Index (PFIv2) performance in the last two decades (2001–2016). *Int. J. Climatol.* 55, joc.6648. <https://doi.org/10.1002/joc.6648>
- Soni, V.K., Pandithurai, G., Pai, D.S., 2016. Is there a transition of solar radiation from dimming to brightening over India? *Atmos. Res.* 169, 209–224. <https://doi.org/10.1016/j.atmosres.2015.10.010>
- Tokarska, K.B., Stolpe, M.B., Sippel, S., Fischer, E.M., Smith, C.J., Lehner, F., Knutti, R., 2020. Past warming trend constrains future warming in CMIP6 models. *Sci. Adv.* 6, eaaz9549. <https://doi.org/10.1126/sciadv.aaz9549>
- Vasconcellos, F.C., Deng, Y., Zhang, H., Martins, G., 2020. Austral summer precipitation biases over tropical South America in five CMIP5 earth system models. *Int. J. Climatol.* 40, 6506–6525. <https://doi.org/10.1002/joc.6595>
- Wang, K., Ma, Q., Li, Z., Wang, J., 2015. Decadal variability of surface incident solar radiation over China: Observations, satellite retrievals, and reanalyses. *J. Geophys. Res. Atmos.* 120, 6500–6514. <https://doi.org/10.1002/2015JD023420>
- Wild, M., 2016. Decadal changes in radiative fluxes at land and ocean surfaces and their relevance for global warming. *Wiley Interdiscip. Rev. Clim. Chang.* 7, 91–107. <https://doi.org/10.1002/wcc.372>
- Wild, M., 2012. Enlightening global dimming and brightening. *Bull. Am. Meteorol. Soc.* 93, 27–37. <https://doi.org/10.1175/BAMS-D-11-00074.1>
- Wild, M., 2009. Global dimming and brightening: A review. *J. Geophys. Res.* 114, 1–31. <https://doi.org/10.1029/2008JD011470>
- Wild, M., Folini, D., Henschel, F., Fischer, N., Müller, B., 2015. Projections of long-term changes in solar radiation based on CMIP5 climate models and their influence on energy yields of photovoltaic systems. *Sol. Energy* 116, 12–24. <https://doi.org/10.1016/j.solener.2015.03.039>
- Yang, L., Jiang, J., Liu, T., Li, Y., Zhou, Y., Gao, X., 2018. Projections of future changes in solar radiation in China based on CMIP5 climate models. *Glob. Energy Interconnect.* <https://doi.org/10.14171/j.2096-5117.gei.2018.04.005>
- Zhang, G., Ma, Y., 2020. Clear-sky surface solar radiation and the radiative effect of aerosol and water vapor based on simulations and satellite observations over Northern China. *Remote Sens.* 12. <https://doi.org/10.3390/rs12121931>
- Zhou, Z., Lin, A., Wang, L., Qin, W., Zhong, Y., He, L., 2019. Trends in downward surface shortwave radiation from multi-source data over China during 1984–2015. *Int. J. Climatol.* 1–19. <https://doi.org/10.1002/joc.6408>
- Zou, L., Wang, L., Li, J., Lu, Y., Gong, W., Niu, Y., 2019. Global surface solar radiation and photovoltaic power from Coupled Model Intercomparison Project Phase 5 climate models. *J. Clean. Prod.* 224, 304–324. <https://doi.org/10.1016/j.jclepro.2019.03.268>

Zuluaga, C.F., Avila-Diaz, A., Justino, F.B., Wilson, A.B., 2021. Climatology and trends of downward shortwave radiation over Brazil. *Atmos. Res.* 250, 105347. <https://doi.org/10.1016/j.atmosres.2020.105347>

GENERAL CONCLUSIONS

In chapter 1, DSWR was evaluated against four reanalysis products (ERA5, MERRA2, JRA55 and CFSR) and two mixed products (GMFD and WFDEI) in relation to grid observations (OBS_BR), on annual and seasonal scales for five regions of Brazil, during the period 1980 - 2016. The results showed that ERA5 delivered the DSWR values closest to OBS_BR for all regions of the country. Also, DSWR showed a positive trend (brightening) in DSWR for all of Brazil, particularly in the N, CW and SE regions. Strong correlations were found between cloud cover and observed DWSR that showed that decadal cloud cover changes are the main contributing factor to the brightening effect in Brazil.

In chapter 2, DSWR and other atmospheric variables related to the PV power potential (P_{PV}) from 47 CMIP6 models were evaluated, compared to ERA5 during the historical period (1981 - 2010). Then, the best four models were chosen - CIESM (M12), MPI-ESM1-2-LR (M39), EC-Earth3-Veg (M22) and FGOALS-g3 (M25) - to determine the impact of climate change on P_{PV} for two future periods: near-term (2021-2050) and end-of-the-century (2071-2100) under the SSP2-4.5 and SSP5-8.5 scenarios. The results showed that P_{PV} will have slight increases only in the north of the N region, south of the NE region, and in the SE region in all scenarios and periods, with maximum growth values of 2.5% under SSP5-8.5 for the near-term future. Despite the greater availability of solar energy, the sensitivity to the increase in TAS of the technology of current P_{PV} systems, would not allow increases in the yield of P_{PV} . On the contrary, as TAS increases, the efficiency of solar panels decreases, canceling the positive effect of the increase in RSDS.

This thesis provides the first assessment of solar radiation incident in Brazil, based on extensive datasets, such as reanalyses, merged, ESMs, as well as the causes of their spatiotemporal variations, and potential applications such as renewable energy. We hope that this study will be an important input for the Brazilian energy sector, as well as for other sectors that involve the use of solar radiation.

In preparing this thesis, it became apparent that future research efforts should focus on:

- Use of regional models with a higher spatial resolution (e.g., CORDEX)

- Use of models with higher temporal resolution (e.g., hourly)
- Evaluate the calibration of the technological constants of P_{PV} systems, to adjust the relationship between climate and P_{PV} technology.
- Establish economic balances (cost/benefit) of the effect of climate change on P_{PV} .
- Build detailed schedules of use of the solar resource for P_{PV} .